

UNCLASSIFIED

AD NUMBER

AD479687

LIMITATION CHANGES

TO:

Approved for public release; distribution is unlimited.

FROM:

Distribution authorized to U.S. Gov't. agencies and their contractors;
Administrative/Operational Use; 1962. Other requests shall be referred to U.S. Naval Postgraduate School, Monterey, CA 93943.

AUTHORITY

USNPS ltr, 18 Oct 1971

THIS PAGE IS UNCLASSIFIED

NPS ARCHIVE
1962
ALDERSON, D.

PLASMA OSCILLATIONS IN A
LOW PRESSURE NEON DISCHARGE

DONALD M. ALDERSON, JR.
and
JOHN D. LEONARD, JR.

LIBRARY
U.S. NAVAL POSTGRADUATE SCHOOL
MONTEREY, CALIFORNIA

PLASMA OSCILLATIONS
IN A
LOW PRESSURE NEON DISCHARGE

by

Donald M. Alderson, Jr.

Lieutenant, United States Navy

and

John D. Leonard, Jr.

Lieutenant, United States Navy

Submitted in partial fulfillment of
the requirements for the degree of

MASTER OF SCIENCE
IN
PHYSICS

United States Naval Postgraduate School
Monterey, California

1 9 6 2

LIBRARY
U.S. NAVAL POSTGRADUATE SCHOOL
MONTEREY, CALIFORNIA

PLASMA OSCILLATIONS
IN A
LOW PRESSURE NEON DISCHARGE

by

Donald M. Alderson, Jr.

and

John D. Leonard, Jr.

This work is accepted as fulfilling
the thesis requirements for the degree of

MASTER OF SCIENCE

IN

PHYSICS

from the

United States Naval Postgraduate School

ABSTRACT

This work is a continuation of plasma oscillation studies of rare gas plasmas extending over the last five years at the U. S. Naval Postgraduate School. A low pressure Neon plasma was studied. Electronic methods of obtaining continuous graphical plots of probe current squared, and first and second derivatives of probe current, with respect to voltage were used. Data derived from probe measurements is presented graphically in the form of: plasma density, space potential, average electron energy, and oscillation intensities, as a function of probe position. Plasma densities derived from the positive ion section of probe current and a Druyvesteyn analysis are correlated with densities derived from detected electron oscillations. A correction factor on the order of $\sqrt{\frac{T_i}{T_e}}$ is shown to be necessary to correlate the density derived by positive ion current with that found by other methods. Electron oscillations were detected on all data runs throughout the length of the discharge, unlike the localized oscillations found in the argon plasma investigated the previous year. Ion oscillations corresponding to those in argon were detected throughout the length of the discharge. The detected electron oscillations corresponded to the Langmuir plasma frequency. Detector current from these oscillations increased by a factor of as much as 10^7 on decreasing plasma density gradients indicating large growth in amplitude and decrease in frequency. The detected ion oscillations corresponded to the predicted Langmuir electrostatic sound waves and were found to peak in amplitude with the electron oscillations. These ion oscillations were assumed to have a wavelength nominally

the length of the plasma column (9cm), and a velocity equal to $\sqrt{\frac{\gamma k T_e}{m_i}}$. These values of velocity and wavelength yielded frequencies of 94 KC and 75 KC in reasonable agreement with the 100 KC and 67 KC detected in a 75 ma and 65 ma discharge respectively. A tentative relation between the effects of ion mass and ionization potential on oscillations and discharge ionization phenomena is made suggesting that plasmas of light mass elements with atoms of high ionization potential may develop very strong electron and ion oscillations.

ACKNOWLEDGMENTS

The writers wish to gratefully express their appreciation to Professor Norman L. Oleson for his encouragement, guidance, and many helpful suggestions during the course of our work. Appreciation is expressed to Professor Carl E. Menneken, Department of Electronics, for his guidance in the techniques of high frequency measurements and the use of the equipment and facilities of his department. Appreciation is also expressed to Professor Gilbert F. Kinney, Chairman of the Department of Chemistry and Metallurgy, whose loan of several valuable pieces of electronic equipment made the continuance of our electronic reduction of data possible. Professor A. W. M. Cooper's effective aid in supplying material for our tube construction as well as his helpful advice is also most appreciated. Thanks are extended to Professor O. B. Wilson for his advice in acoustic phenomena. We wish also to extend our thanks to Professor K. G. Emeleus, Queens University, Belfast, Ireland, whose visit to our laboratory helped us considerably in interpreting some of the anomalous effects in our discharge. Appreciation is also expressed to our predecessors Captain L. H. Putnam, U. S. A., and Captain H. D. Collins, U. S. A., for their effective design of semi-automatic data recording equipment that made probe investigations in our work much easier. Thanks are given to Messrs. Kenneth C. Smith, Milton K. Andrews, Robert C. Moeller, Allen N. Goodall, and Allen J. White for their ever ready assistance and advice in technical matters. Especial appreciation is expressed to Mr. John M. Calder whose technical competence in the art of glass blowing, and experimental vacuum tube construc-

tion, aided us innumerable times in our work.

TABLE OF CONTENTS

| Section | Title | Page |
|---------|---------------------------|------|
| 1. | Introduction | 1 |
| 2. | Previous Work | 3 |
| 3. | Anomalies of NEON | 9 |
| 4. | Equipment | 14 |
| 5. | Procedures | 23 |
| 6. | Results | 29 |
| 7. | Interpretation of Results | 36 |
| 8. | Conclusions | 50 |
| 9. | Recommendations | 53 |
| 10. | Bibliography | 92 |
| | Appendix I | |

LIST OF ILLUSTRATIONS

| Figure | Subject Title | Page |
|--------|---|------|
| A | General Structure of a Gas Discharge | 5 |
| B | Collision Probability for Argon and Neon, for Electrons of Various Energies | 12 |
| C | Ionization Efficiency of Electrons in Neon and Argon | 12 |
| D | Probe Attenuation vs Frequency | 20 |
| 1 | General Experimental Equipment Arrangement | 54 |
| 2 | Frequency Detection Equipment | 55 |
| 3 | Probe Circuitry | 56 |
| 4 | Discharge Tube | 57 |
| 5 | Discharge Tube Details | 58 |
| 6 | D. C. Circuitry | 59 |
| 7 | Tube Characteristics Curves , Argon | 60 |
| 8 | Relaxation Oscillations in Neon | 61 |
| 9 | Collapsed Discharge in Neon | 61 |
| 10 | Tube Characteristics Curve, Neon, Run 1 | 62 |
| 11 | Tube Characteristics Curve, Neon, Run 2 | 62 |
| 12 | Probe Characteristics Curve, Near Cathode | 63 |
| 13 | Probe Characteristics Curve, Near Beginning of Region of Maximum Interaction | 64 |
| 14 | Probe Characteristics Curve, within the Region of Maximum Interaction | 65 |
| 15 | Probe Characteristics Curves, Anode Side, Beyond Region of Maximum Interaction | 66 |
| 16 | Probe Characteristics Curves, Anode 5 ^{mm} from Probe | 67 |

| Figure | Subject Title | Page |
|--------|--|------|
| 17 | Probe Characteristics Curves , Anode 20 ^{mm} from Probe | 68 |
| 18 | Probe Characteristics Curves , Anode 35 ^{mm} from Probe | 69 |
| 19 | Probe Characteristics Curves , Anode 50 ^{mm} from Probe | 70 |
| 20 | Probe Characteristics Curves , Anode 65 ^{mm} from Probe | 71 |
| 21 | Space Potential vs Distance , Run 1 | 72 |
| 22 | Space Potential vs Distance , Run 2 | 72 |
| 23 | Space Potential vs Distance , Run 2 | 72 |
| 24 | Space Potential vs Distance , Run 2 | 72 |
| 25 | Energy Distribution Function | 73 |
| 26a | Energy Distribution Function | 73 |
| 26b | Energy Distribution Function | 73 |
| 27 | Energy Distribution Function | 74 |
| 28 | Energy Distribution Function | 74 |
| 29a | Electron and Ion Densities vs Distance , Run 1 | 75 |
| 29b | Electron Density and Detector Current vs Distance , Run 1 | 76 |
| 30 | Electron and Ion Densities vs Distance , Run 2 | 77 |
| 31 | Electron and Ion Densities vs Distance , Run 2 | 78 |
| 32 | Electron and Ion Densities vs Distance , Run 2 | 79 |
| 33 | Electron Density , Space Potential , and Electron Temperature vs Distance , Run 1 | 80 |
| 34 | Electron Density , Space Potential , and Electron Temperature vs Distance , Run 2 | 81 |
| 35 | Electron Density , Space Potential , and Electron Temperature vs Distance , Run 2 | 82 |

| Figure | Subject Title | Page |
|--------|--|------|
| 36 | Electron Density, Space Potential, and Electron Temperature vs Distance, Run 2 | 83 |
| 37 | Ion Oscillation, Photograph | 84 |
| 38 | Ion Oscillation, Photograph | 84 |
| 39 | Ion Oscillation, Photograph | 84 |
| 40 | Ion Oscillation, Photograph | 84 |
| 41 | Ion Oscillation, Photograph | 84 |
| 42 | Ion Oscillation Intensity, Electron Density, and Detector Current vs Distance, Run 1 | 85 |
| 43 | Ion Oscillation Intensity, Electron Density, and Detector Current vs Distance, Run 2 | 86 |
| 44 | Ion Oscillation Intensity, Electron Density, and Detector Current vs Distance, Run 2 | 87 |
| 45 | Ion Oscillation Intensity, Electron Density, and Detector Current vs Distance, Run 2 | 88 |
| 46 | Photograph of Contaminated Sections of Discharge Tube and Internal Structure | 89 |
| 47 | Normal Glow Discharge, Photograph | 90 |
| 48 | Electron Temperature and Electron Density vs Anode Cathode Separation | 91 |

List of Symbols

- A - Area of probe
- γ - Adiabatic compression coefficient
- e - Electronic charge
- \bar{e}_v - Average electron energy
- f_e - Frequency of electron oscillation
- f_i - Frequency of ion oscillation
- I_C - Cavity wave meter, detector current
- I_d - Discharge current
- I_p - Probe current
- k - Boltzman's constant
- λ - Wave length
- m_e - Mass of electrons
- m_i - Mass of ions
- n_e - Electron density
- n_i - Ion density
- T_e - Electron temperature
- T_i - Ion temperature
- V_d - Discharge voltage
- V_i - Amplitude of ionic oscillation
- V_p - Probe potential
- V_{sp} - Space potential

1. Introduction.

In the years since World War II, the field of plasma physics has grown rapidly and with ever increasing importance. The study of plasmas has brought new knowledge into the fields of thermo-nuclear processes, radio communications, electronic circuitry, astrophysics, space propulsion, ballistic re-entry phenomena, and the views of science on cosmology. While these subjects are by no means the limit of its influence, they serve to illustrate the wide ranging effects of this specific field of basic research.

The term plasma was originally defined by Langmuir and Tonks (4), and they stated:

The word 'plasma' will be used to designate that portion of an arc type discharge in which the densities of ions and electrons are high but substantially equal. It embraces the whole space not occupied by the sheath.

Plasma is not a rare manifestation of matter as might first be expected by a casual glance at our immediate environment, but embraces very probably 99% or greater of the total matter in our universe. It is only in the dense matter environment such as laboratory facilities on earth where its existence must be so carefully sustained. It exists naturally in the universe from the fringes of our ionized upper atmosphere throughout interstellar space, and the unbelievably energetic plasma phenomena occurring on the sun directly affect our lives on this planet.

Plasmas generated under careful laboratory conditions have received increasing attention in the field of thermo-nuclear fusion devices. Initial attempts to generate a sustained thermo-nuclear reaction have met with

repeated failures in a succession of experiments, both in this country and overseas. It is becoming increasingly apparent that an understanding of the simple basic behavior of plasma and its inherent instabilities is a necessity before more complex procedures of containment can be applied to it.

It is toward this goal of better understanding of the basic phenomena in plasma physics that this particular research is carried out. This project is a continuation of the group work guided by Professor N. L. Oleson in the field of rare gas plasmas. In particular it is an investigation into the electron-ion oscillation instabilities that occur in a low pressure Neon discharge.

2. Previous Work.

Probe study of the characteristics of low pressure gaseous discharge tubes was placed on a firm theoretical foundation by Langmuir and Mott-Smith during 1924 in their analysis of a mercury vapor arc using probes (or collectors) of various geometries. (1)

Further studies by Langmuir (2) in 1925 showed that three separate energy groups of electrons were apparently present in the discharge. He classified them as "primary electrons," "secondary electrons," and "ultimate electrons." The primary electrons were those which kept nearly all the momentum gained in the cathode ion sheaths. The secondary and ultimate electrons were two groups with Maxwellian distributions of energy, the secondary's distribution proportional to the primary's energy and the ultimate electron's distribution independent of the primary's and lower than the secondary's. This indicated that some energy transfer mechanism existed in the discharge which Langmuir called scattering. Dittmer (3) disproved the hypothesis that a new mechanism, such as the possible large increase in the target area of excited molecules was the cause of scattering, by showing that the scattering reached a constant value at some distance from the cathode. Dittmer found that the region of scattering approaches the cathode as the tube current is increased and predicted that high scattering of electrons might be due to oscillation in the plasma. However, he was unable to detect such oscillations with the equipment available at that time.

Tonks and Langmuir (4) provided a simple theory for electron and ion

oscillations, by treating the electrons as simple oscillators held in a jelly-like substance being the ions of the plasma. They predicted electrons oscillations having a natural frequency;

$$\omega_e = \left(\frac{n e^2}{\pi m_e} \right)^{\frac{1}{2}}$$

and ion oscillations with an upper frequency limit of;

$$\omega_i = \left(\frac{m_e}{m_i} \right)^{\frac{1}{2}} \omega_e$$

Tentative verification of the theory was obtained by detecting oscillations which corresponded reasonably well with those predicted.

Merril and Webb (5) in their investigation in a low pressure mercury arc discharge, using probe techniques, found scattering occurred in narrow regions, and was associated with oscillations, agreeing within ten per cent of the Langmuir frequency. Their conclusions were that scattering was due to oscillations receiving energy from the fast electron group. Continuing these investigations in the period 1947 to 1954, Armstrong, Emeleus, and Neill established that (a) oscillations are reproducible, (b) oscillations varied in frequency and magnitude over tube characteristics (6) and (c) the frequency of oscillation, the Langmuir frequency, was independent of probe bias over a large range, and varied directly with gas pressure (7, 8).

Emeleus (9) demonstrated the value of visual observations in a typical low voltage argon plasma in the micron pressure range. A sketch illustrating the major sectors follows:

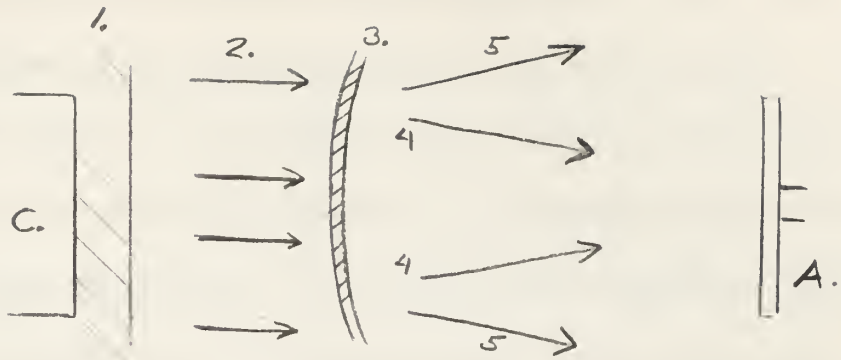


Fig. A. C, cathode; 1, cathode sheath, 2, primary beam; 3, meniscus, 4, 5, scattered beams; A, anode

Investigation of probe data during discharge studies by Easley (10) demonstrated the importance of probe cleanliness for accurate measurement technique.

Oleson and Found (11) have shown that nonlinear log plots of probe data were obtained in discharges with striations present.

It became increasingly evident that new methods of determining actual energy distributions in low pressure discharges was necessary since the assumption of a strictly Maxwellian energy distribution was not at all times valid. In 1939 Druyvesteyn (12) demonstrated that the electron energy distribution function, $N\phi(eV)$ could be found from the following formula:

$$N\phi(eV) = \frac{2}{Ae} \left(\frac{2m_e V_p}{e} \right)^{\frac{1}{2}} \frac{d^2 I_p}{dV_p^2}$$

Where $N\phi(eV)$ is the number of particles of energy per unit volume, and in this work in units of reciprocal electron volts and reciprocal cubic centimeters, i.e. $eV^{-1} cm^{-3}$; A is probe area, and m_e , e , I_p and V_p represent the quantities tabulated in the Table of Symbols and Abbreviations.

Waymouth (13) illustrated the utility of this expression for use in cases where departure from normally assumed energy distributions exists.

R. H. Sloane and E. I. R. MacGregor (14) and R. L. F. Boyd and N. D. Twiddy (15) utilized modifications of a suggestion by Emeleus for obtaining the energy distribution. It was shown that a small a-c signal on the probe would yield a D. C. increase directly proportional to the second derivative of the probe current-voltage relationship.

Boyd and Twiddy (15) also demonstrated that for a non-isotropic discharge a cylindrical probe will give an energy distribution which will attain negative values between major electron groups.

An R-F technique of determining plasma frequency was discovered by Takayama and Ihegumi (16) who found that if an R-F signal is superposed on a probe maintained negative to space potential that a marked resonant increase appears in probe circuit current at the Langmuir frequency

Allis (17) and D. W. Mahaffey (18) have correlated plasma oscillation growth and decreasing plasma density gradients. Mahaffey reported an eighty-five per cent correlation between these parameters in a micron pressure mercury arc discharge. Putman and Collins (19) in previous work with N. L. Oleson also demonstrated the connection of these parameters in a low pressure argon discharge wherein peak oscillation intensity occurred along a decreasing density gradient.

In 1949 Bohm and Gross (23) proposed a theory for plasma oscillations which postulated that a longitudinal traveling potential field could be excited by a beam of high velocity electrons in transit through the plasma. This in turn would provide a mechanism for energy transfer from

the beam to the plasma.

Looney and Brown (24), however, in attempting to utilize this mechanism by using a second beam of electrons were unable to find the predicted oscillations, but rather postulated that they had found standing waves in the plasma. They attributed these waves to interaction of the beam with large sheaths on the beam electrodes.

Demirkhanov, Gevorkov, and Popov (25) have shown that these oscillations can be produced as predicted, and have attributed the mechanism causing the effects found by Looney and Brown to secondary electrons ejected by the impinging beam on the anode. These secondary electrons oscillate in a potential well in front of the anode from which ejected.

G. D. Boyd, L. M. Field, and R. W. Gould (26) have also shown that this transit mechanism for electron plasma oscillations does occur and have succeeded in exciting them with a velocity modulated beam of electrons and have demonstrated that they grow in amplitude as they wave through the plasma.

I. Alexeff and R. V. Neidigh (27) in recent work at Oak Ridge National Laboratories have found correlations between acoustic theory and kilocycle oscillations in a spherical glass discharge tube. The predicted Langmuir electrostatic ion sound waves are believed to have been successfully observed with the following characteristics:

- a. Sinusoidal waveform.
- b. Higher frequency modes of oscillation not integral multiples of the fundamental theory (This is in agreement with the boundary conditions of acoustic

theory.

- c. Frequency proportional to $M_i^{-1/2}$.
- d. Frequency proportional to D^{-1} (D is tube diameter).
- e. Frequency yields a value for electron temperature (T_e)
in agreement with values obtained by the other methods.

3. Anomalies of Neon.

In extension of the continuing project of studies of low pressure gaseous discharge phenomena, it was suggested by Professor N. L. Oleson, that a Neon plasma be investigated, to further extend data in this field.

Prior to introducing Neon into this system Argon had been utilized for a test discharge and curves, as shown in Fig. 7, quite typical of those found by Putnam and Collins (19) for current-voltage characteristics were traced. Slightly higher values of current were found due to the larger surface area of the cathode presently installed.

The system was thoroughly baked twice at 350 degrees Centigrade and flushed with Neon twice prior to taking any tube characteristic curves and making a data run. After the second bake out and flushing, the system was evacuated to 2.7×10^{-7} mm. of (Hg). The system was then filled with 9.6 microns (Hg) of Neon at room temperature, and the cathode brought up to operating temperature. Pressure then stabilized at 10 microns.

It became immediately apparent upon taking the initial tube current-voltage characteristic curve that Neon was behaving considerably different in the same system than had Argon. Discharge currents were lower throughout the operating range for similar voltages, and severe instability occurred in the discharge at currents higher than 75 ma., at 10 microns pressure, and at lower currents at lower pressures. At currents below 30 ma. at 10 microns pressure violent relaxation oscillations occurred, Fig. 8, which sporadically would extinguish the discharge completely. Voltage had to then be increased until re-ionization occurred.

The relaxation oscillations were dampened as much as possible by placing a large resistance next to the cathode in the discharge current circuit, and a large capacitor across the tube itself. The values of these circuit elements were adjusted until an optimum damping effect was reached. The values used for these components were 5500 ohms and 10 microfarads.

The instability occurring at the higher current range could not, however, be diminished except by going to considerably higher pressures. At a pressure estimated at 50 microns - 70 microns it was possible to maintain a stable discharge up to 150 ma., however, since no accurate method was available of measuring this pressure, so that a return to the exact pressure could always be assured, it was decided to work in the more limited 10 micron range.

This high current discharge instability occurred in the following manner, and its threshold was always reproducible at ~ 75 ma. at 10 micron pressure. When 75 ma. was reached, the voltage would slowly climb from its initial value to about 60 volts, then it would jump almost instantaneously to 325 volts. The current would decrease in a similar manner, slowly at first then almost instantaneously to a value of 15 ma., a value below the thermionic emission current of the cathode in high vacuum (22 to 35 ma.). The discharge in this form appeared as a narrow beam in the center of the tube with an apparent focus, independent of anode-cathode spacing, at about 40mm. from the cathode. Fig. 9.

It was first thought that this might be due to the focusing effect of the slight cathode face curvature, however, when the anode was placed within

10 mm. of the cathode or less, the phenomena still occurred, so this hypothesis does not seem to be borne out. Further investigation of the literature revealed that Neon has been used extensively in slow sweep cathode ray tubes for "gas focusing" and is most effective in the 4 microns - 6 microns range, Cobine (20). The 4 microns - 6 microns range is where the most severe form of this instability occurred, which we termed a "collapsed discharge," and tube currents of 40 ma. to 50 ma. were the maximum which could be sustained without collapsing. It is therefore believed that this effect was the primary reason for this upper limit instability in the Neon plasma.

A cursory investigation by oscilloscope in this discharge form was remarkable for the absence of any oscillations and extremely low noise. The cavity wavemeter was also unable to detect any high frequency oscillations. Visual observations showed only a minor amount of the typical red glow associated with the normal Neon discharge illustrating low excitation and ionization occurring in this form.

Further search into the literature while investigating this phenomenon revealed some other anomalies of Neon which it is felt deserve attention.

It has been mentioned previously that lower currents were obtained throughout the current-voltage characteristic curves for Neon when compared with Argon. This at first seemed easily attributable to the higher ionization potential of Neon, 21.5 V, vice that of Argon, 15.7 V, however, it further became apparent that it was remarkable that such a comparable discharge did in fact occur at all.

Neon exhibits little Ramsauer-Townsend effect throughout a voltage range of 0 to 100 volts, and when compared with Argon its electron collision probability (P_t) is much smaller in our system's operating range.

Fig. B. from R. B. Brode (21) illustrates this effectively.

More explicitly, its relative ionization in comparison with Argon can be seen to be quite small as illustrated in Fig. C. from Von Engel (22).

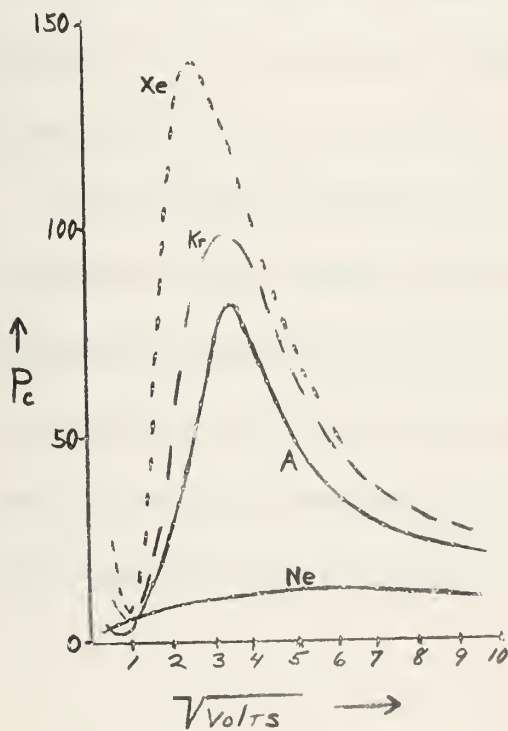


Fig. B. Probability of collision (P_c) in Ne, A, Kr, Xe.

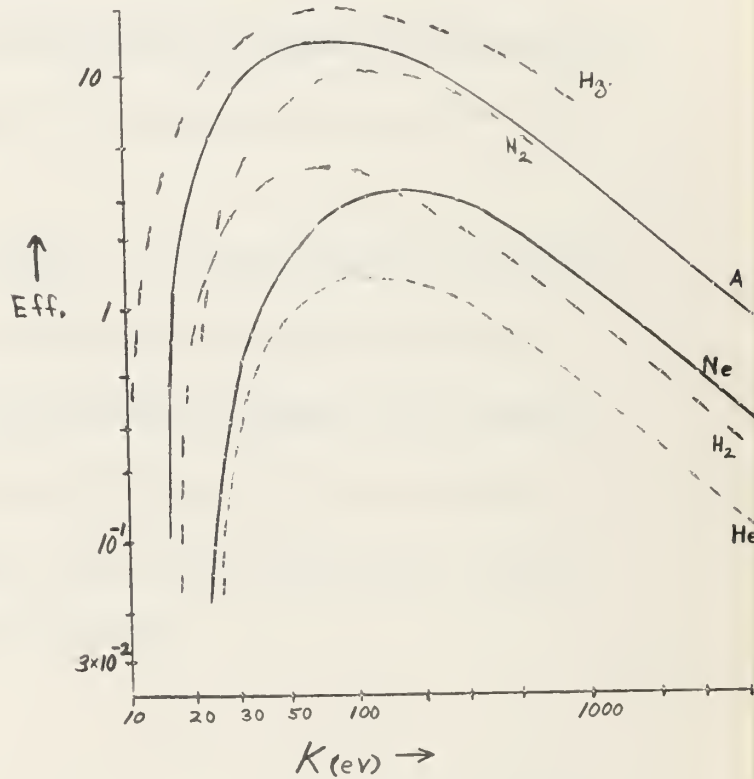


Fig. C. Ionization efficiency in various gases as a function of electron energy K .

and although this data was taken at 1 mm pressure, we believe an order of magnitude extrapolation to a lower pressure is consistent for comparison.

Also, the mean free path of an electron in Neon at a pressure of 10 microns is, from kinetic theory, 5.76 cm. a value which should be reasonably accurate since Neon having a tightly bound closed outer electron shell approaches the classic spherical atom. This would lead one to believe that

the ionization of Neon would be considerably dependent on the cathode-anode spacing of the discharge up to 5 cm. or so, and relatively independent at greater distances.

However, none of these effects were apparent in our discharge tube in the range expected. The currents as stated before were slightly lower than for Argon, but only by a factor of a few per cent at the most. The current and voltage were completely independent of cathode-anode spacing, as near as one could tell by reading a well calibrated milli-ammeter, for distances of 10 mm. to 100 mm.

We therefore conclude that ionization is occurring rapidly within a few millimeters of the cathode and that the plasma may exist because of its oscillations interaction with the electron beam immediately upon leaving the cathode. As discussed later in the conclusion of our investigation, oscillations were found up to at least 2 mm. of the cathode face, which would certainly tend to confirm this hypothesis.

4. Equipment.

Figs. 1 through 3 are photographs of the laboratory equipment arrangement. The equipment used in the experiment can be classed into four general headings:

1. Gaseous discharge tube
2. Vacuum system
3. Frequency detection and measuring equipment
4. D. C. electrical circuits.

Discharge Tube. The tube envelope was locally manufactured using Pyrex glass and salvaged tungsten-uranium glass seals. Tube design criterion was based upon having a sealed system which could be subjected to bake out and, at the same time, allow a maximum amount of variation in the geometrical parameters

The electrodes were all mounted on cylindrical iron cores sealed in pyrex to enable the electrodes to be moved within the tube by application of an external magnetic field.

Electrical leads to the electrodes were coiled multi-strand oxygen-free copper, insulated where necessary with ceramic beads. Attachment to the tungsten seals at both the tube and electrode seal was by means of spot-welded nickel straps.

The cathode was an indirectly heated dispenser type cathode supplied by Semicon of California, Incorporated. This cathode has an evaporation rate of one microgram per centimeter per hour and negligible sputtering. This gives the dispenser cathode considerable advantage over the conventional oxide coated cathode as regards tube contamination in this type of

work. The cathode was 28.5 millimeters long, 22.1 millimeters in diameter, and had a concave face with a radius of curvature of 36.7 millimeters. The heaters for the cathode were locally manufactured from 20 mil malleable tungsten wire wound into a coil of approximately 15 turns and 14.2 millimeters in diameter. To prevent shorting between adjacent turns, the cathode was lined with two close-fitting alumina rings and an alumina disk at the face (see Fig. 5). To obtain the operating temperature of 1075°C , required approximately 12.5 amperes. About one-half hour was needed to reach this temperature equilibrium.

The cathode was mounted to the transport by means of a molybdenum jacket spot welded to four tungsten support rods (see Fig. 5). The rear of the cathode was closed with molybdenum to minimize darkening of the tube by depositions of alumina and tungsten.

The anode was a 26 millimeter diameter, 20 mil thick nickel disk supported by a tungsten rod enclosed in a pyrex sheath.

The probes were constructed of 5 mil tungsten wire sheathed in pyrex to within 3.9 millimeters of the end. To prevent conduction on the surface of the glass due to contamination, the probe has a 5 mil stand off from the glass sheath (see Fig. 5). The double probe was not used due to breakage in the final stage of assembly.

Construction Problems. Early in the work, it was necessary to open the discharge tube due to an open cathode heater. This operation started a long chain of difficulties which terminated in a virtual re-building of the tube.

The original heaters were constructed of 10 turns of 15 mil tungsten with an overall diameter of 17 millimeters. These heaters were coated with

a thin alumina coating to prevent shorting between adjacent turns. Several of these heaters were used; however, it was found that their useful life was quite short. It appeared that at the temperatures required for operation, the alumina would flake off and adjacent turns would short as the heater sagged. The next attempt to solve the heater problem was to use an alumina support on the center leg of the heater to give some additional rigidity to the heater. Somewhat greater success was obtained with this configuration. While some shorting did occur, it did not appear to be progressive. Semicon of California donated the present cathode, which in its original configuration had its heater potted in cast alumina. This would seem to be an ideal configuration, but the structure appears to be extremely fragile, perhaps too fragile, for an experimental arrangement. After two failures with this configuration and upon consultation with Semicon, the configuration described in Fig. 5 was used.

In early attempts it was found that only very low emission currents could be obtained from the cathode. It was then discovered that the cathode was extremely sensitive to chloride poisoning, contamination by low vapor pressure metals, and contamination by water vapor and oxygen.

The majority of these contamination problems were solved by proper activation of the cathode. The chloride poisoning, however, was irreversible, destroying the usefulness of the cathode in general; if localized, it disturbed the emission in the vicinity of the poisoning.

Activation of the cathode should be attempted after bake out. The procedure is basically to bring the cathode to operating temperature (1100°C)

in a high vacuum $\sim 10^{-6}$ millimeters of Hg, and apply a potential from anode to cathode of approximately 500V. As the cathode becomes activated, a tube discharge current will be observed which will increase with time until activation is completed, at which time it will become constant. This procedure will require about two hours, depending upon the degree of cathode contamination.

As mentioned previously, chloride contamination results in permanent damage to the cathode. The migration of other metallic ions to the emitting surface may also produce permanent damage to the cathode. It is therefore necessary to keep low vapor pressure metals remote from the hot cathode. The materials recommended for cathode mounting are tungsten, tantalum, or molybdenum. Early attempts were made using a tantalum anode with the cathode heat shield and mounting of tantalum. On completion of bake out, it was noted that the tantalum anode was plated with a rather heavy coating of cupric, cuprous oxides and copper. The other tantalum surfaces were plated with a thin copper coating, in addition a powdery deposit of copper was found on the glass envelope (see Fig. 45, a, b, c). The only possible source for the copper was from the multi-strand copper wire. In view of these observations, it was postulated that the tantalum acts as a copper "getter" lowering the partial pressure of copper in the system, thereby permitting additional boil off of copper. If it were absolutely necessary to have copper and tantalum simultaneously in the system, this problem could possibly be minimized by an extremely slow bake out, always maintaining a vacuum in the order of 10^{-5} millimeters of Hg.

The final configuration utilized a nickel anode with all cathode mountings of molybdenum. A heat shield was not mounted. Mechanical joints were utilized wherever possible due to difficulty in welding molybdenum and tungsten even when using platinum as a "wetting" agent.

All copper leads were spot welded and supported with nickel straps. This procedure minimized the amount of heat applied to the copper wire and reduced the possibility of contamination from either silver solder or flux.

Vacuum System. The vacuum system was capable of a vacuum in the order of 10^{-7} millimeters of Hg and tested leak free with the Veeco MS-9 Helium leak detector which was capable of detecting leaks as small as 1×10^{-18} cubic centimeters per second. Pumping was done with a three stage air-cooled oil diffusion pump and mechanical fore-pump. The vacuum system was divided into two sections: "internal" discharge tube, and vacuum gauges; and the "external" oil manometer and gas bottles for neon and argon gas. The "internal" system was isolated from both the pumps and the "external" system by liquid nitrogen traps. All stopcocks were vacuum type lubricated by Type N Apiezon grease. The oil in both the manometer and diffusion pump was Octoil-S. The "internal" system was baked out by a portable oven, while the "external" system was baked out with heating tapes. The anode was out gassed by means of an induction heater.

Vacuum measurement in the high vacuum region 10^{-4} to 10^{-7} millimeters Hg was by means of a Veeco RG-75 ionization gauge. To measure micron range pressures, a modification was made to the Veeco Vacuum Gauge RG 31A by installing an additional range resistor to the circuit to provide a 10^{-3} millimeter scale. This additional resistor in the pressure

multiplier circuit extended the scale of the meter by serving as a meter shunt for the ion current from the RG 75 ionization gauge. This modification gave continuity when compared to the 10^{-4} millimeter scale. On the basis of the manufacturer's claim for the RG 75 tube of linearity to 10^{-3} , we assumed linearity for the 1-10 micron range.

A Westinghouse type 7903 high pressure ionization gauge was installed in the system, however, control circuit difficulties precluded its use during our work. This instrument operates in the range of from 1×10^{-5} to 5×10^{-1} millimeters of Hg and offers considerable utility for further work.

High Frequency Measurement. A cavity wave meter, Test set, Model AN/UPM 2, frequency range 80-1220 megacycles, was used to detect electron oscillation frequencies by capacitive coupling with a wire probe. The dc-signal from the detector crystal of the cavity wave meter was fed to a Hewlett-Packard Model 425 A dc micro-volt-ammeter. Currents as small as 10^{-12} amperes could be detected with this instrument.

In previous work concern had been expressed that at the frequencies of interest (k-mcs) range excessive attenuation of signal might occur due to the coiled leads from the probe and their path through the iron case of the transport. To investigate this problem, the probe assembly was removed from the tube and measurements taken to determine the losses. A signal was fed to the probe from a Hewlett-Packard 612 A frequency generator (450-1230 mcs) losses were measured through a detector crystal and a Hewlett-Packard 415 Standing Wave Ratio Meter for various configuration of the single probe the following results were noted.

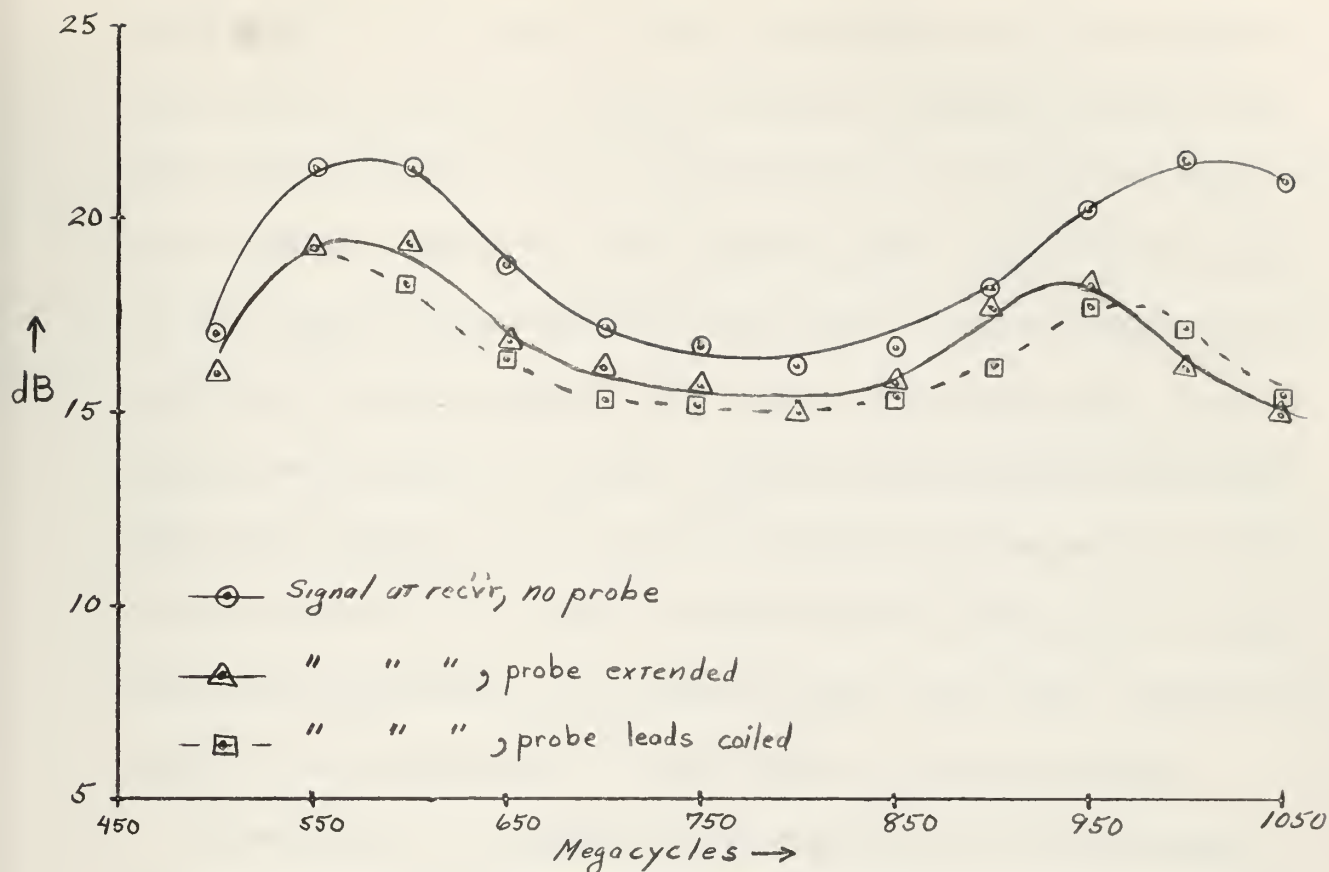


Fig. D. Probe Attenuation vs Frequency.

The characteristics for the double probe was far more complex and indicated quite high attenuation.

Ion oscillation were detected and measured with a Tektronix Type 543 oscilloscope.

The circuits for obtaining frequency data were simply coaxial lines from the probe to the wave meter in the case of electron oscillations, and to the oscilloscope through a 1000 cycle high pass filter for ion oscillations. The high pass filter was necessary due to a high background of electrical noise in the laboratory.

Probe Circuits. Two sources of power were available to the probe The time varying signal was supplied by a Hewlett Packard Low Frequency Function Generator, Model 202 A, which was set for triangle wave output

varying linearly with time. The output signal was set to 15 volts peak to peak excursion and fed to a gain ten amplifier in the Donner Analog Computer, Model 30¹ with problem board Model 30-6. The amplified signal was then biased by means of the initial condition power supplies of the computer. This signal was then supplied to the probe to obtain the desired positive and negative voltage excursions with respect to the anode. For a constant voltage power supply to the probe, two of the initial condition power supplies of the computer were connected in series and connected to the probe. This method was used to outgas the probe by ohmic heating prior to taking each probe characteristic. The voltage outputs of the initial condition amplifiers were calibrated with a Donner Model 50 Comparator Bridge.

Probe current as a function of probe potential was passed through a resistance on the order of 500 ohms where a voltage proportional to probe current was obtained. (The effect on probe potential due to voltage drop in the resistance is less than one per cent and considered negligible.) This voltage was fed through two gain ten amplifiers on the computers. The amplified signal was then supplied to the F. W. Mosely Autograph X-Y recorder Model 2-S² either: direct as I_p , $\frac{dI_p}{dV_p}$, $\frac{d^2I_p}{dV_p^2}$ or I^2 vs V_p .

¹The Donner Analog Computer, Model 30, has 10 operational amplifiers which operate in the range -100 to +100 volts with a long time stability better than 0.5% of full scale value, maximum drift characteristic of 4 millivolts per hour with a short term random drift less than ± 2 millivolts. Five initial condition regulated d.c. power supplies, 0 to 100 volts are available on the computer.

²The F.W. Mosely Autograph X-Y Recorder, Model 2-S which has a range on the horizontal axis of from 0-7.5 millivolts to 0-150 volts full scale. The vertical axis has a range of 0-5 millivolts to 0-100 volts full scale. Input impedances on both scales are in the order of 2 megohms. This equipment is accurate to 0.25% of full scale on all ranges when calibrated. Calibration drift is negligible.

The X-Y recorder was operating with a sweep period of 20 seconds. The derivatives were obtained by two cascade R-C differentiator circuits with a time constant of .025 seconds. The I_p^2 was obtained by supplying the amplified voltage signal to both the X and Y inputs of a Donner Electronic Function Multiplier, Model 33. This equipment would accept inputs of ± 100 volts in either or both X and Y inputs and produces an output of $-0.01 XY$. Use of this equipment was discontinued on the second run due to alignment difficulties at the last moment before the run.

5 Procedures

General Procedure. Prior to making a data run, the system was taken to as low a vacuum as possible, in the order of 10^{-5} millimeters of Hg, and then baked out with the portable oven at 350°C for a period of 10 to 15 hours. During this time, external tubing was heated to 350°C with heating tape. Upon completion of the bake out, vacuums in the range of 2×10^{-7} millimeters of Hg were obtainable. The next step was to bring the cathode to temperature with the pumps still on the system. Since it was found that the alumina in the cathode would absorb considerable amounts of gas, the following steps were taken: when the vacuum stabilized, the cathode heater was secured; after the cathode had cooled, a charge of neon was admitted to the system with the pump secured; the cathode was again brought to temperature and a discharge fired for from 15 minutes to one half hour, at which time the system was again pumped down to about 10^{-7} millimeters of Hg. This procedure of flushing and filling would be repeated two or three times to minimize the amount of foreign gas in the tube. The tube was again filled with neon and allowed to pump down to 9.2 microns as measured with the Veeco ionization gauge. While the absolute error of the Veeco gauge modification described on page 19 may be large, it is considered that the pressures are reproducible to within two-tenths of a micron.

Upon completion of the filling process, the cathode was brought to operating temperature and allowed to reach equilibrium. One-half to three-quarters of an hour were allowed for equilibrium to be achieved.

During this time, the electrodes were positioned with the cathetometer using the following procedure: the cathetometer was set at its reference value for the cathode. The cathode was then moved with the solenoid until its face was lined up with the reference mark of the cathetometer. The cathetometer was then traversed to the probe position and this distance recorded. Next the cathetometer was traversed to the desired anode position and the anode moved to coincide with the reference mark of the cathetometer. All measurements were made in the same direction to minimize backlash errors. These procedures should allow electrode placement accurate to within 0.1 millimeters. These same procedures were carried out, as applicable, for all subsequent electrode positioning.

A discharge was then obtained with the oscilloscope across the tube. The value of resistance in the tube power supply circuit and capacitance across the tube were varied to minimize relaxation oscillations as observed with the oscilloscope. The X-Y recorder was then put in the discharge circuit to record the tube characteristic, V_d as a function of I_d . With this information recorded, the X-Y recorder was placed back in the probe circuitry.

The procedures from this point on became repetitive for each of the desired probe positions and were as follows:

A. To observe ion oscillations, the anode was grounded, the oscilloscope lead was directly coupled to the probe and the shield grounded common with the anode. In the first data run, the frequency and amplitude of the ion oscillations were read directly from the scope display. During the second data run, all scope displays were photographed and analyzed

at a later time.

B. Next the cavity wave meter was capacitively coupled to the probe and a frequency search conducted. The deflection of the micro-micro ammeter at resonance from its ambient value was recorded as a measure of the electron oscillation amplitude. In many cases the deflections are very slight, a few per cent of the ambient current. It was therefore imperative that the search be conducted very slowly to prevent resonance dips from being masked by random meter fluctuations which were not reproducible.

C. The next step involved allowing the discharge circuit to float. At the same time, the probe circuitry which had been isolated from the discharge tube during frequency measurement, was then directly coupled to the probe. The output of the function generator was set for a triangle wave and adjusted to 15 volts peak to peak and fed to the X-axis of the X-Y recorder. The same signal was supplied to a nominal gain ten amplifier which was then calibrated to give a peak to peak excursion of 150 volts. This output was then biased by an initial condition power supply to, in the first run +43 to -107 volts and in the second run from +30 to -120 volts as measured between probe and anode. (See Fig 5)

The current drawn by the probe was passed through a resistance R_p to provide a voltage signal proportional to the probe current. This voltage signal was supplied to two gain ten amplifiers of the computer. The resistance R_p was adjusted to provide an output from the amplifiers of less than 100 volts, the maximum scale value for the Y axis of the X-Y recorder. The amplified voltage signal proportional to probe current was now plotted

as a function of probe potential. This same voltage signal was also fed through a pair of R-C differentiators in cascade. The outputs of this circuit were then plotted as $\frac{dI_p}{dV_p}$ and $\frac{d^2I_p}{dV_p^2}$ as a function of V_p . (See Fig. 6)

Prior to each data plot, the probe circuits were isolated from the probe and a voltage of approximately +125 volts was applied to the probe to outgas it by ohmic heating.

To allow for the differences in amplitude of the various signals, the calibrated scales of the X-Y recorder were changed, I_p vs V_p was plotted on 100 volts full scale and 10 volts full scale. The first derivative was plotted on 10 volts full scale, while the second derivative was plotted on 1 volt full scale. Attempts were made to use the 100 millivolt scale to enlarge the plot for the second derivative, but the response was quite noisy and did not appear to be reliable enough for use.

D. During the collection of probe data, the cathode temperature and heater current were monitored to keep the cathode within $\pm 5^\circ\text{C}$ of the selected operating temperature. Discharge voltage and current were recorded for each probe position. During the first run, discharge current was continuously recorded in order to determine the effect on discharge current of drawing probe current. No discernable effect was noted even for maximum values of probe current and its use was discontinued.

E. At the completion of data collection for each probe position, the electrodes were repositioned and the balancing of the amplifiers checked. The entire procedure for a single probe position required approximately twenty minutes.

F. At the completion of each run, it was necessary to calibrate the data curves. This was done by computing the current necessary to produce the given voltage across resistance R_p . The first derivative curves were calibrated by measuring the slope of I_p vs V_p curve at a voltage corresponding to a maximum of the first derivative. The same procedure was carried out on the first derivative to calibrate the second derivative. The calibrations thus obtained were then checked against other sections of the curves, a good correlation was obtained. These calibrations are considered to be accurate at the maximum values to within $\pm 5\%$ of the true value as represented on the plots.

Data Run I. The first data run consisted of an investigation of a 75 milliampere discharge in neon by taking data every two millimeters over a length of 40 millimeters. The data recorded on this run was I_p vs V_p , I_p^2 vs V_p , $\frac{dI_p}{dV_p}$ vs V_p , $\frac{d^2I_p}{dV_p^2}$ vs V_p , electron oscillation frequency and amplitude, ion oscillation frequency and amplitude for each of the 19 probe positions. The purpose of this investigation was to determine the character of a neon discharge and to determine regions of maximum interest for further investigation.

Data Run II. The second data run was taken in a 65 milliamper discharge and was set up primarily to determine the effect of a concave cathode face on the characteristics of the discharge, and to investigate the character of a discharge wherein the effects of Ramsauer free path are minimized, as in the case of neon. (See p. 12).

The program consisted of taking probe data with the probe at 5, 10, 15, 18, 21, 23, 28, 33, 35 millimeters from the cathode. For each of these

positions, the anode was to be located at 5, 20, 35, 50, 65 millimeters from the probe. The data recorded for this run was I_p vs V_p , $I_p \times 10$ vs V_p , $\frac{dI_p}{dV_p}$ vs V_p , $\frac{d^2I_p}{dV_p^2}$ vs V_p , electron oscillation frequency and amplitude, ion oscillation frequency and amplitude.

6. Results.

Tube current-voltage characteristics curves are shown for data runs 1 and 2 in Figs. 10 and 11. Both these runs were made at 10 microns pressure. Run 1 was conducted at 75 ma discharge current, and run 2 at 65 ma discharge current. A comparable curve for Argon is shown with that for Neon in Fig. 10. The various curves in Fig. 11 illustrate the absence of any effect due to increased anode-cathode separation from 10mm to 75mm. Only the general shape of these curves is reproducible since the power supply voltage was changed by hand. The difference between them is attributable to this factor. It was found that if the voltage was stopped at any point, the current would reach an equilibrium value independent of Cathode-Anode spacing.

The region of instability which eventually results in a collapsed discharge follows the rather short level section of the curve. The voltage rise in this part of the curve is clearly evident. A photograph of the relaxation oscillations occurring below 30 ma. is shown in Fig. 8., one of a collapsed discharge in Fig. 9.

Typical probe characteristic curves for run 1 are shown in Figs. 12, 13, 14, and 15. They are for probe positions near the cathode (Fig. 12), at the beginning of the region of maximum interaction (Fig. 13), within the region of maximum interaction (Fig. 15). Probe characteristics curves for run 2 with a fixed cathode-probe distance of 15.5mm and anode to probe distances of 5, 20, 35, 50, and 65 mm are shown in Figs. 16, 17, 18, 19 and 20 respectively. These illustrate the gradual decrease then the increase in length

of the high energy tails on that section of the second derivative giving the energy distribution of the randomized electron group, and the gradual decrease then the increase in size of that section representing the "beam" electrons. This result occurs as the anode-cathode distance is increased.

The second derivatives of I_p with respect to V_p are seen from these curves to approach zero more rapidly than they should. A changing slope may be seen on the curves representing the first derivative extending out to a considerably greater negative voltage than is indicated by the second derivative plot. Corrections made for this effect are discussed in our conclusions.

It was noticed from these curves, which were traced from a positive to negative probe voltage, that the inertia of the plotting arm of the X-Y recorder causes a shift to the right, or toward to more negative voltage, for both the first and second derivative plots. This is illustrated by comparing the location of the maximum value of slope of the I_p vs V_p curve with the maximum value of the first derivative, and the maximum value of the first derivative with the zero of the second derivative. A shift along the horizontal scale of minus 1 volt in each case is seen.

The character of the representative curve in the region of maximum interaction (Fig. 13) illustrated the effect of the strong oscillations occurring at this point on the first and second derivative plots.

Representative plots of space potential vs distance along discharge are shown in Figs. 21, 22, 23, and 24. Fig. 21 for the first data run shows the close agreement obtained between the zero of the $\frac{d^2 I_p}{dV_p^2}$, the maximum of

$\frac{dI_p}{dV_p}$, and the "first break" in the $\ln I_p$ vs V_p plot for probe curves taken in the most "Maxwellian" section of the discharge, on the anode side of the maximum interaction region.

Several electron energy distributions are shown in Figs. 25, 26 a and b, and 27. These were obtained by plotting $V_p^{1/2} \frac{d^2 I_p}{dV_p^2}$ vs probe retarding potential directly from the probe curves after correcting for space potential. The presence of the beam electrons at 45 to 50 volts energy is clearly seen in Fig. 25, a position 6 mm. from the cathode in run 1. Fig. 26 a and b illustrates the "smeared out" appearance of the distribution in the maximum interaction region, 30 mm. from the cathode, and Fig. 27 shows the randomized "near Maxwellian" distribution well past the interaction region 38 mm from the cathode. These latter two positions are also from run 1.

There is an absence in all these distributions of any intermediate or very high energy electron groups. One distribution from run 2 is included in Fig. 28. This was the only distribution which shows three distinct energy groups in a total of 64 probe positions in both runs.

Electron and ion densities are shown in Figs 29 a and b, 30, 31 and 32, for run 1, and three groups of 40 mm, 55 mm and 70 mm anode-cathode spacing from run 2, as a function of distance along the discharge. The plots show the densities predicted from frequency, the Druyvesteyn analysis, and the slopes of the positive ion I_p^2 vs V_p portion of the probe curve. The last method's results are shown in run 1 both corrected and uncorrected for the ratio of ion to electron temperatures, $\frac{T_i}{T_e}$.

The correlation between electron density and oscillation (or detector

current) intensity is shown in these figures wherein the density in this case is derived from the frequency detected. The maximum error in detected frequency is less than 2 megacycles in the general range of our operation with the AN/UPM2 cavity wave meter. The maximum error in detector intensity is ± 3 units of the various scales used. In general both of these are within the plotting circles on the graphical plots. A plot of density (derived from frequency) with space potential (V_{sp}) and electron temperature (T_e) is shown in Figs. 33, 34, 35, and 36.

Photographs of ion oscillations varying from 50 KC to 66.7 KC are shown in Figs. 37, 38, 39, 40, and 41 for run 2. A possible higher frequency component of 300K (is discernable superposed on the lower frequency traces. No ion oscillations near the upper limit predicted by Langmuir (about 2.3mc for our discharges) were detected. Plots of the ion oscillation amplitude vs distance are shown together with plots of electron oscillation intensity and density, in Figs. 42, 43, 45, for both runs 1 and 2.

Electron oscillations were detected throughout the discharge in all runs. The oscillation frequency in general varied from 700 megacycles near the cathode to a predominant 500 megacycle range throughout the rest of the tube. Usually a slightly higher frequency was found near the anode, and several other frequencies would appear sporadically on the anode side of the maximum interaction region. Possible explanation for these frequencies are covered in section 7 of this work.

A tabulated result of all frequencies detected in run 2 follows

| Cathode to probe (mm.) | Probe to Anode (mm.) | Electron Osc.Freq. Fe (mc) | Electron Osc.Amp. Ic amperes | Ion Osc. Freq.Fi (kc) | Ion Osc. Amp. Vi (mv) |
|------------------------------|----------------------------|----------------------------------|------------------------------------|-----------------------------|-----------------------------|
| 5 | 5 | 944.5 | 1.5×10^{-11} | - | - |
| 5 | 20 | 539 | 6×10^{-11} | 66.7 | 4 |
| - | - | 675 | 4×10^{-11} | - | - |
| 5 | 35 | 702 | 5×10^{-11} | 62.5 | 26 |
| 5 | 50 | 705.5 | 5×10^{-11} | 60.6 | 17 |
| 5 | 65 | 708 | 4×10^{-12} | - | 4 |
| 10.5 | 5 | 846 | 3×10^{-9} | 55.5 | 13 |
| - | - | 885 | 3×10^{-9} | - | - |
| 10.5 | 20 | 547.5 | 1.8×10^{-10} | 50.0 | 10 |
| - | - | 685.5 | 4×10^{-11} | - | - |
| 10.5 | 35 | none observed -- | - | - | 6 |
| 10.5 | 50 | 599 | 1×10^{-11} | 54.0 | 7 |
| 10.5 | 65 | 599 | 4×10^{-12} | 58.9 | 6.5 |
| 15.5 | 5 | 686.5 | 6×10^{-7} | 43.0 | 40 |
| - | - | 838 | 1×10^{-7} | - | - |
| 15.5 | 20 | 553.5 | 2×10^{-7} | 68.8 | 18 |
| - | - | 1010.5 | 2×10^{-8} | - | - |
| 15.5 | 35 | 546.5 | 1.5×10^{-7} | 54.0 | 21 |
| 15.5 | 50 | 523.5 | 4×10^{-9} | 58.9 | 6.5 |
| - | - | 590 | 5×10^{-10} | - | - |
| 15.5 | 65 | 591 | 2×10^{-11} | - | 8 |

| Cathode to probe (mm) | Probe to Anode (mm.) | Electron Osc.Freq Fe (mc) | Electron Osc.Amp. Ic Amperes | Ion Osc. Freq. Fi (kc) | Ion Osc. Amp Vi (mv) |
|------------------------------|----------------------------|---------------------------------|------------------------------------|------------------------------|----------------------------|
| 18 | 5 | 563 | 1×10^{-5} | 55.5 | 86 |
| - | - | 671 | 1×10^{-5} | - | - |
| 18 | 20 | 557 | 7×10^{-6} | 58.7 | 66 |
| 18 | 35 | 546.5 | 5×10^{-6} | 54.8 | 64 |
| 18 | 50 | 528 | 4×10^{-6} | 55.5 | 32 |
| 18 | 65 | 509 | 2.3×10^{-6} | 55.3 | 24 |
| 21 | 5 | 502 | 5×10^{-7} | 57.2 | 52 |
| 21 | 20 | 514.5 | 3×10^{-7} | 57.2 | 43 |
| 21 | 35 | 510.5 | 1×10^{-7} | 58.0 | 39 |
| 21 | 50 | 503 | 1×10^{-4} | 62.5 | 36 |
| 21 | 65 | 493 | 1×10^{-7} | - | - |
| - | - | 552 | 5×10^{-8} | - | - |
| 23 | 5 | 505 | 5×10^{-6} | 60.6 | 50 |
| 23 | 20 | 535 | 2×10^{-6} | 54.0 | 46 |
| 23 | 35 | 542 | 4×10^{-7} | 62.5 | 32 |
| 23 | 50 | 557 | 1×10^{-7} | - | 36 |
| 23 | 65 | 544 | 7×10^{-8} | 60.6 | 40 |
| 28 | 5 | 549 | 3×10^{-7} | 52.0 | 50 |
| 28 | 20 | 387 | 1×10^{-10} | 53.3 | 49 |
| - | - | 545 | 1×10^{-11} | - | - |
| 28 | 35 | 538 | 1×10^{-11} | 53.3 | 72 |

| Cathode to probe (mm.) | Probe to Anode (mm.) | Electron Osc.Freq. Fe (mc) | Electron Osc.Amp. Ic amperes | Ion Osc. Freq. Fi (kc) | Ion Osc. Amp. Vi (mv) |
|------------------------------|----------------------------|----------------------------------|------------------------------------|------------------------------|-----------------------------|
| 28 | 50 | 589.5 | 1×10^{-11} | 56.3 | 90 |
| - | - | 543 | 3×10^{-11} | - | - |
| 28 | 65 | 481.5 | 2×10^{-11} | 58.8 | 32 |
| - | - | 534 | 5×10^{-11} | - | - |
| 33 | 5 | 544.5 | 1.5×10^{-7} | 55.5 | 44 |
| 33 | 20 | 546.5 | 1×10^{-8} | 48.7 | 30 |
| 33 | 35 | 388.5 | 1×10^{-8} | 69.0 | 34 |
| - | - | 544.5 | 1×10^{-8} | - | - |
| 33 | 50 | 384 | 1×10^{-8} | 58.8 | 64 |
| 33 | 50 | 529 | 5×10^{-9} | - | - |
| 33 | 65 | 383 | 2×10^{-9} | 58.8 | 60 |
| - | - | 530 | 8×10^{-9} | - | - |
| 35 | 5 | 531 | 2×10^{-7} | 53.3 | 38 |
| 35 | 20 | 383 | 1×10^{-7} | 62.5 | 18 |
| - | - | 532 | 2×10^{-8} | - | - |
| 35 | 35 | 385 | 2×10^{-8} | 55.5 | 48 |
| - | - | 535 | 2×10^{-9} | - | - |
| 35 | 50 | 386.5 | 2×10^{-8} | 51.3 | - |
| - | - | 529 | 1×10^{-8} | - | - |
| 35 | 65 | 386.5 | 1×10^{-8} | 58.8 | - |
| - | - | 529 | 5×10^{-9} | - | - |

7. Interpretation of Results.

General

It was found in preliminary work that analyzing space potential, electron density, and temperatures by those methods of Langmuir which assume Maxwellian distribution of electron energies produced an extremely poor correlation with data obtained through the several other methods. In view of the general non-Maxwellian behavior of the electron energy distribution function, and the I_p vs V_p curves, it was decided to rely upon those methods of analysis which are not predicated upon a Maxwellian type distribution of electron energies.

Before introducing the data from our probe investigations of the discharge, its reduction, and our conclusions, we believe that some amplification of our statement concerning the existence of oscillations close to the cathode and the bearing of these oscillations on the maintenance of the plasma in Neon is in order.

We believe that these oscillations are connected with an early interaction of the beam electrons with the gas after they leave the cathode sheath. Classical kinetic theory, and experimental results of electron ionization efficiency, discussed in section 3 of this paper, predict a much lower ionization of the Neon than that which we have found in this region, and also predict a definite increase in ionization with increased cathode-anode spacing out to a distance equal to the mean free path. We found that this increase did not occur, and that a relatively constant value of plasma density existed throughout the discharge, differing by a factor of

three at the most.

It is believed that a mechanism described as follows may account for this.

The high energy electron beam emitted from the cathode will cause some ionization after leaving the cathode sheath. The beam will then continue to interact with this rarified plasma adding kinetic energy to the electrons and ions through the mechanism described by Bohm and Gross (23). This would have two effects, first prevent recombination of ion electron pairs, and second, cause increased ionization by the plasma electron-gas atom collisions taking place in the region. If true this would indicate that two complementing ionization mechanisms might occur in a gas, and help to explain the lack of oscillations found near the cathode by Putnam and Collins (19) in the Argon discharge. Argon would ionize far more readily due to the resonance effect (Raumsauer effect) near its ionization potential as seen in Figs B and C section 3, than does Neon. This rapid ionization due to electron collision, and Argon's increased mass over Neon, would mean that beam electrons traveling sufficiently close to an atom would cause more ionization by this collision effect and transfer less energy to the ions due to their traveling potential field effect. Also, the Argon plasma electrons in this region may not be able to gain large amplitude oscillations since they can more readily ionize their nearest neighbor atoms than in the corresponding case of Neon.

Another factor entering into the absence of these oscillations in Argon could well be our extreme good fortune in capacitively coupling our wave-

meter to probe. We were able, after many tries, to find an extremely sensitive coupling which allowed us to detect oscillation amplitudes down to 10^{-12} amps in detector current. These frequencies near the cathode were always very weak (10^{-11} amps) and a small change in coupling impedance could easily have prevented their detection.

Probe Characteristic Curves.

It is noted in inspection of the probe characteristic curves that the relative density of the energy distributions changes with increased anode cathode separation for a single probe position with respect to the cathode. In fact as seen in Fig. 48, the high energy beam group increases, after a gradual decrease, with increased separation as does the randomized plasma electron group.

We conclude from these effects that two mechanisms are occurring. The first which yields our initial high density with the anode close to the probe is the emission of secondary electrons caused by the beam impinging on the anode. Moving the anode away from the probe would cause the effect of these secondaries to decrease, since they are trapped in space within a few millimeters of the anode (25).

The second mechanism which would cause the significant increase of these groups as the anode is moved farther from the cathode is not at all clear. We have several hypothesis and they are:

1. Possible convergence of peripheral beam electrons toward center of discharge as anode is moved further away

2. Possible influence of field lines of concave surface of cathode causing a slight focusing effect on beam when anode spacing is large.
3. A high positive space charge found 20 to 30 mm from cathode in plasma may tend to attract peripheral beam electrons toward the center of the discharge. Fig. 21 illustrates an example of this charge and its location in the plasma.

From the appearance of the probe curves in the region of maximum interaction as illustrated in Fig. 13, the difficulty of extracting information about electron energy distributions in this area becomes apparent. The effect of the beam plasma interaction on the second derivative of I_p with respect to V_p is so large, that no absolutely valid information could be taken by the Druyvesteyn method in this region. In all figures showing data plots where this effect occurred we have shown cross hatched areas. It is noted that in general it is these regions where our data correlation is poorest. In other areas we believe the correlation to be quite good. The example probe characteristic curve shown in Fig. 13 is the most severe example of this disturbance. It was quite reproducible, and it can be seen that the second derivative was traced three separate times. The disturbance is also apparent on inspection of the I_p vs V_p and $\frac{dI_p}{dV_p}$ vs V_p curves.

Electron Energy Distributions.

An analysis of the electron energy distribution was carried out using the method of Druyvesteyn (12). The product of $V_p^{1/2} \frac{d^2 I_p}{dV_p^2}$ was plotted against V_p to obtain the shape of the energy distribution function. The area

under this curve could then be interpreted as the electron density by numerical integration where

$$N\phi(\text{eV}) = \frac{2}{Ae} \left(\frac{2me}{e}\right)^{\frac{1}{2}} V_p^{\frac{1}{2}} \frac{d^2 I_p}{dV_p^2}$$

where N = electron density in electrons/cm³ -eV

A = area of probe

For our situation it was determined that

$$N\phi(\text{eV}) = 2.72 \times 10^{13} V_p^{\frac{1}{2}} \frac{d^2 I_p}{dV_p^2} \quad \text{and} \quad N = \int N\phi(\text{eV}) d(\text{eV})$$

for all regions where the second derivative has positive finite value. The results of this procedure produced electron densities which were in error, when compared with the densities obtained by the relationship $N = \left(\frac{f}{8980}\right)^2$, by a factor of about 1.5 when compared at all points. Upon further inspection of the probe characteristics curves, it became apparent that not all electron energies were being included in the energy distribution. By inspection of the $\frac{dI_p}{dV_p}$ vs V_p curves (Figs. 12 through 20), it can be seen that there is a recognizable slope which extends out to approximately -65 volts. At the same time, it can be seen that the effect of this slope does not indicate in the plot of the second derivative of current with respect to voltage. We therefore concluded that perhaps a relatively large number of electrons which should have been included in our energy distribution had been missed. To obtain an approximation to the magnitude of this loss, we assumed that the trailing edge of the energy distribution (Fig. 27) from the

last readable value obtained from second derivative would continue out as a straight line to zero at -65 electron volts energy, rather than to where the second derivative had appeared to have gone to zero. This operation increased the value of the electron density by a factor of about 1.4. Having established why our electron densities were in error and realizing that this method of correction left a great deal to be desired due to the small magnitude of the effects as plotted, we decided to apply a constant correction for what we felt was the mean distribution of missing electron energies.

This correction was obtained by picking four densities obtained from $n = \left(\frac{f}{8980}\right)^2$ and comparing them to $n = k \int v^{1/2} \frac{d^2 I_p}{dv^2}$, where k is to be our empirically arrived at constant. This gave us a value for k of 4.4×10^{13} and n was then considered to be $n = 4.4 \times 10^{13} \int v^{1/2} \frac{d^2 I_p}{dv^2}$. When this correction was applied to the remaining 37 energy distributions, a good correlation was obtained as noted in Figs. 29a, 30, 31, and 32. It can also be seen in these figures that the correlation is poorest in the region of maximum interaction where the second derivative of current with respect to voltage becomes difficult if not impossible to evaluate (see Figs. 13 and 14).

Plasma density was also obtained from an analysis of the positive ion region of the probe characteristics curves by the method of Langmuir (\pm). Ion densities are obtained from the relationship:

$$n_i^2 = -\frac{\pi^2 m_i}{2e^3 A} \frac{d(I_p^2)}{dV_p}$$

where n_i = ion density in ions/cm³

A = probe area in cm²

m_i = mass of ion

This analysis of the positive ion region does not assume a Maxwellian energy distribution as does the similar Langmuir method for finding electron density by the slope of the I_p^2 vs V_p curve in the electron region of the curve. The required slopes were obtained by squaring the values of I_p for every five volts V_p for the linear positive ion portion of the I_p vs V_p curves. When the ion densities were computed by this method, they were found to be about three times greater than the densities obtained by Druyvesteyn analysis and from the relationship $n = \left(\frac{f}{8980}\right)^2$ (Fig. 29a). L. S. Hall (28) has postulated a proportionality factor for the Langmuir relationship which is "expected to be in the order of $\frac{T_i}{T_e}$ ". We made attempts to bring our ion densities into better agreement with electron density by applying this proportionality factor "in the order of $\frac{T_i}{T_e}$ ". In computing the correction, we used for T_e the mean energy of the randomized plasma electrons. For T_i , we assumed a constant ion temperature across the discharge of 1000°K, which seemed reasonable for our discharge. The next step was to correlate n (electrons) = $\sqrt{\frac{k T_i}{T_e}} n_i$ where for a best fit $k = 3$. This produced a relationship n (corrected) = $\sqrt{\frac{3 T_i}{T_e}} n_i$. When this correction was applied to all of the data points of run one and two, Figs. 29a, 30, 31, and 32 resulted.

It was considered significant that the agreement obtained between this method and the Druyvesteyn analysis agreed both in shape and magnitude, though showing some deviation from the densities obtained from $n = \frac{f}{8980}$.²

It was further considered significant that this correction removed the major fluctuation in ion density in the region of the anode. It was noted that the agreement was poorest in the region of maximum interaction as might be expected.

To further investigate the proportionality factor, we analyzed the data of Putnam and Collins (19) which had also shown an ion density considerably higher than the electron density in Argon. Using the same technique and assumptions, we were able to obtain the same sort of correlation

described above by using a correction formula, $n \text{ (corrected)} = \sqrt{\frac{12 T_i}{T_e}} n_i$.¹

Space Potential vs Distance.

The plot of space potential vs distance for run 1 with a constant anode-cathode spacing of 40 mm shows an interesting effect which we corroborated by three separate methods. The data was taken from the zero of the second derivative of I_p with respect to V_p , the maximum value of the first derivative of I_p with respect to V_p , and the first break from linearity of the $\ln I_p$ vs V_p curve. The latter method, as stated previously, is not to be relied on too heavily because of our non-Maxwellian electron energies, however, the gross effect of an increasing space potential some 10 mm away from the anode is quite apparent. In the most Maxwellian section of the discharge, i.e., on the anode side of the maximum interaction region, we find close agreement between all three methods of determining the space potentials.

¹Note, it might be significant that $\sqrt{\frac{12 T_i}{T_e}} = 2\sqrt{\frac{3 T_i}{T_e}}$ and that atomic weight of A is twice that of Ne.

We have therefore decided to rely most heavily on the zero of the second derivative for our absolute value of space potential² in all runs, and only this value was plotted for our 40 mm, 55 mm, and 70 mm (anode cathode spacing) groups from run two.

Unhappily in these runs (which were actually a collection of data from our investigation of the effects of various anode cathode spacings with a fixed cathode probe distance) we have few probe positions. However, we believe that the effect of increasing space potential some 30 mm from the cathode may be indicated in them. There is a slight but definite increase in the second 40 mm group and the 55 mm group in Figs. 22 and 23.

We are far from being positive about what causes this positive space charge effect, however, we postulate three mechanism which could account for it.

First, the cathode face curvature may result in some "bunching" of field lines in this area causing the ions to remain there, whereas the more mobile, more energetic electrons could escape.

Second, the ion focusing effect of neon, mentioned in section 3, may be at a maximum in this area, causing the ions to collect in the region.

Third, the beam electrons which have been randomized in direction in the maximum interaction region may be leaving this area toward the Tube walls as the "electron cloud" drifts down the tube toward the anode with

²This method was brought to our attention by Professor K. G. Emeleus of Queens University, Belfast, Ireland, who very kindly allowed us to view an as yet unpublished thesis of A. Garscadden during a visit to our laboratory.

the normal electron drift velocity of the discharge

Electron Oscillations.

The correlation between electron oscillation amplitude (from detector current intensity) and electron densities as illustrated in Figs. 33, 34, 35 and 36, we believe to be extremely significant. Fig. 33 illustrates an almost mirror image effect between these two parameters. Figs 34, 35 and 36 also show remarkably good correlation, and we feel that these are of special value in corroborating this effect since they are taken from a collection of discharges with the same cathode-anode spacing, discharge current, and pressure, but over a period of several hours with two complete changes of gas in our system.

This effect agrees with the theory that these oscillations should grow traveling down a decreasing plasma density gradient. Putnam and Collins (19) also found this effect as did Mahaffey, et al (18). However, Mahaffey's group believed that many of the small intensity changes in this data might be due to a "frequency pulling effect" of the probe. Since Demirkhanov, Gevorkov, and Popov (25) were able to correlate many of their frequencies detected by probe, with signals detected by receiving equipment using an antennae outside their discharge tube, we believe that our frequencies detected through the probe are correct, and hence the densities obtained from them through the relation $n = \left(\frac{f}{8980}\right)^2$ are accurate.

It should be noted that the intensity values are plotted on a rough logarithmic scale, and that small decreasing density changes yield very large changes in oscillation intensity. We conclude, therefore, that the

oscillations do start on peak plasma densities and grow rapidly down the decreasing density gradient, and that minor density changes have large effects on increasing and decreasing the amplitude of these oscillations.

We have also found, as illustrated in Figs. 33, 34, 35, and 36, that the plasma density follows quite well the average electron temperature (plotted in electron volts) as calculated from the energies described by our distribution function. This result is to be expected, because the areas of higher electron energy should be able to maintain a more dense plasma. The higher energy electrons will have less chance of ion-electron recombinations and aid in ionizing neutral atoms in this region.

The result in turn gives us further evidence for the accuracy of our Druyvesteyn analysis of electron energy distributions, since we used this to predict our average energy, whereas the densities which are correlated with these energies come directly from the detected frequencies.

The method used to determine these energies was basically a numerical integration of the electron distribution function in the following manner:

$$\langle \bar{eV} \rangle = \frac{\int V_p N \phi(eV) d(eV)}{\int N \phi(eV) d(eV)} .$$

Electron oscillations were found, as tabulated in section 6 for run 2, to extend from cathode to anode in both data runs 1 and 2. The increase in frequency found near the anode we attribute to the increased density of electrons resulting from secondary emission from the anode. Even very low energy electrons have a considerable secondary emission effect on

nickel (the anode material)³, and the range of this effect agrees quite well with what would be necessary to produce the increased frequency in this region. The previously mentioned positive space charge on the anode side of our maximum interaction region would aid in removing these electrons from the anode upon their emission.

Ion Oscillations.

Ion oscillations were also found throughout the tube, and they were seen to peak in amplitude with the electron oscillation intensity. Photographs of these oscillations show this effect (Figs. 37, 38, 39, 40, and 41) as does the plot of oscillation intensity illustrated in Figs. 42, 43, 44, and 45. The amplitude of the ion oscillations, although peaking with the amplitude of the electron oscillations, shows none of the minor variations which in the case of the electron oscillations are attributed to increasing and decreasing density changes.

No ion oscillations were found in the 2.3 megacycle range as predicted by the Langmuir relationship $f_i = f_e \left(\frac{M_e}{M_i} \right)^{1/2}$. All oscillations detected were of a much lower frequency, and we believe that these are the electrostatic sound waves predicted by Langmuir and Tonks (29).

Using this assumption we investigated the boundary conditions on our plasma column in order to infer what mode of longitudinal oscillation might be expected. A visual inspection demonstrated that the most

³H.S.W. Massey and E.H.S. Burhop, Electron and Ion Impact Phenomena, Clarendon Press (1952) Chapter V of this text gives a comprehensive discussion of this phenomena. The curves for Copper having a value of maximum emission coefficient similar to Nickel, p. 306, illustrates the small but finite emission which may be expected from primaries of 40 volts and below.

probable situation was that of a free boundary surrounding the plasma on all sides. The glowing plasma column was surrounded by a dark space approximately one centimeter thick between itself and the tube walls. This space we believe consists primarily of neutral atoms within which ion-electron recombinations are occurring

Simple acoustic analogy (30) indicates a longitudinal mode of vibration for this boundary condition wherein the frequency is related to the length of the vibrating column by the expression:

$$f = \frac{nc}{2l} \quad \left(\frac{n}{2l} = \frac{1}{\lambda} \right)$$

where f is frequency, n an integer, c the wave velocity, and l the column length. Langmuir and Tonks predicted a wave velocity on the order of $c = \sqrt{\frac{\Upsilon k T_e}{M_i}}$ and when this expression is introduced into the frequency equation the results are:

$$f = \frac{n}{2l} \sqrt{\frac{\Upsilon k T_e}{M_i}}$$

The above expression was used to predict frequencies from data runs 1 and 2, and the following assumptions were made.

- a. $n = 2$; since Langmuir indicated a low frequency cutoff wherein λ was on the order of the discharge tube dimensions.
- b. $l = 9$ cm; the approximate length of our plasma column.
- c. $\Upsilon = 5/3$; as used by Alexeff and Neidigh (27)
- d. kT_e ; Boltzman's constant x electron temperature, the value used was actually the average value of (eV) converted to ergs at the location where ion oscillations were a maximum. For run 1, (eV)

= 9 electron volts, for run 2 (eV) = 6 electron volts.

Utilizing these assumptions in the equation, with the appropriate value of the electron temperature for each run, gave the following results.

$$C_{run 1} = \sqrt{\frac{\gamma k T_e}{m_i}} = \sqrt{\frac{1.67 \times 14.4 \times 10^{-12} \text{ ergs}}{3.35 \times 10^{-23} \text{ gms}}} = 8.46 \times 10^5 \text{ cm/sec}$$

$$f_{run 1} = \frac{8.46 \times 10^5 \text{ cm/sec}}{9 \text{ cm}} = \sim 94 \text{ kilocycles}$$

$$C_{run 2} = \sqrt{\frac{\gamma k T_e}{m_i}} = \sqrt{\frac{1.67 \times 9.6 \times 10^{-12} \text{ ergs}}{3.35 \times 10^{-23} \text{ gms}}} = 6.91 \times 10^5 \text{ cm/sec}$$

$$f_{run 2} = \frac{6.91 \times 10^5 \text{ cm/sec}}{9 \text{ cm}} = \sim 75 \text{ kilocycles}$$

We feel that these values agree reasonably well with the predominant frequencies detected in run 1 of ~ 100 KC, and those detected in run 2 of $\sim 60 - 67$ KC.

8. Conclusions.

In general, it is our belief that the following conclusions may be drawn from our work.

First, the mechanism of oscillation generation does occur quite close to the cathode in our type of discharge tube, and may be dependent upon several factors. These factors are: the mass of the gas ion, the ionization probability of the atom, the ionization potential of the atom, and the plasma density in this region.

In neon, wherever we placed the probe, we detected oscillations which correlated with the predicted Langmuir frequency of $f = 8980 n^{1/2}$. In Argon and other gases, however, these oscillations have been considerably more localized, usually in the vicinity of the meniscus or maximum beam-plasma interaction region.

We postulate that the lighter mass of the neon atom, its low ionization probability, and its higher ionization potential allows the plasma electrons and ions near the cathode to oscillate with greater amplitude than in the case of such gases as Argon, where, in this region, the electrons, in gaining a few volts of energy, would soon cause other ionizations rather than continue to oscillate and increase in amplitude of oscillation. Thus, although oscillations would occur in this region, they would tend not to grow in amplitude, and be extremely weak in intensity. Even in Neon, our weakest signal was in this region and was of the order of 10^{-11} amperes.

It would be expected that once the beam electrons became randomized with the plasma in the maximum interaction region that these effects would be minimized allowing detectable oscillations in all gases, since all the plasma electrons have a much greater average energy and would remain in an oscillating state in the ion matrix.

The mechanism of interaction itself we believe to be that predicted by Bohm and Gross, wherein a traveling potential field is set up by the beam in transit through the plasma.

Second, at the face or cathode side of the maximum interaction region, we see in our discharge complete randomization of the electron beam with the plasma. We call it the "brick wall effect" since it appears as if the beam electrons are suddenly stopped in their transit of the tube and scattered isotropically. The intensity of oscillations in this region and further on in the interaction region reached values of 10^{-4} amperes of detector current rather than the 10^{-7} and 10^{-11} amperes elsewhere in the discharge. We postulate that these violent oscillations and their associated micro-fields are literally breaking up the directed beam.

Third, we believe we have shown that plasma densities derived from slopes of the ion portion of the curve do indeed need to be corrected by some function of $\frac{T_1}{T_e}$. The gross correction we made to our own data and that of Putnam and Collins' work in Argon illustrated that reasonably good correlation with densities predicted from other methods could be obtained. Also, in the region where ion oscillations were most intense, and ion energies greatest, use of our assumed correction factor based on our

average ion temperature, showed the poorest correlation with other densities determined.

Fourth, the ion oscillations which we detected and photographed, we conclude are the electrostatic sound waves predicted by Langmuir. They agree well with his predictions and appear to be related by wave length to the longitudinal dimensions of our plasma column

Fifth, we have found that in neon the anode-cathode spacing has little effect on frequency once the anode is sufficiently far from the cathode that beam electrons do not emit copious quantities of secondary electrons. We do not know why the high energy beam electron group seems to grow with very large spacing but we have postulated three hypothesis in the preceding section.

Sixth, we believe our high current instability effect as discussed in section three is due to ion focusing of the electron beam. It is an extremely quiescent discharge with no detectable ion or electron oscillations occurring. We have recently put Argon in our tube and were able to draw up to 700 milliamperes without the discharge collapsing, so we now believe even more firmly that this effect is an anomaly of neon.

Seventh, and possibly the most important, we believe we have definitely confirmed the violent growth in amplitude of the electron oscillations on a decreasing plasma density gradient. Even the fine structure of the curves show this effect, and we feel it is predominantly real rather than a probe-plasma interaction.

9. Recommendations .

In keeping with our observations and results, the following areas are recommended for further investigation:

a. Continue this type of investigation in other gases in an attempt to determine whether ion mass and ionization potential are major factors in establishing the intensity of electron and ion oscillations and their location in the discharge. An investigation of discharges at similar currents, pressures, and anode cathode separation using He, Ne, Ar, Kr, Xe, and mixtures of these should prove definitive in this investigation.

b. As an adjunct of the investigation recommended above, additional information should be obtained regarding the possible ion mass dependence on the form of the T_i/T_e correction to the ion densities obtained by analysis of the positive ion region of the probe characteristics curve.

c. Further investigation should be made of the low frequencies found in the kilocycle range to determine if they are longitudinal ion oscillations as supposed, radial modes of vibration, or a coupled oscillation which might be a function of both sides.

d. Additional techniques which are recommended include: use of a high sensitivity UHF receiver to be used in an attempt to detect oscillations external to the discharge, and addition of a spectrographic analysis capability which will be extremely important, if mixed gases are used.



Fig. 1. General experiment equipment arrangement

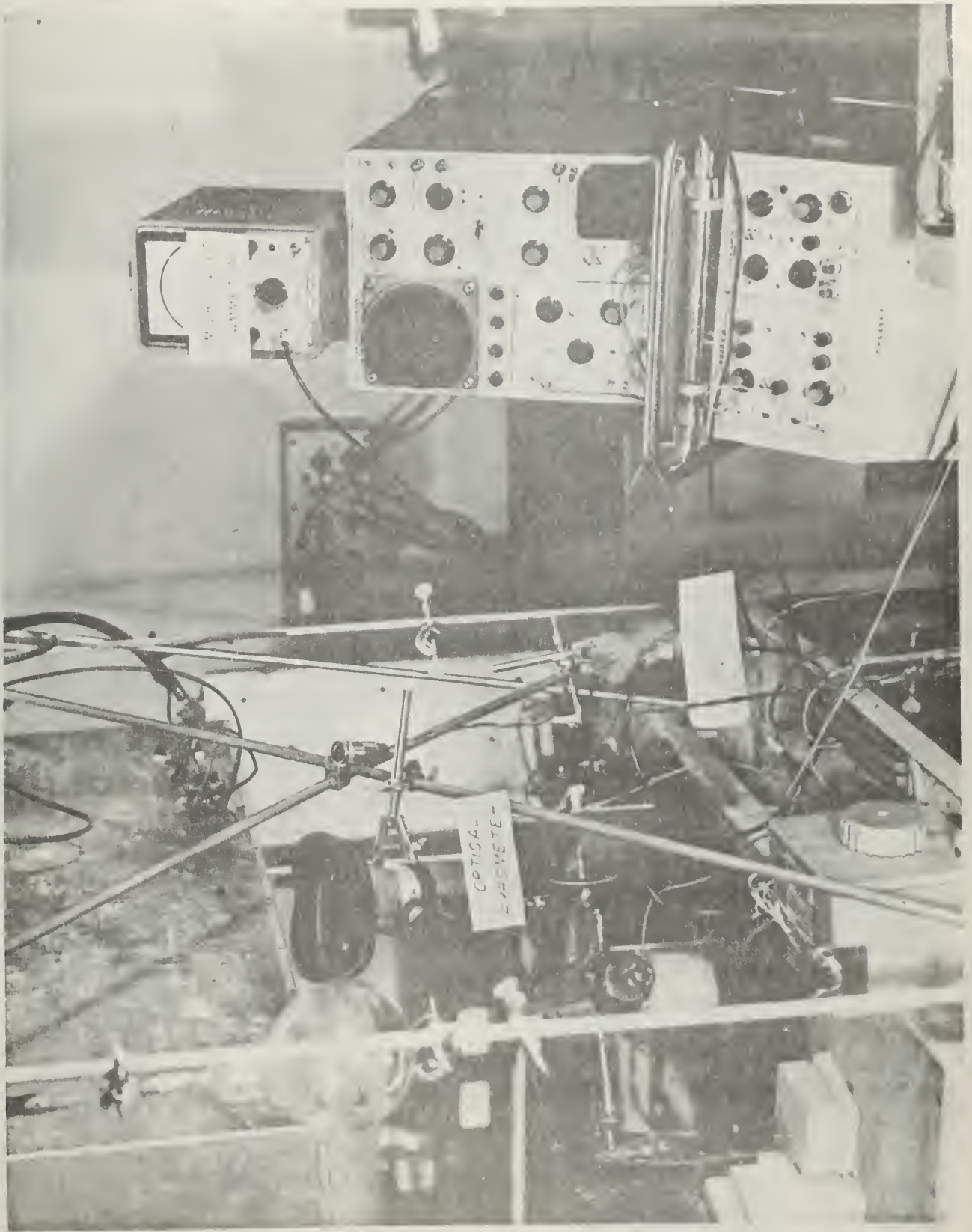


Fig. 2. Frequency detection equipment



Fig. 3. Probe circuitry

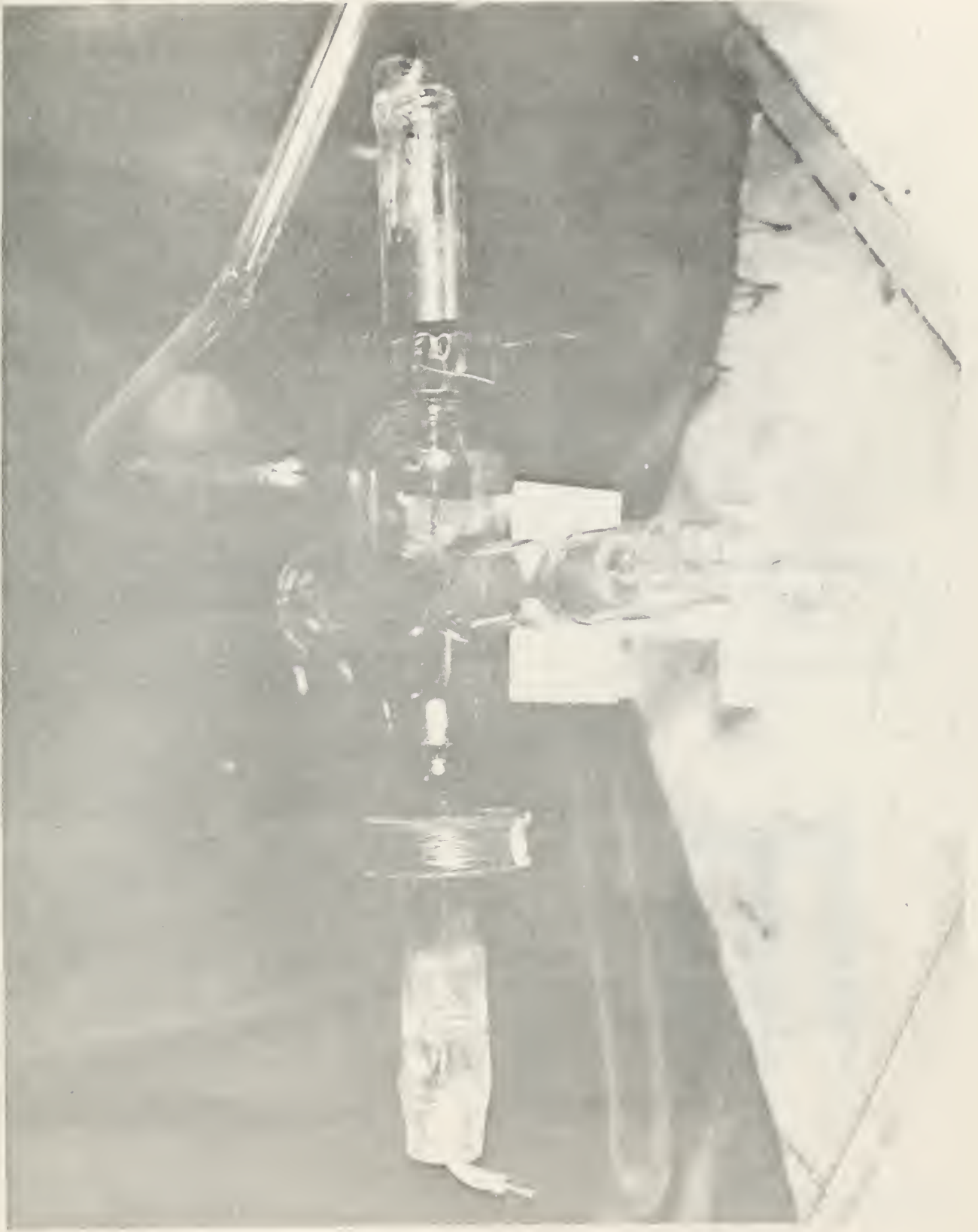
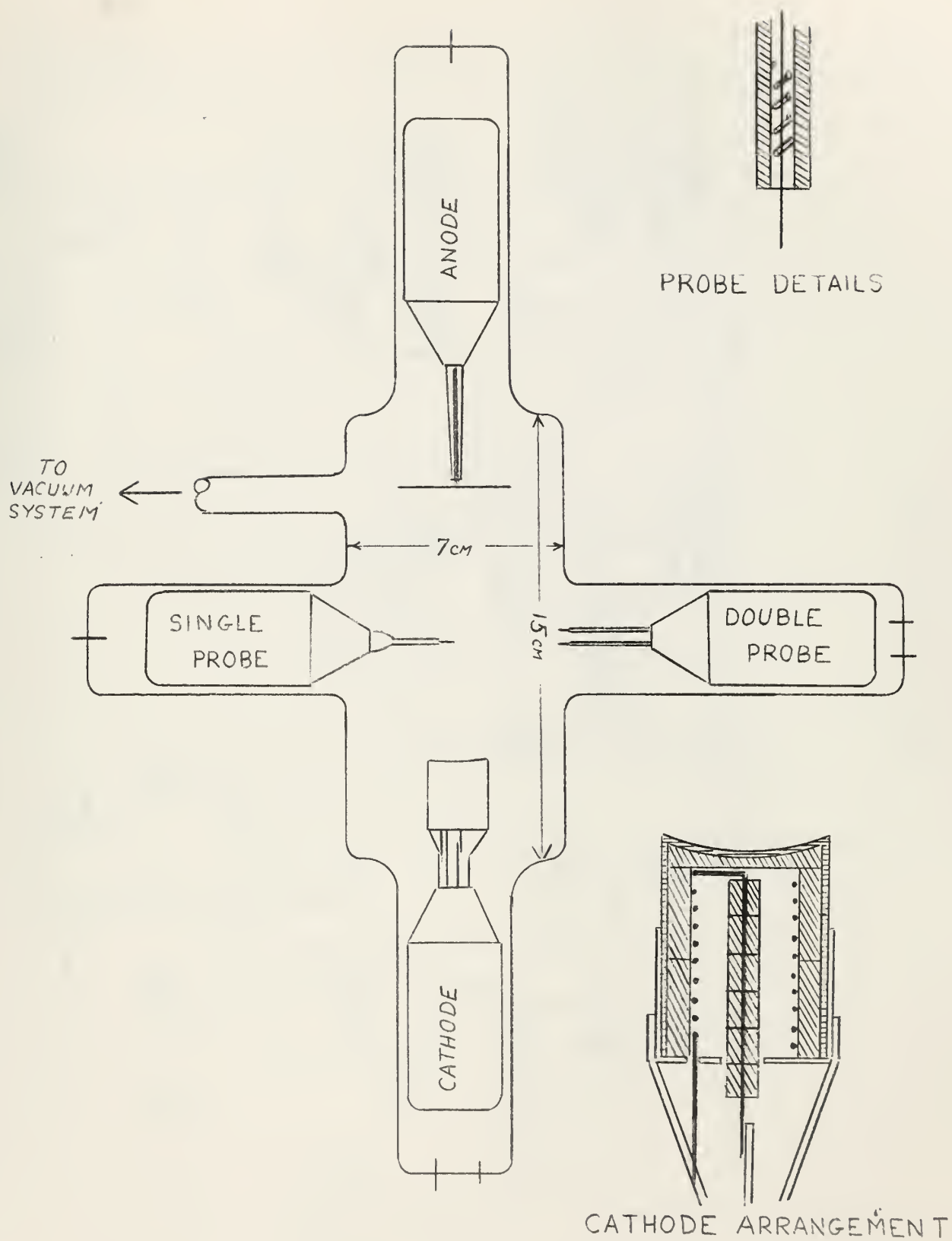


Fig. 4. Discharge tube.



TUBE DETAIL (NOT TO SCALE)

Fig. 5.

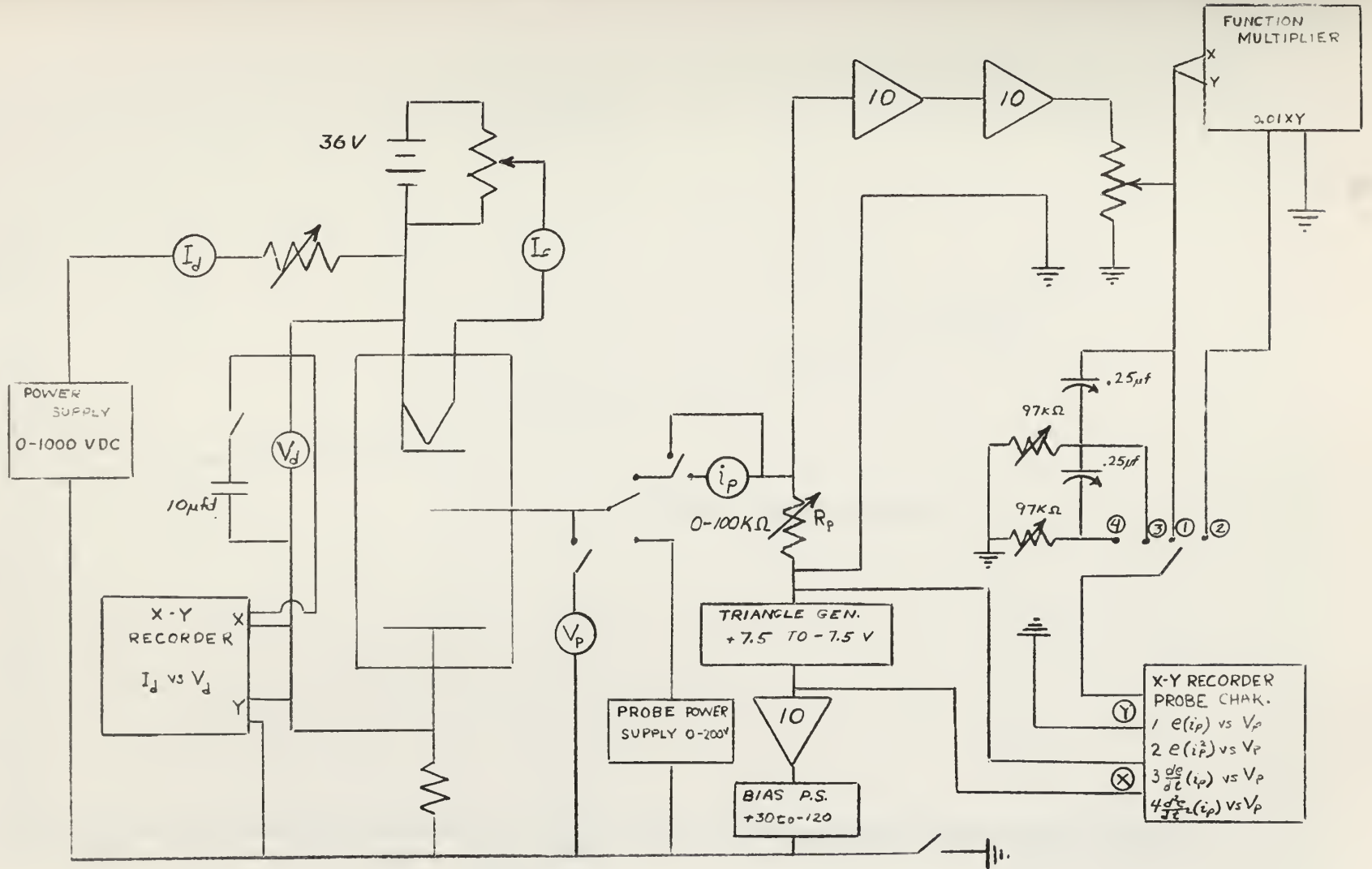


Fig. 6. D. C. Circuitry

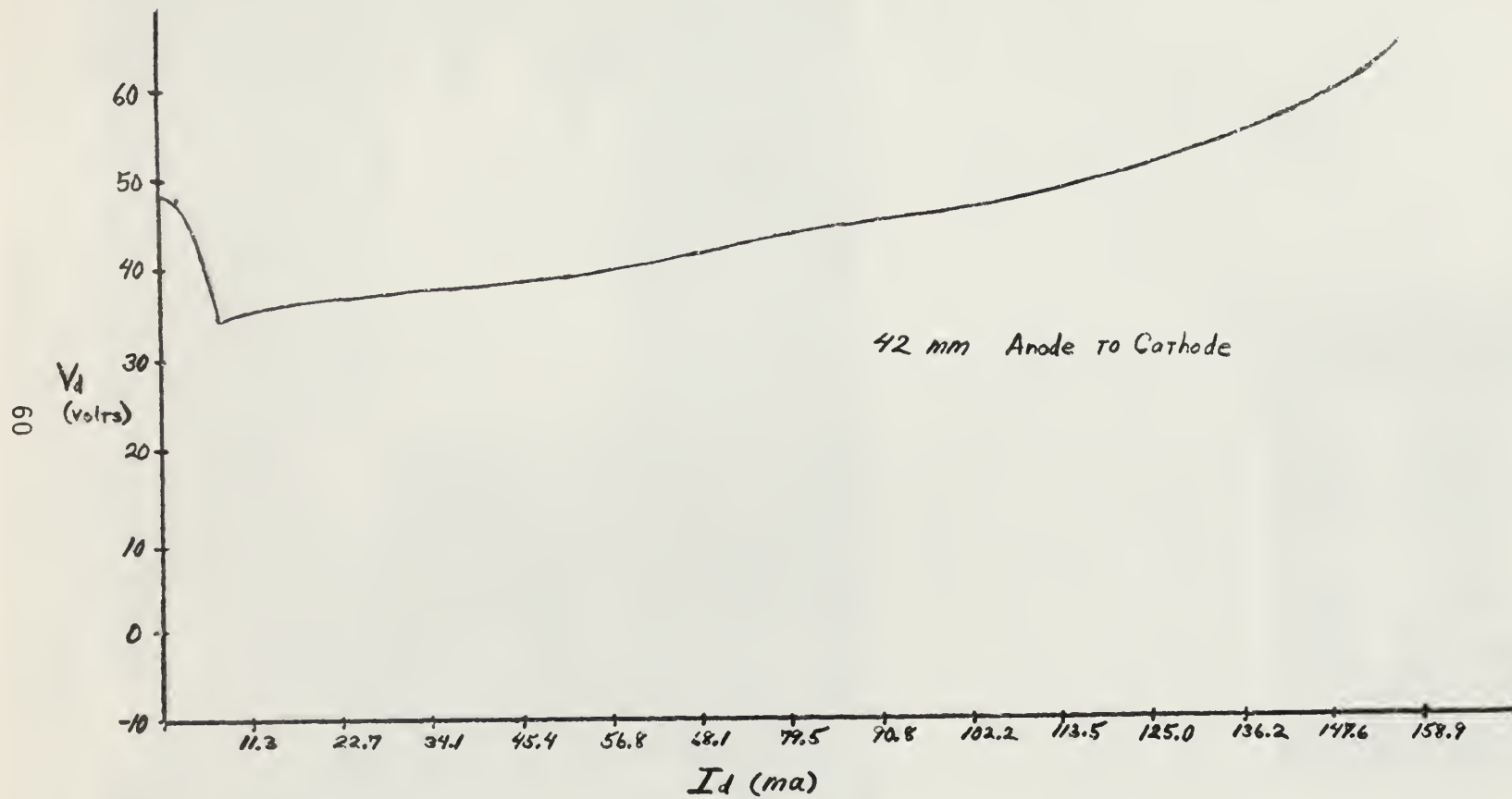


Fig. 7. Tube characteristics curve, Argon

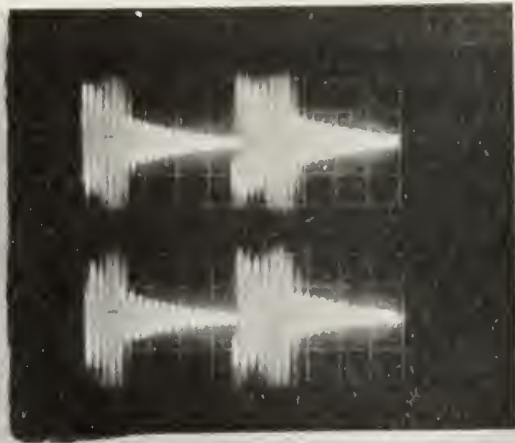


Fig. 8. Oscilloscope Photograph of typical relaxation oscillations

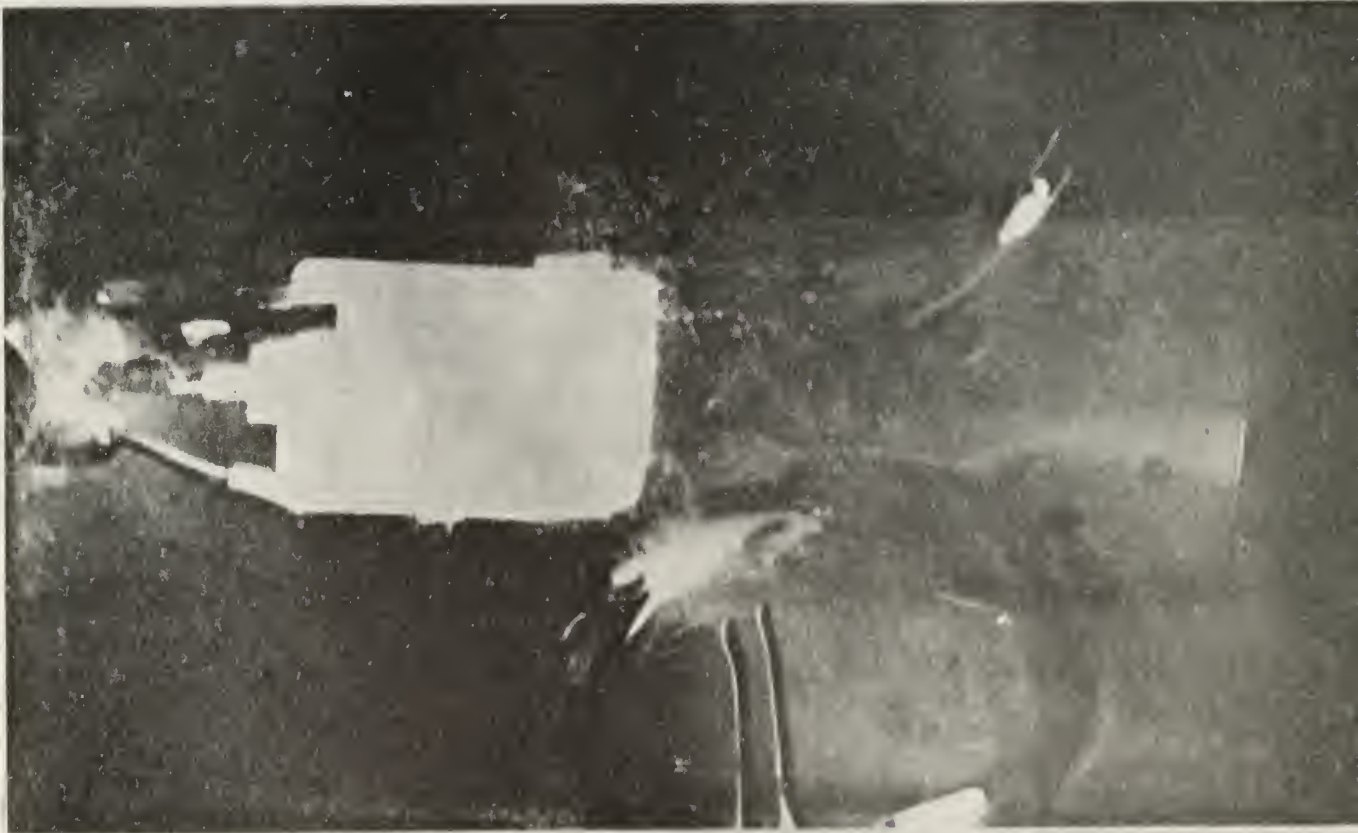


Fig. 9. Photograph of collapsed discharge in Neon.

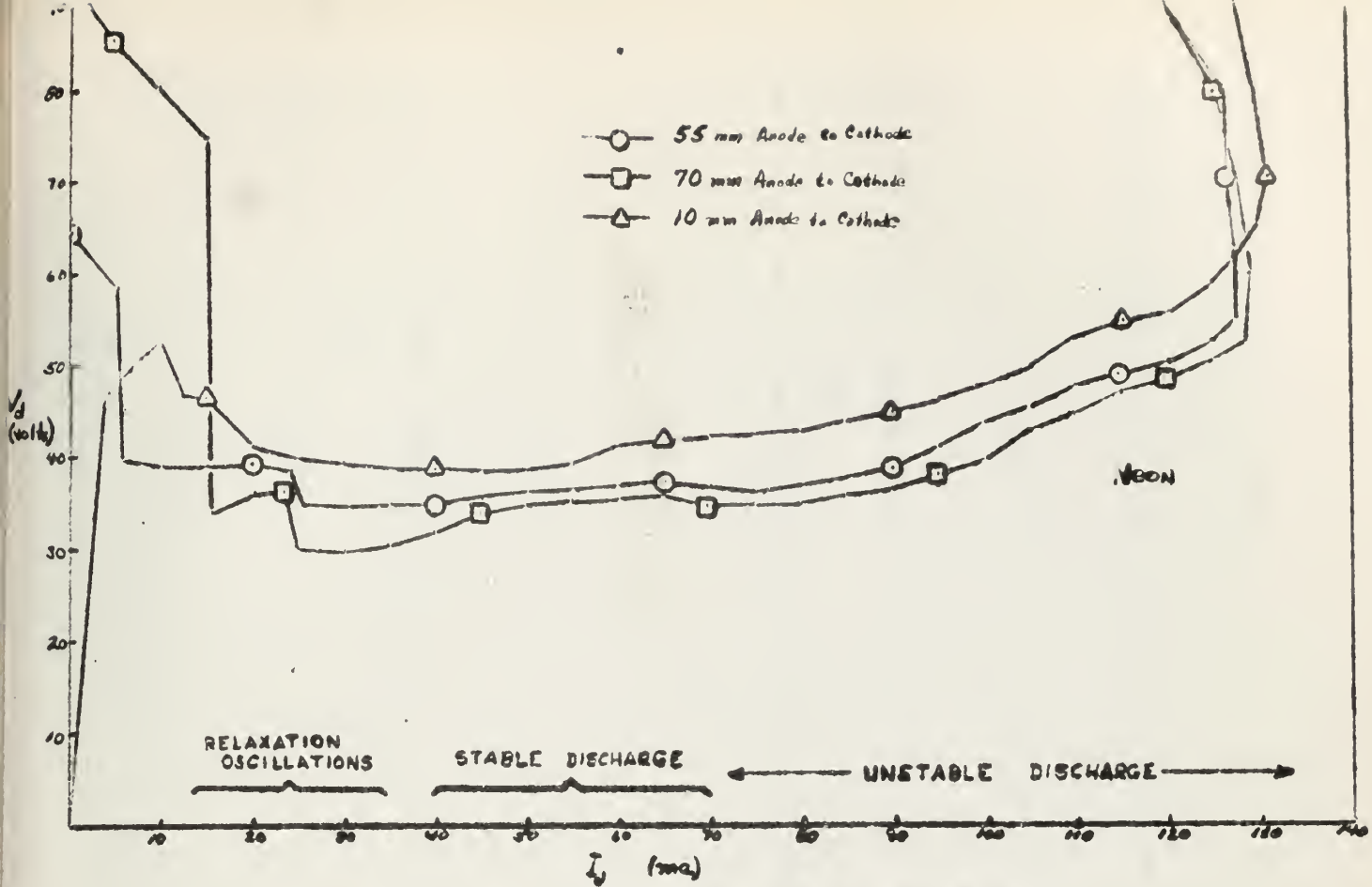


Fig. 11. Tube characteristics curve Run 2

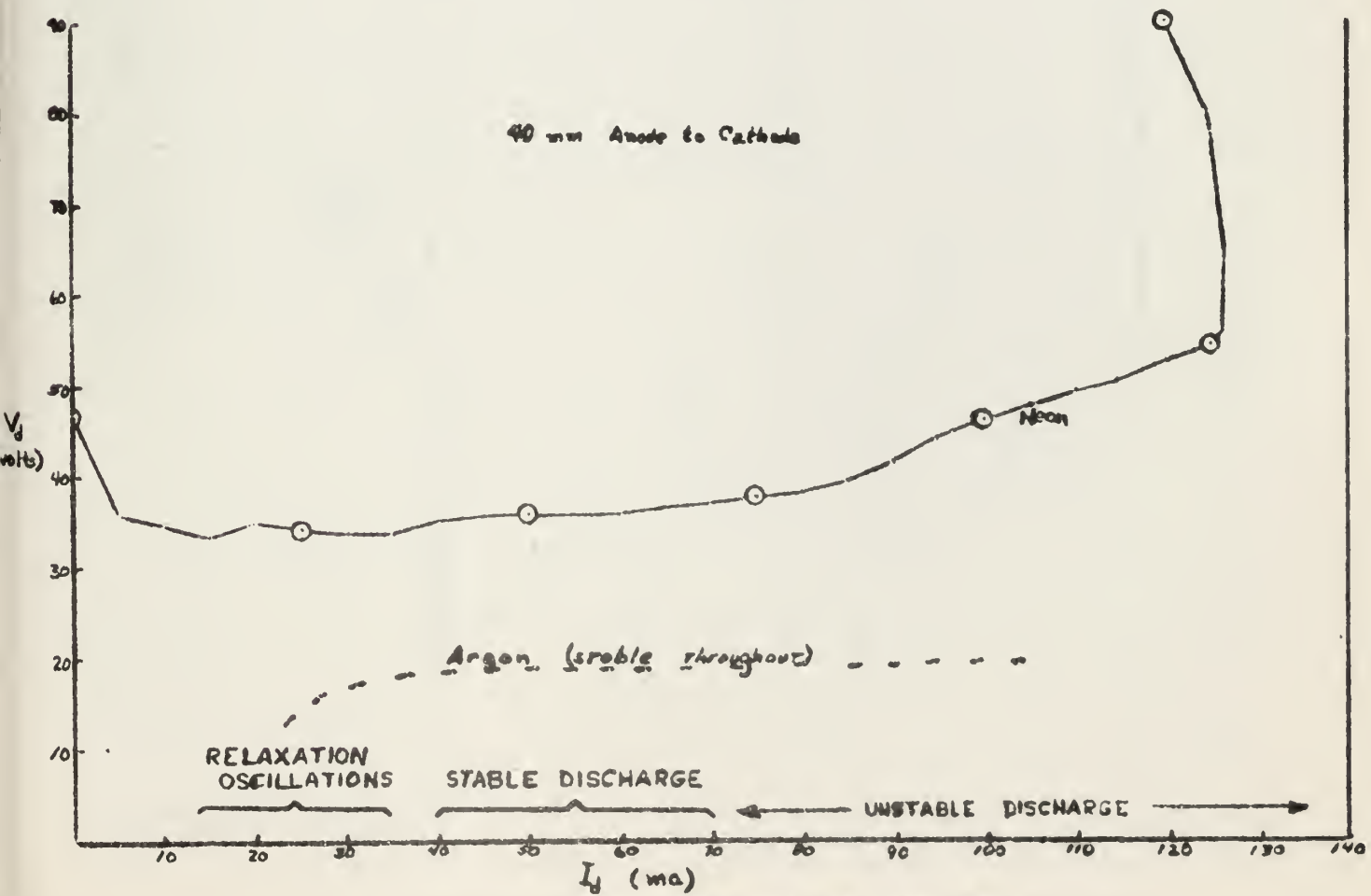


Fig. 10. Tube characteristics curve Run 1

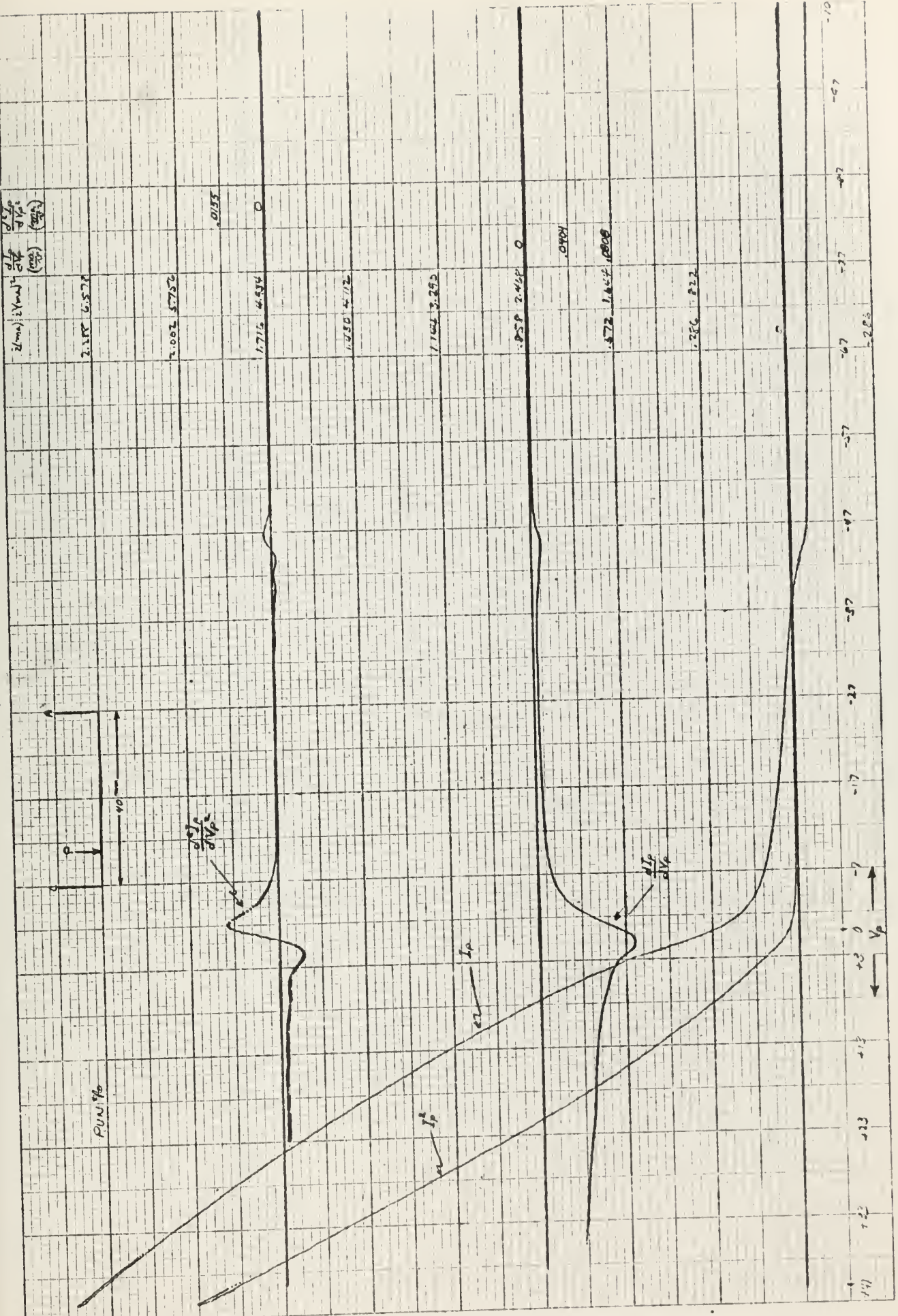


Fig. 12. Probe characteristics curve, Run 1, near cathode

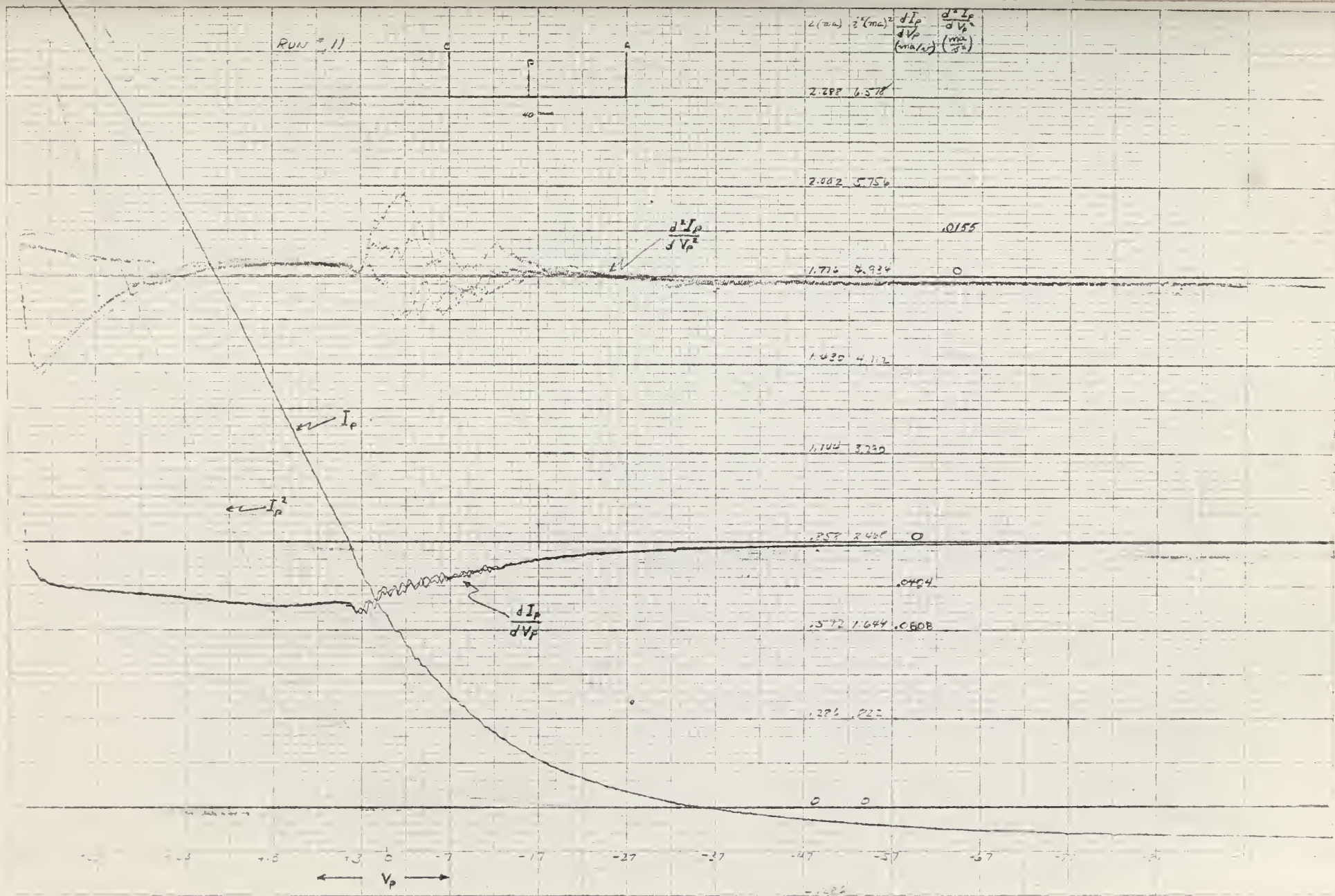


Fig. 13. Probe characteristics curve, Run 1, near beginning of maximum interaction region

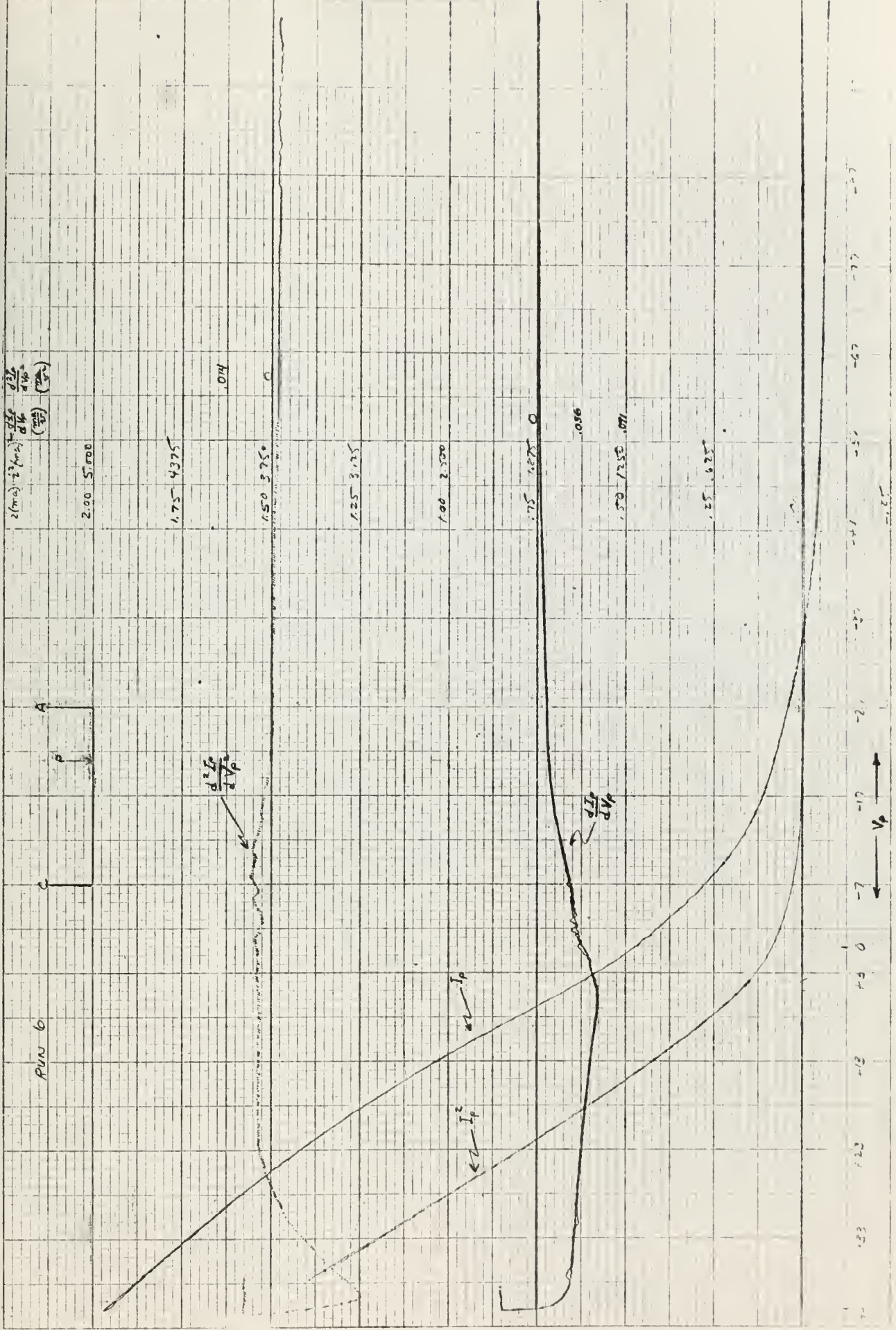


Fig. 14. Probe characteristics curve, Run 1, within region of maximum interaction

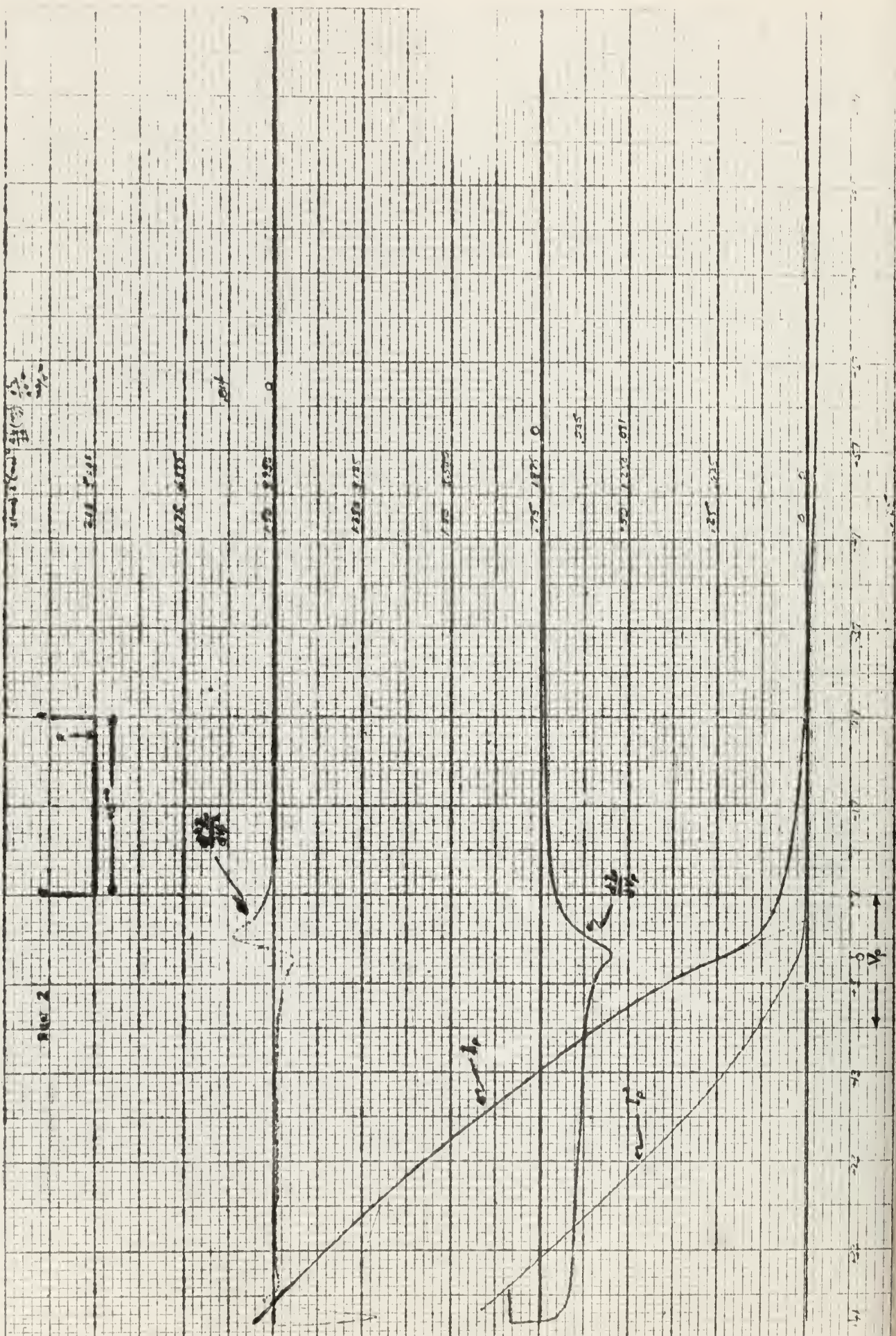


Fig. 15. Probe characteristics curve, Run 1, near anode past region of maximum interaction

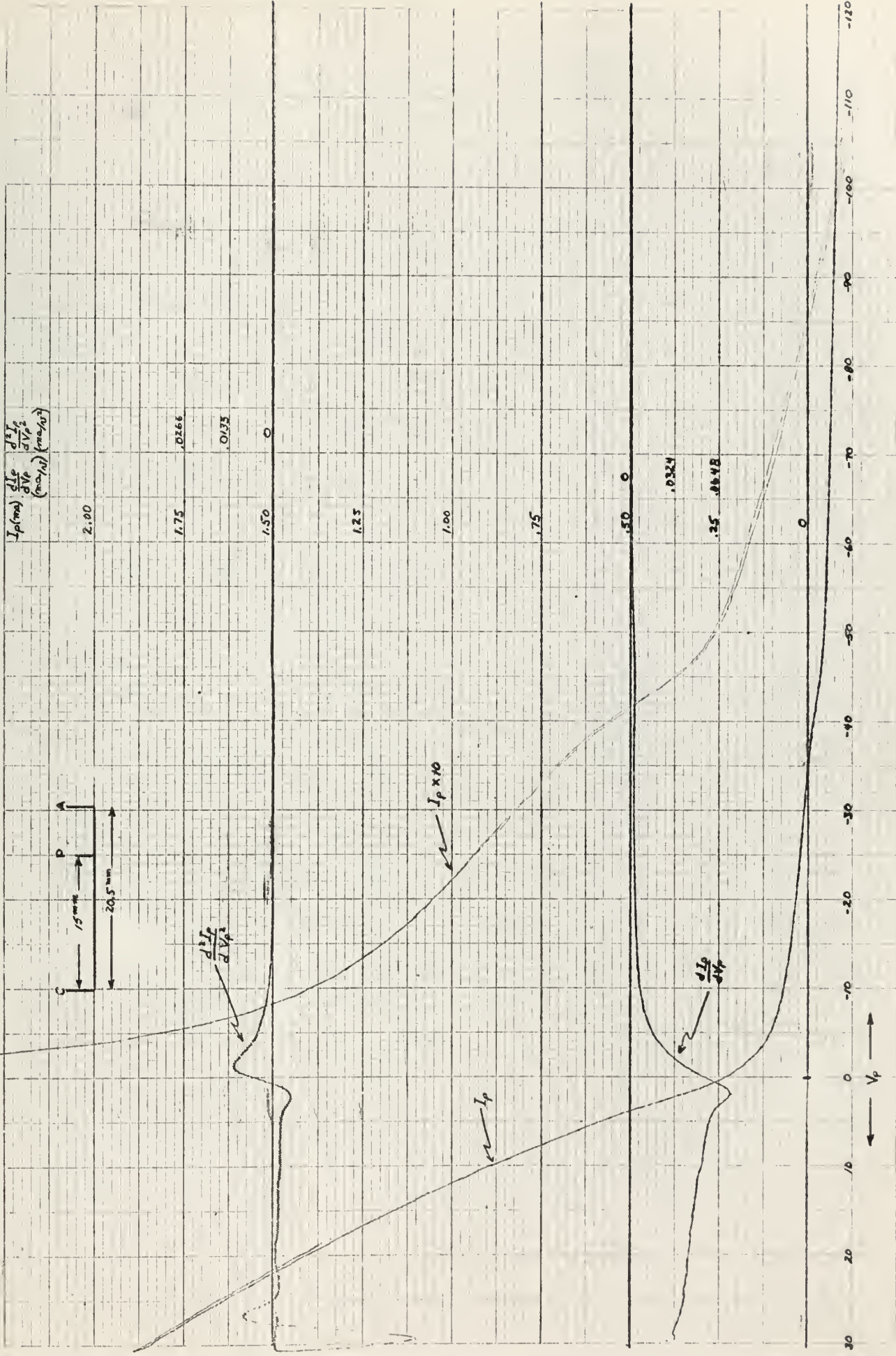


Fig. 16. Probe characteristics curve, Run 2, Anode 5mm from probe

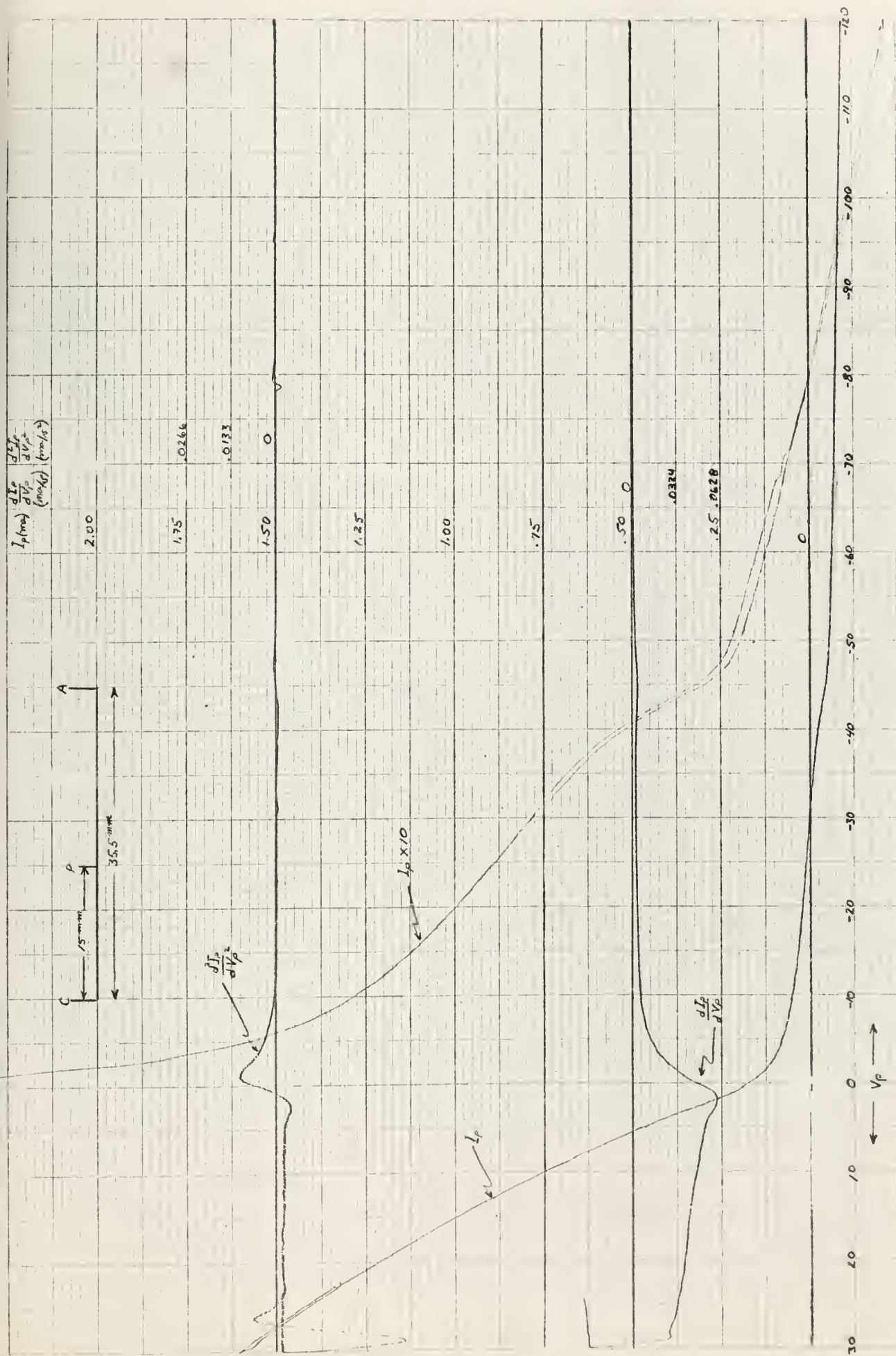


Fig. 17. Probe characteristics curve, Run 2, Anode 20 mm from probe

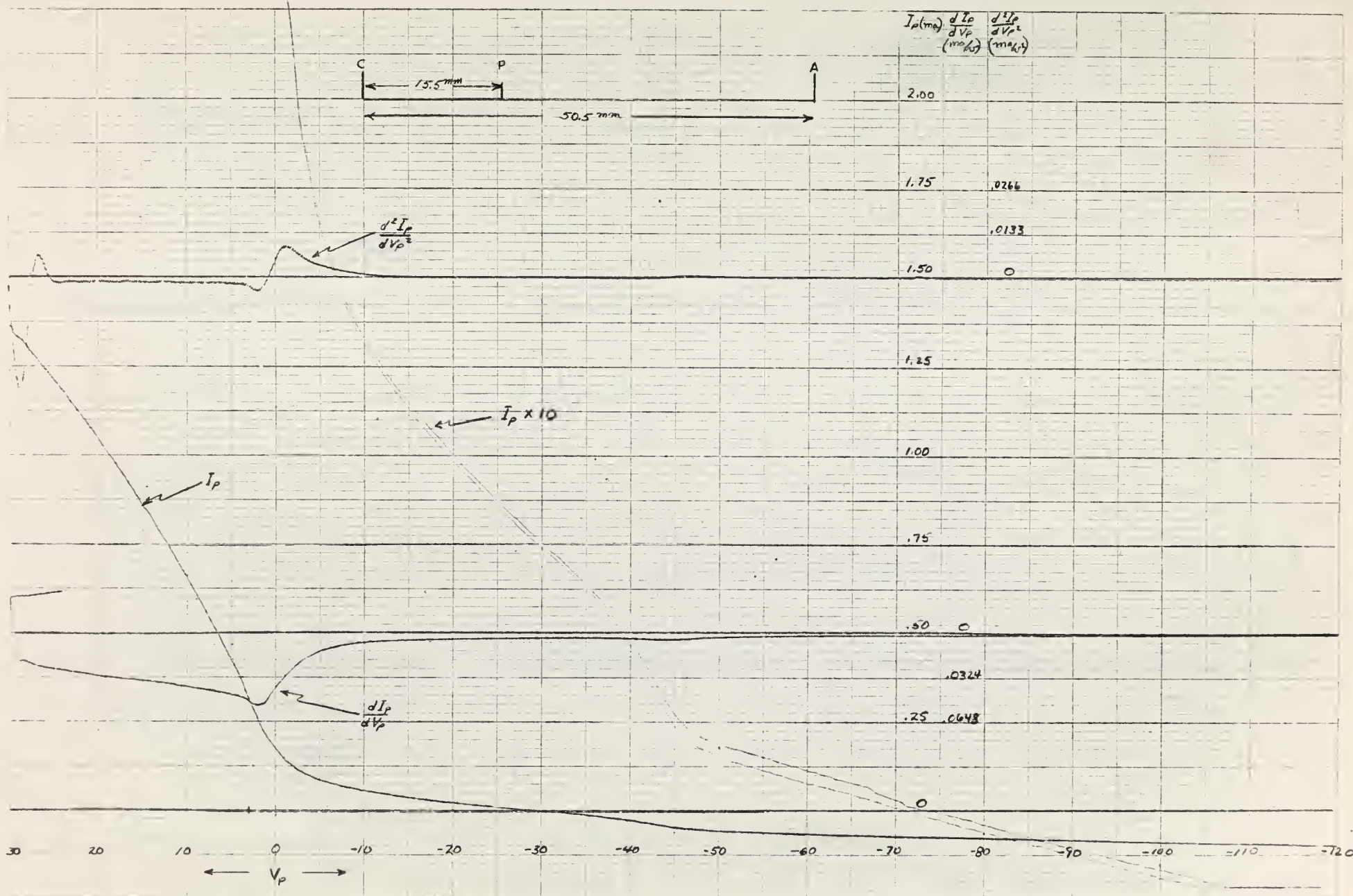


Fig. 18. Probe characteristics curves,
Run 2, Anode 35 mm from probe

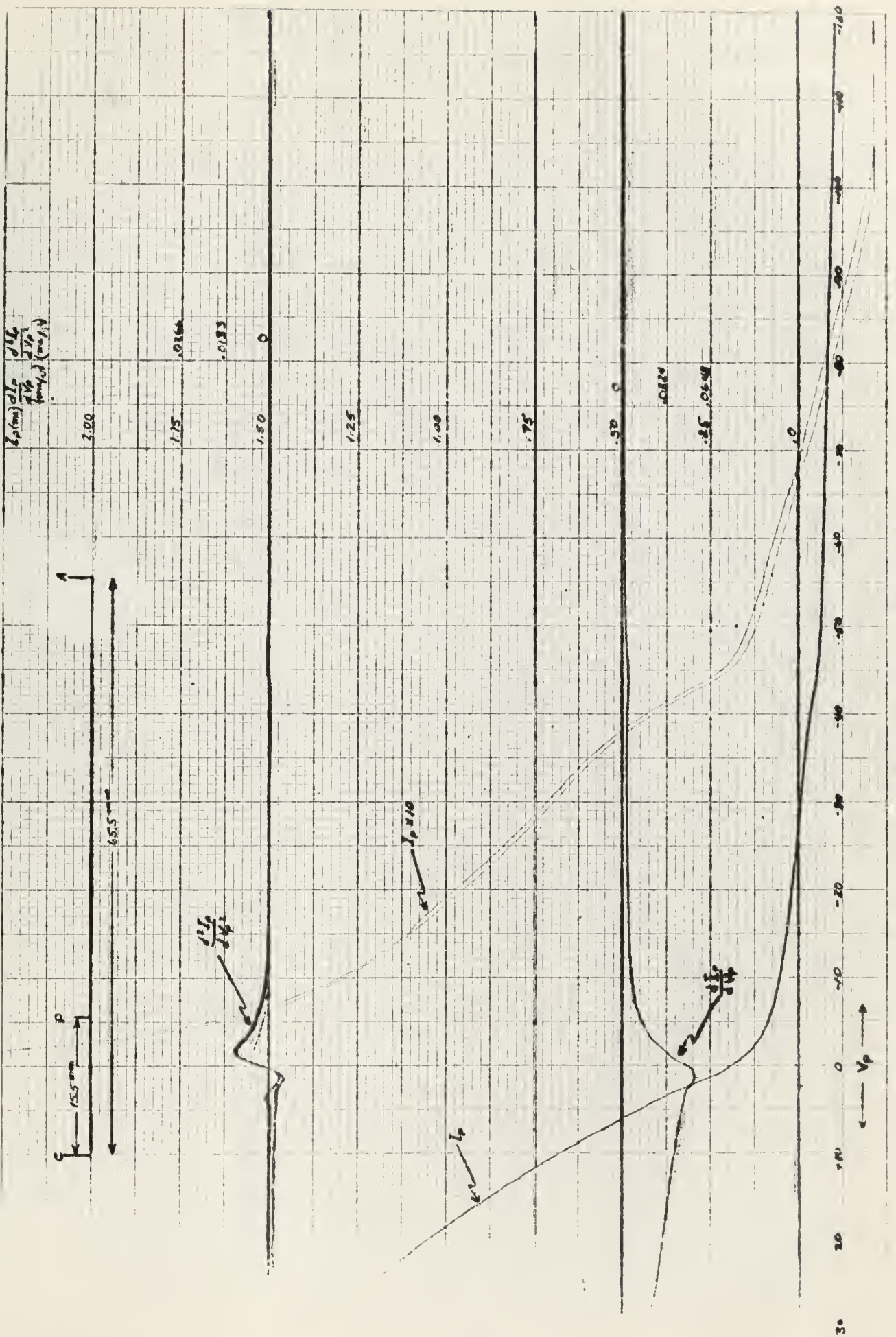


Fig. 19. Probe characteristics curves, Run 2, Anode 50 mm from probe

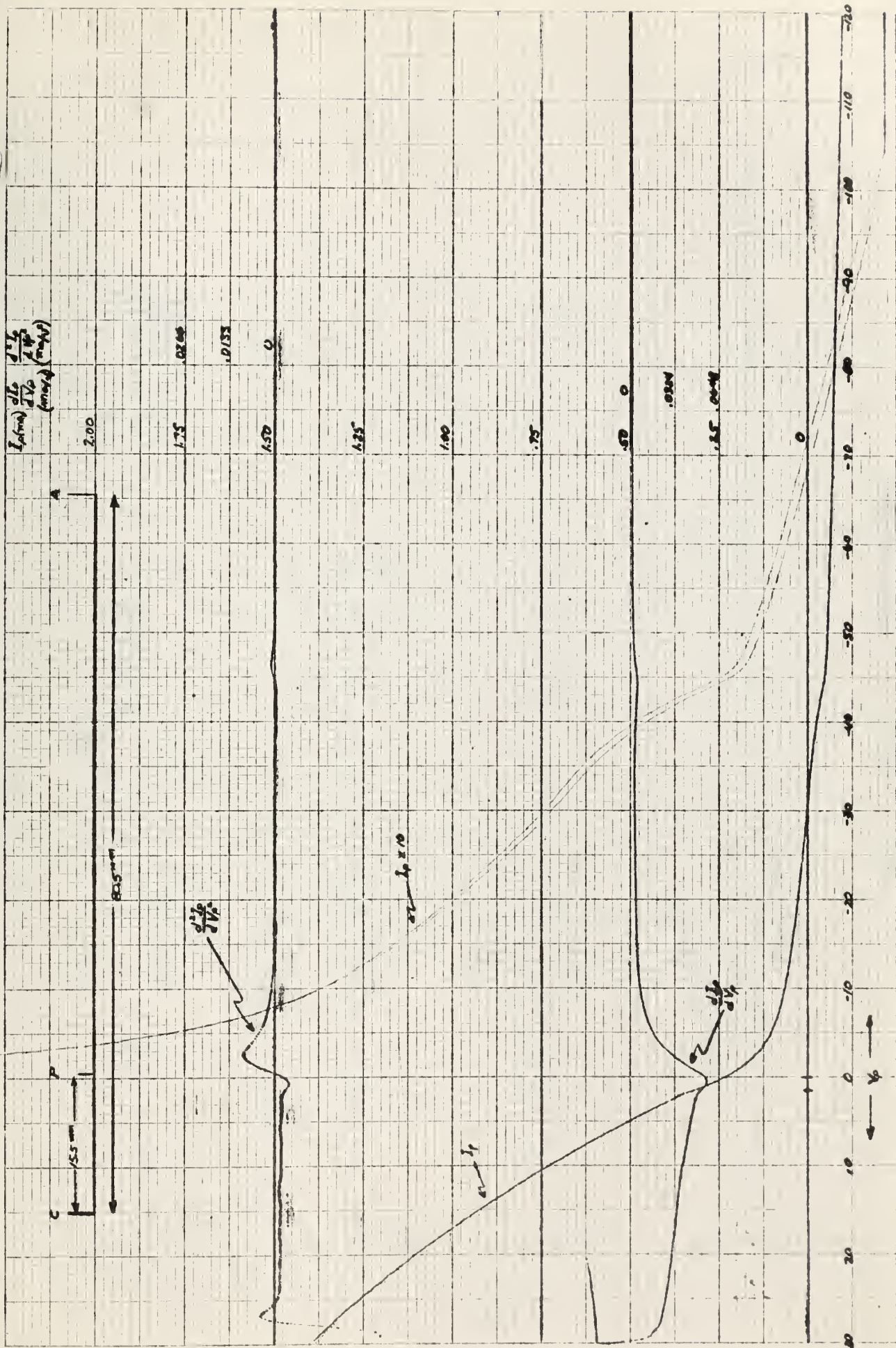
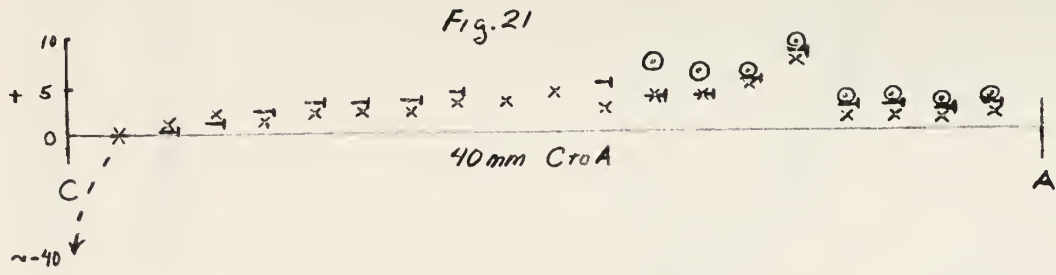
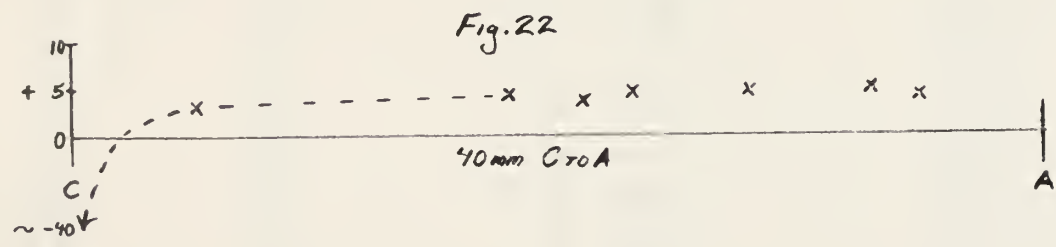


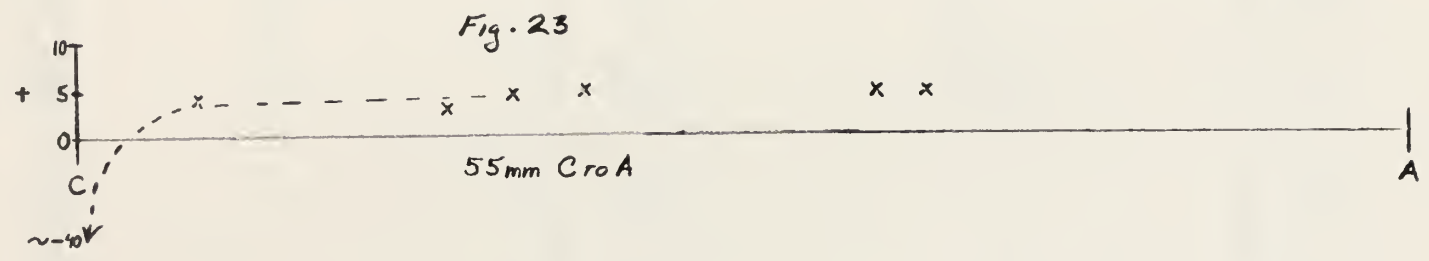
Fig. 20. Probe characteristics curves, Run 2, Anode 65 mm from probe



o V_{sp} from $\ln I_p$ vs V_p
 x V_{sp} from max. $\frac{dI_p}{dV_p}$
 + V_{sp} from "0" $\frac{dI_p}{dV_p}$



72



Figs. 21 through 24. Space Potential

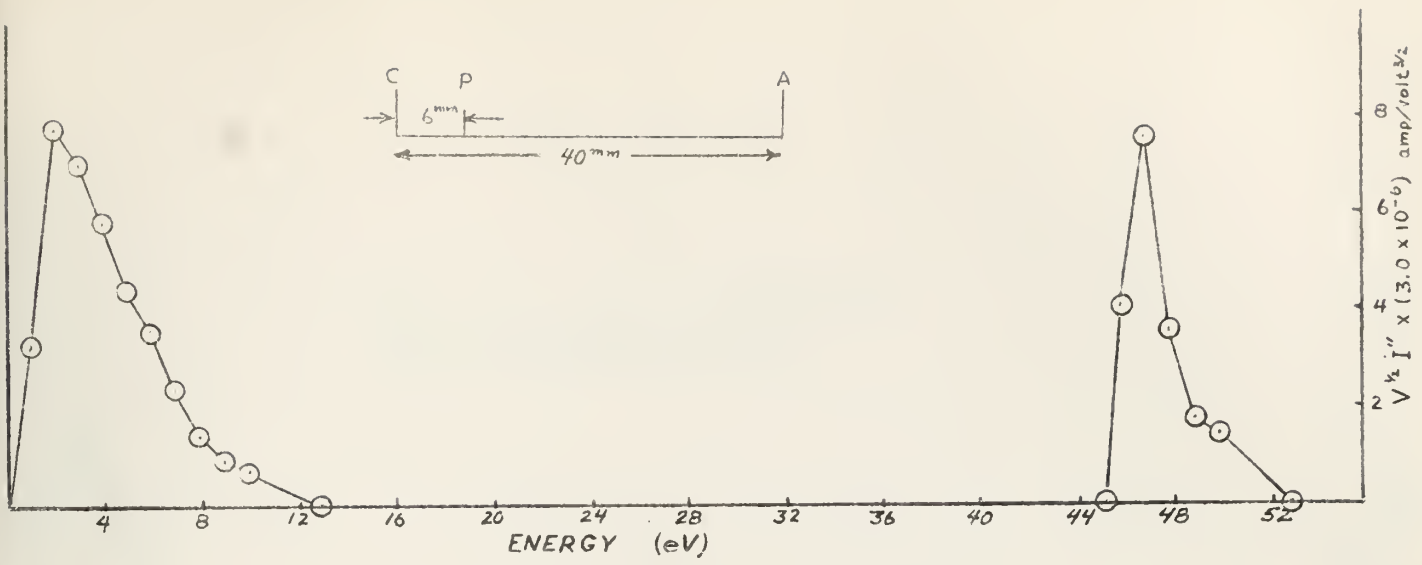


Fig. 25. Energy distribution function

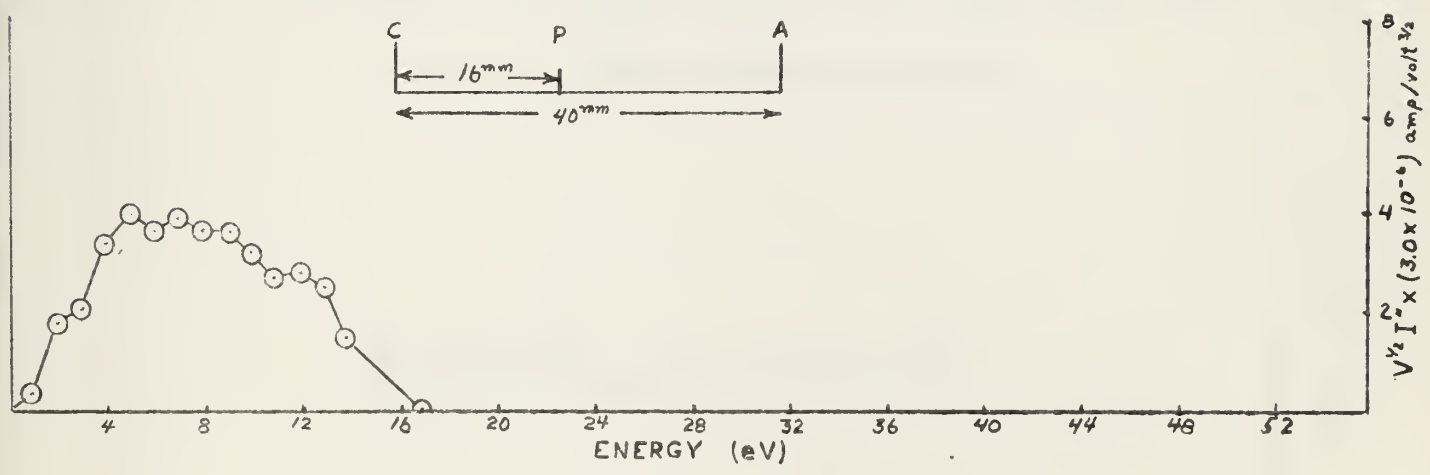


Fig. 26a. Energy distribution function

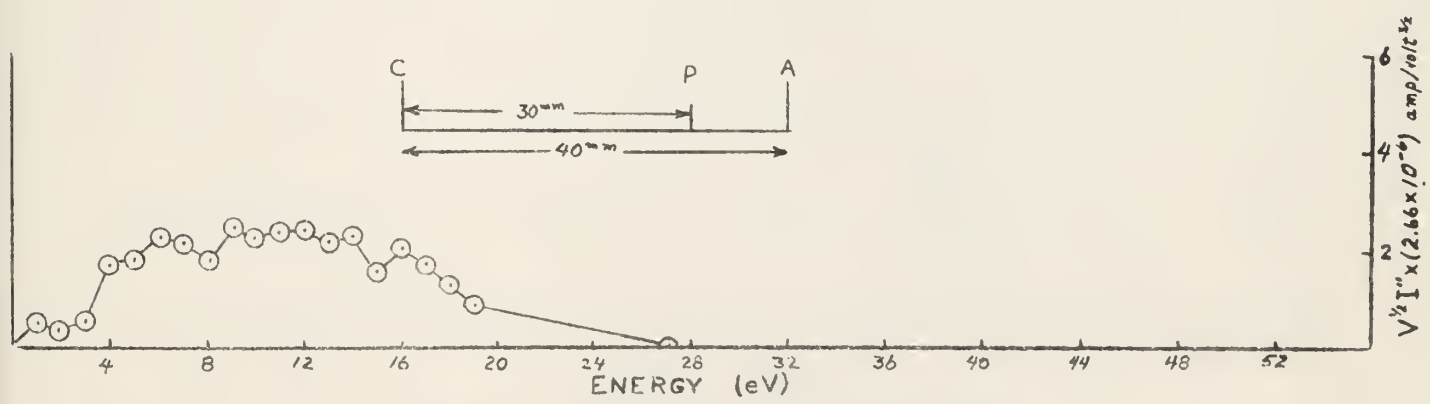


Fig. 26b. Energy distribution function

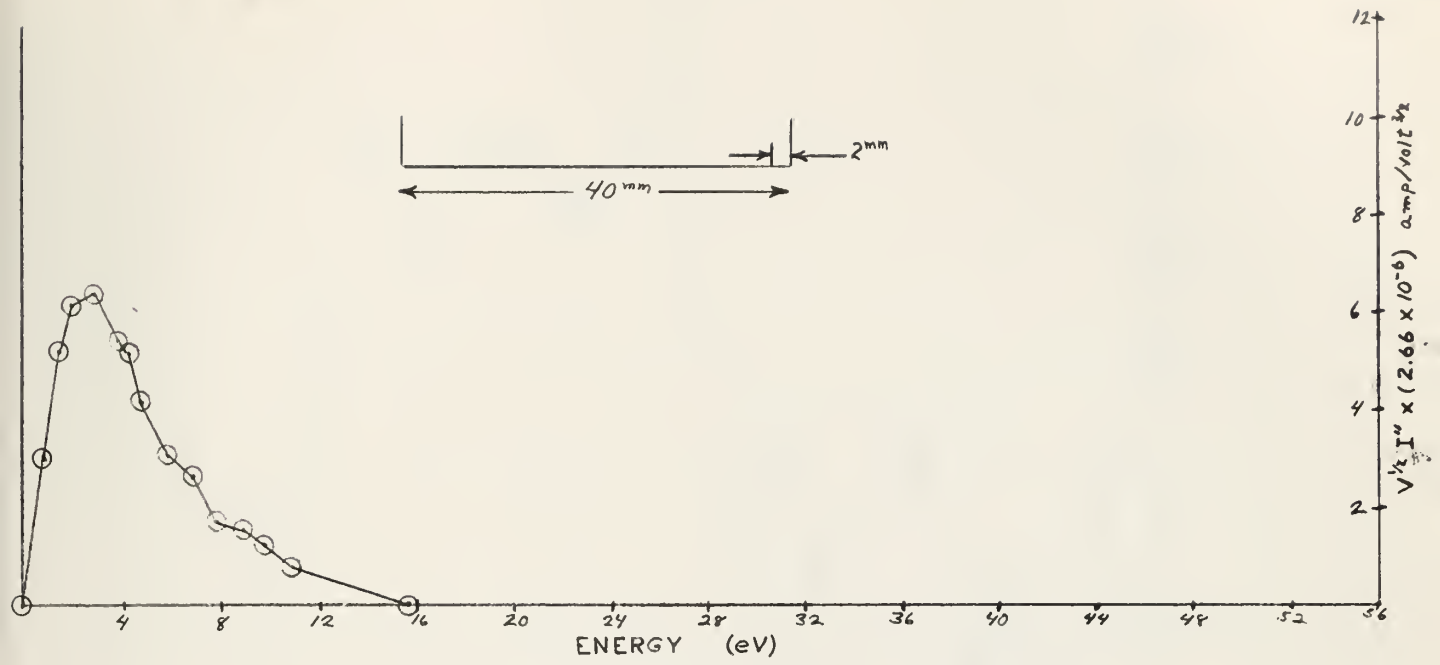


Fig. 27. Energy distribution function

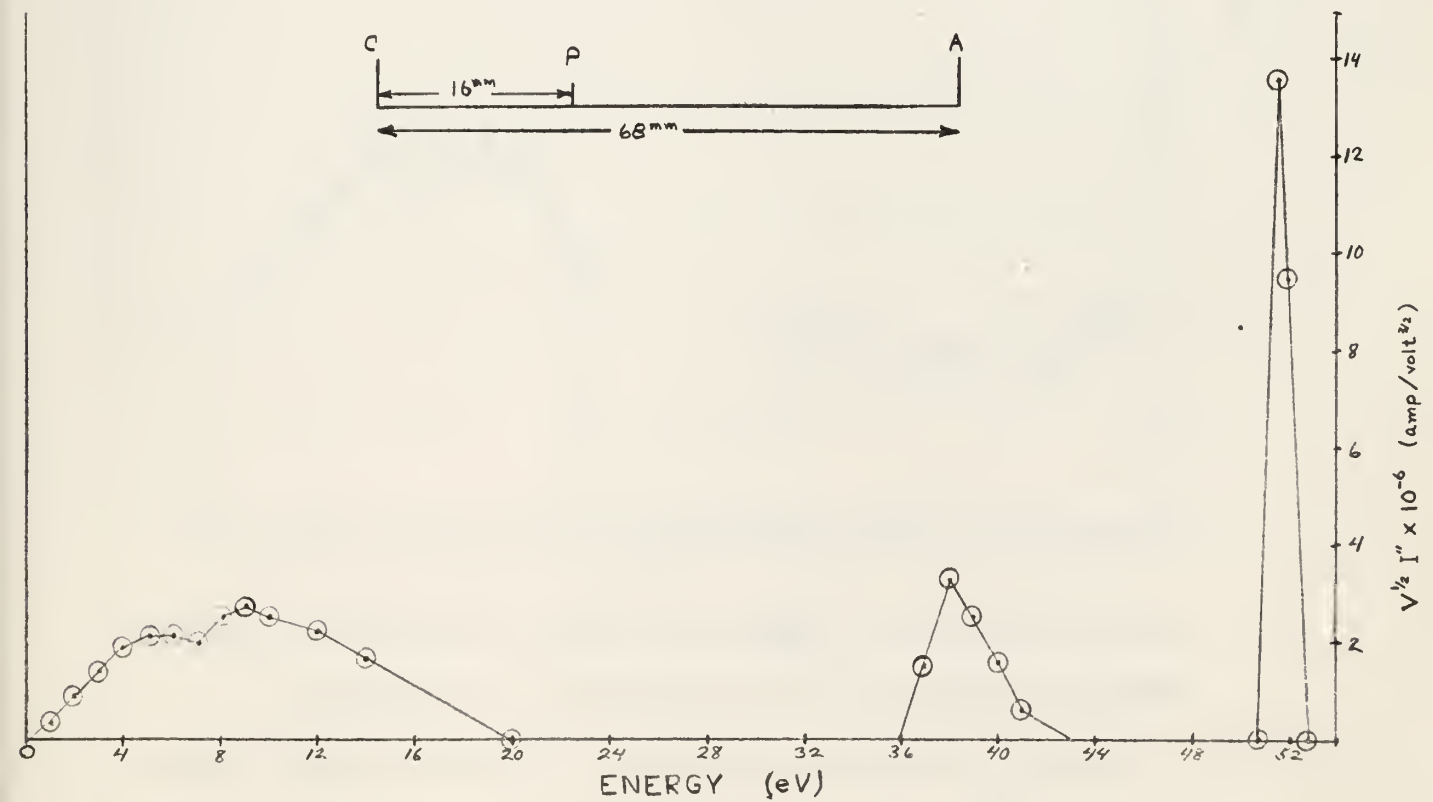
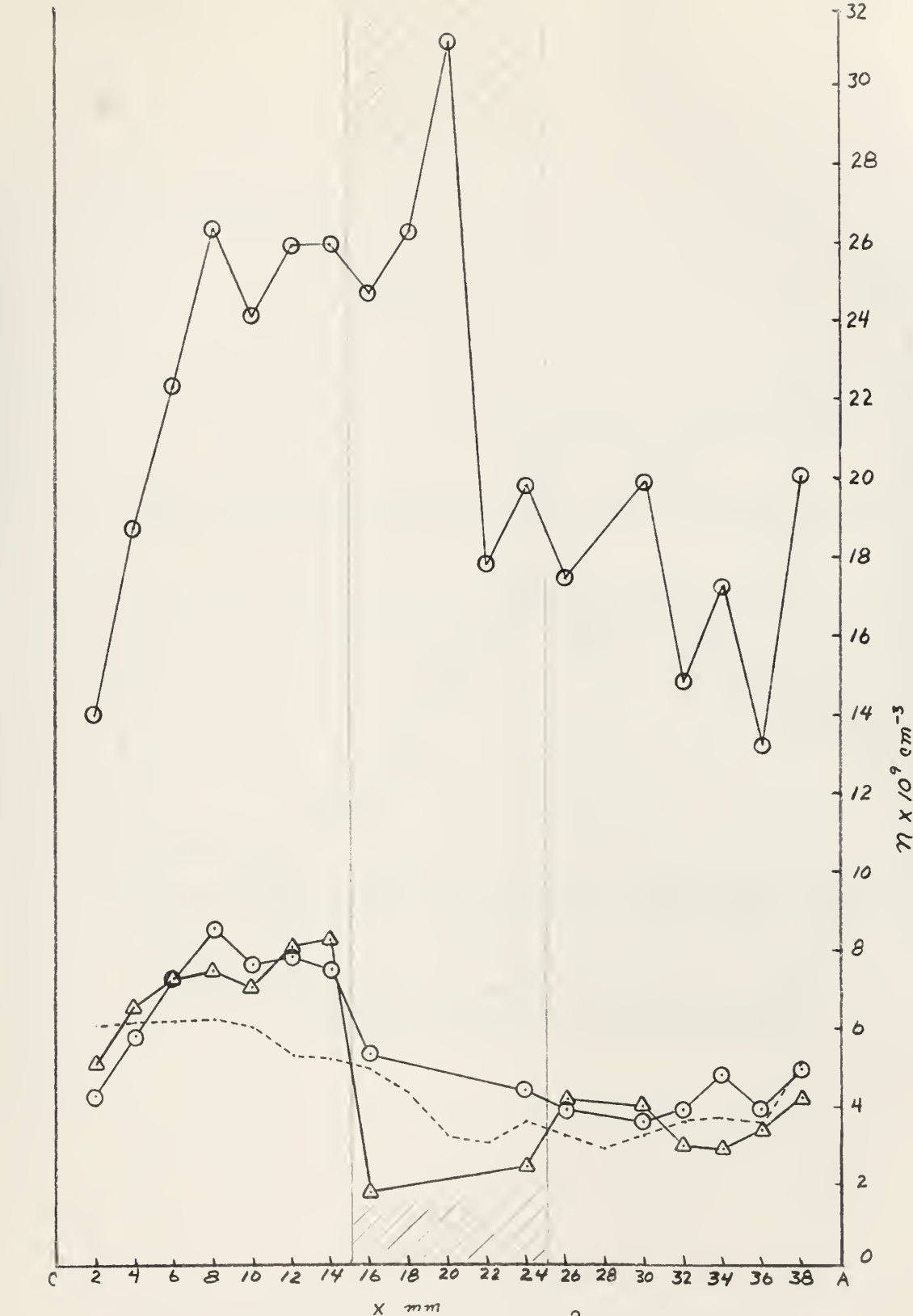


Fig. 28. Energy distribution function



- Ion density, n_i , obtained from $\frac{d(I_p)^2}{dV_p}$ uncorrected (upper)
- Ion density, n_i , corrected for electron temperature (lower)
- △— Electron density, n , obtained by Druyvesteyn analysis
- Electron density, n , obtained by $= \left(\frac{f}{8980}\right)^2$

Fig. 29a. Electron and ion density vs distance, Run 1

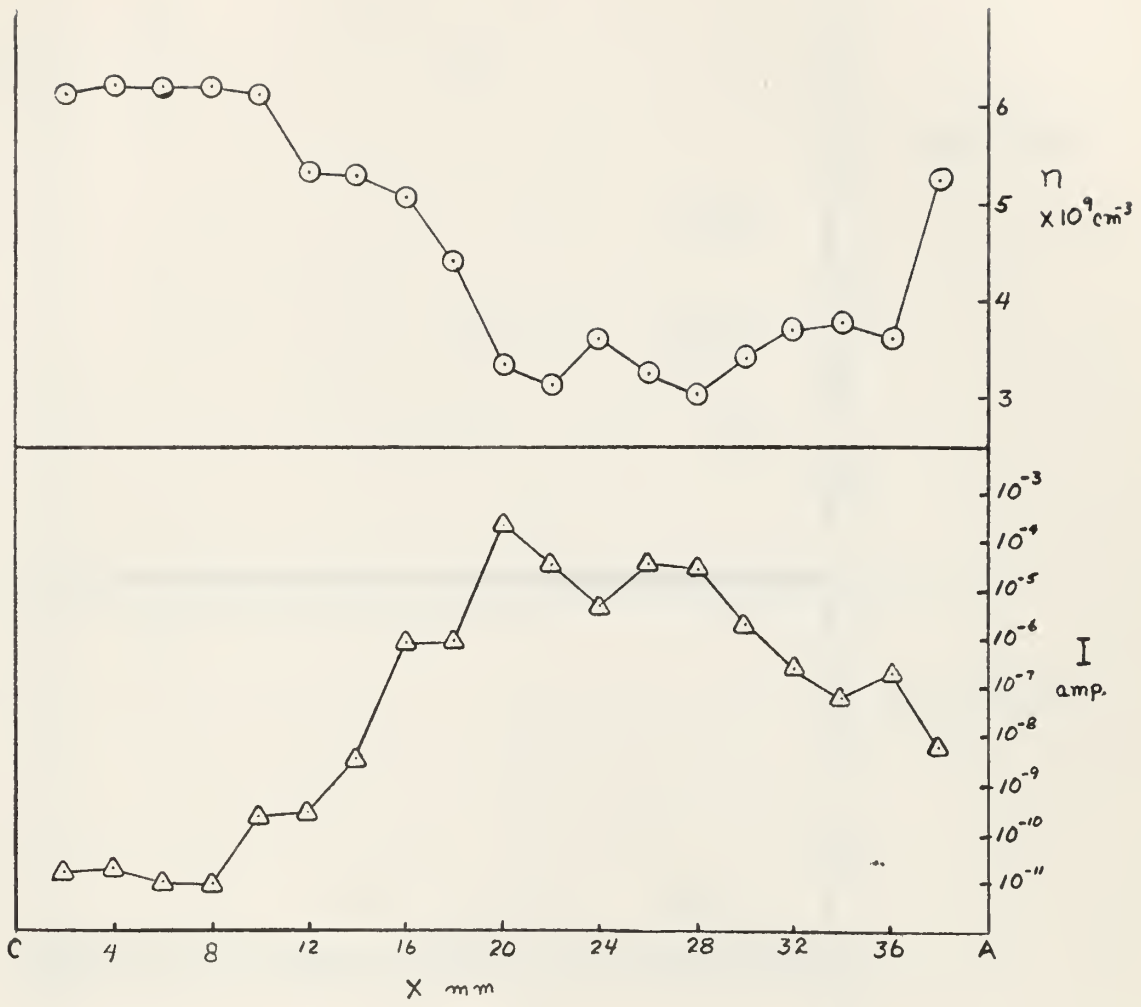


Fig. 29 b. Intensity of detector current, I_c , and electron density, n , vs distance, Run 1

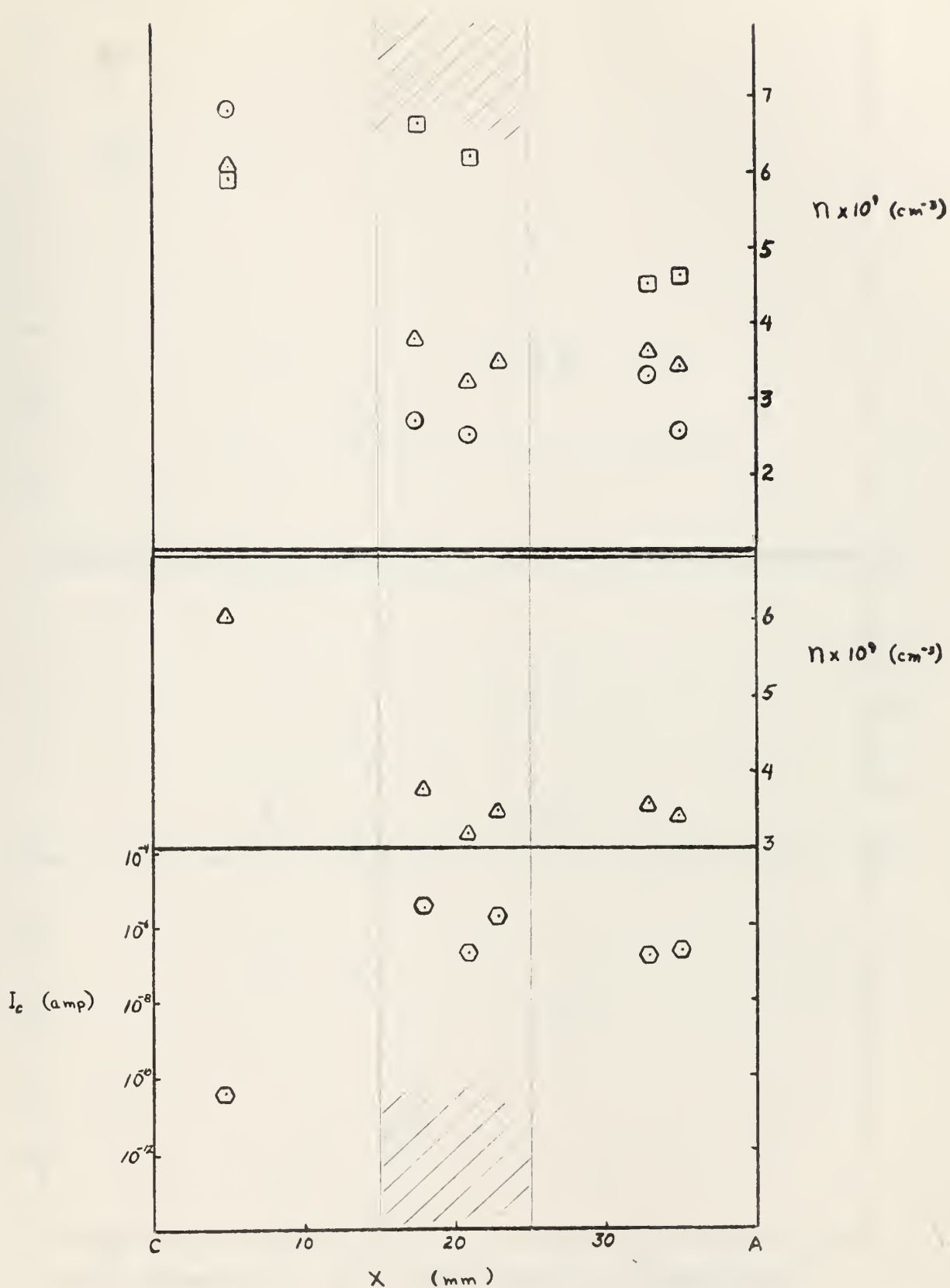


Fig. 30. Upper plot: (\odot) electron density by Druyvesteyn
 (\triangle) electron density by frequency
 (\square) ion density (corrected)

Lower plot: Intensity of detector current I_c , and
 electron density, n , vs distance, Run 2

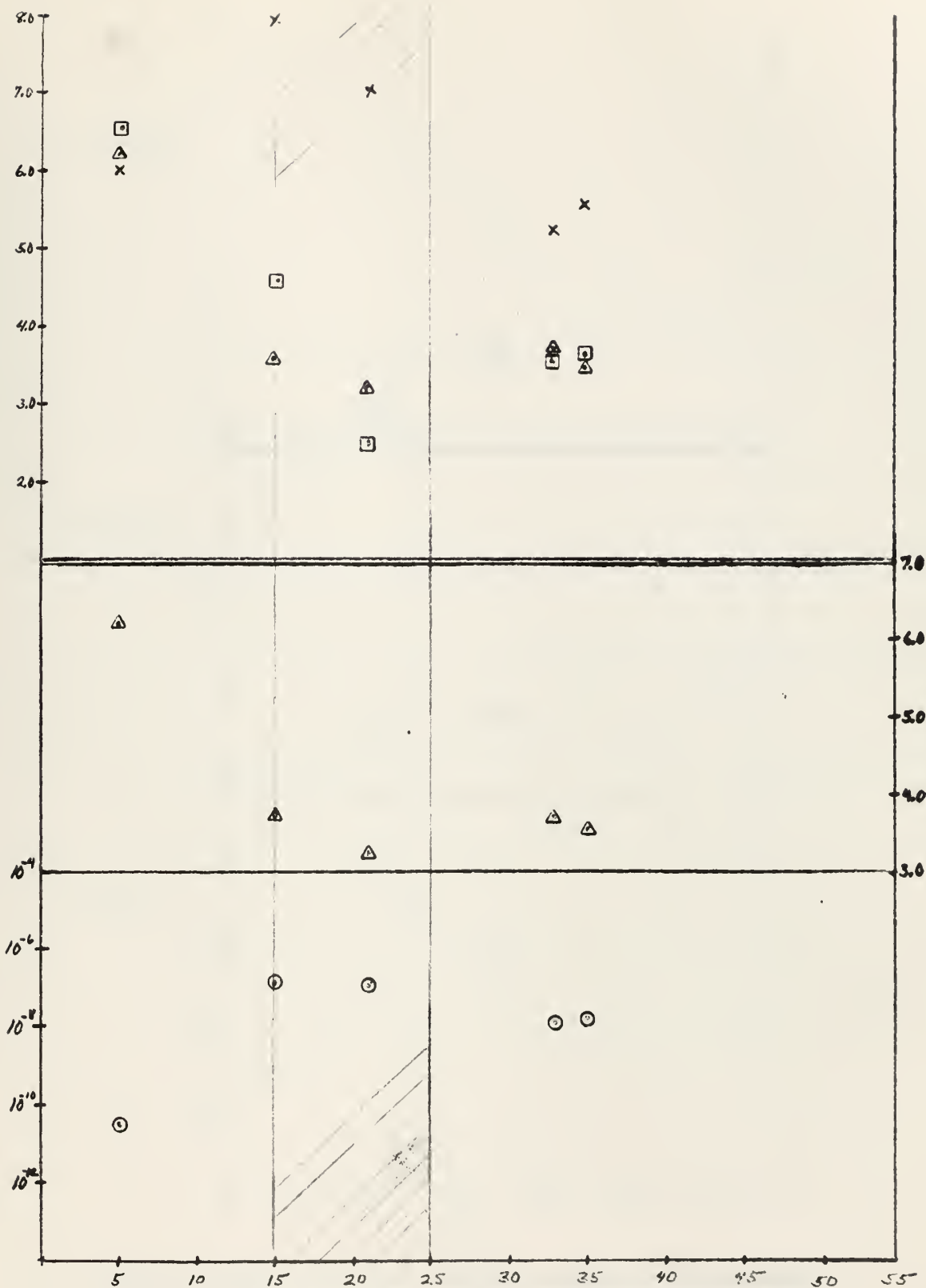


Fig. 31. Upper plot: (\square) electron density by Druyvesteyn
 (\triangle) electron density by frequency
 (\times) ion density (corrected)

Lower plot: Intensity of detector current, I_c , and
 electron density, n , vs distance, Run 2

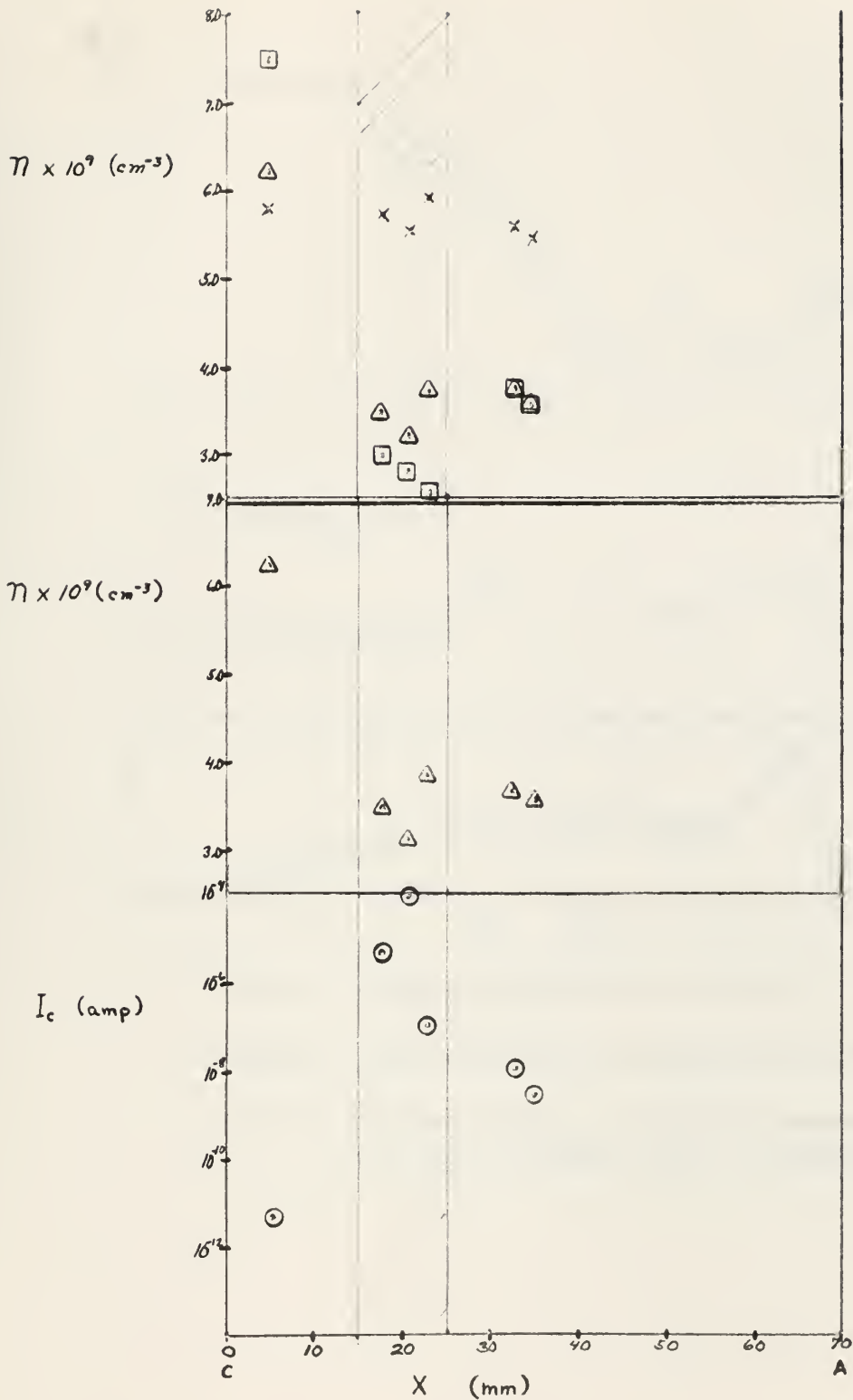
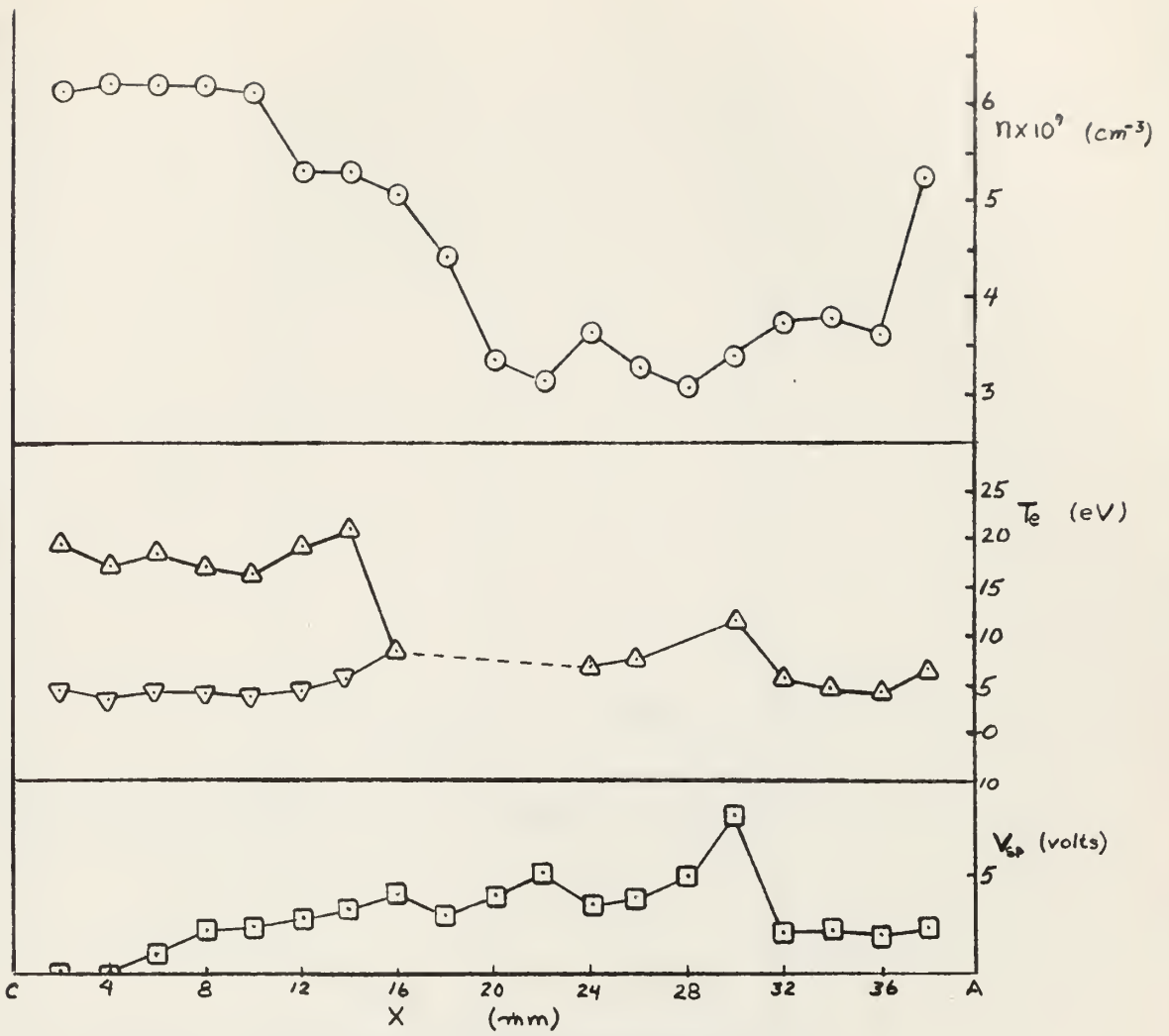


Fig. 32. Upper plot: (□) Electron density by Druyvesteyn
 (△) Electron density by frequency
 (x) Ion density (corrected)

Lower plot: Intensity of detector current, I_c , and
 electron density, n , vs distance, Run 2



- △— Mean temperature, all electrons
- ▽— Mean temperature, randomized electrons

Fig. 33. Electron density, n , electron temperature, T_e , and space potential, V_{sp} , vs distance, Run 1

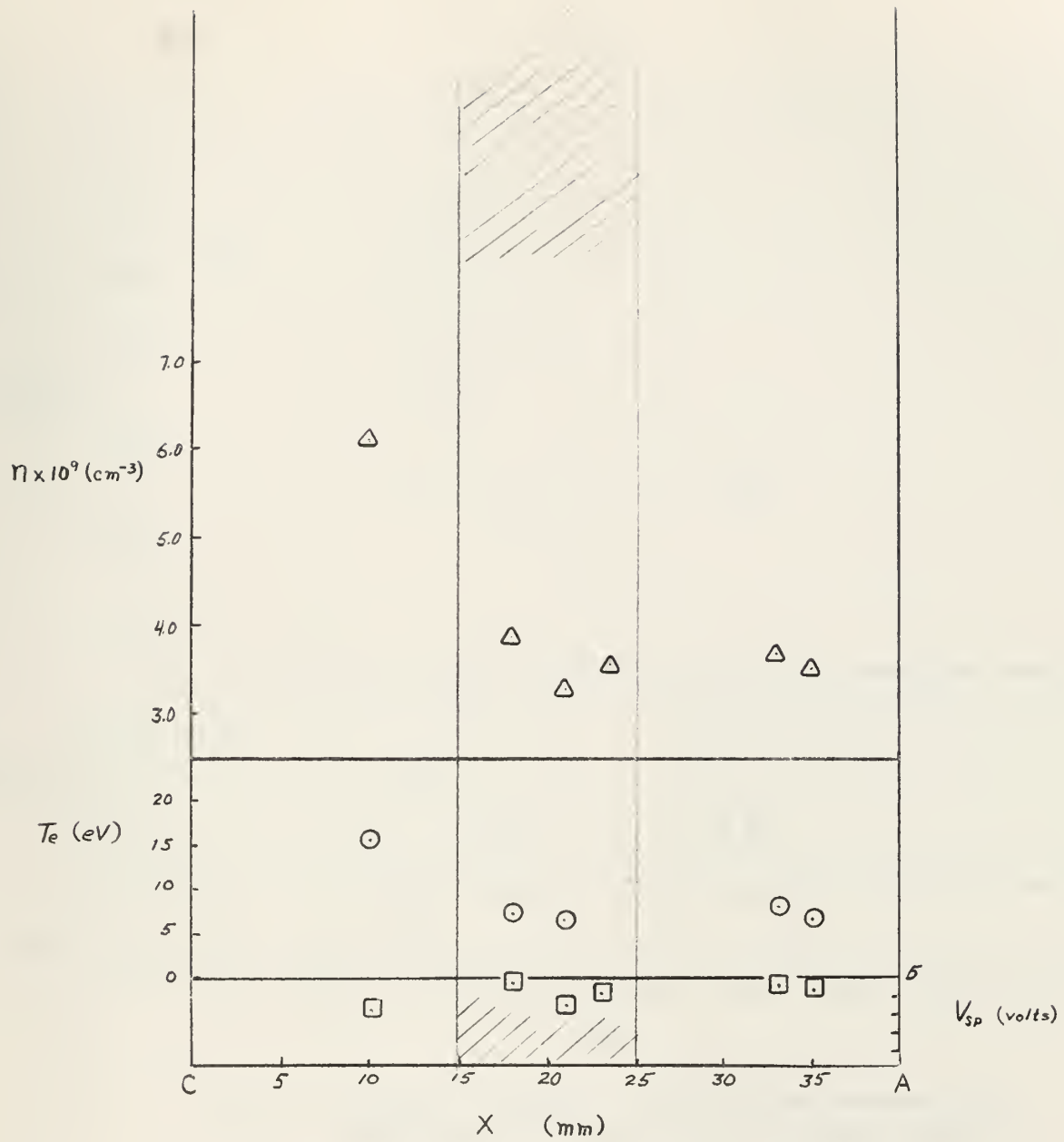


Fig. 34. Electron density, n , electron temperature, T_e , and space potential, V_{sp} , vs distance, Run 2

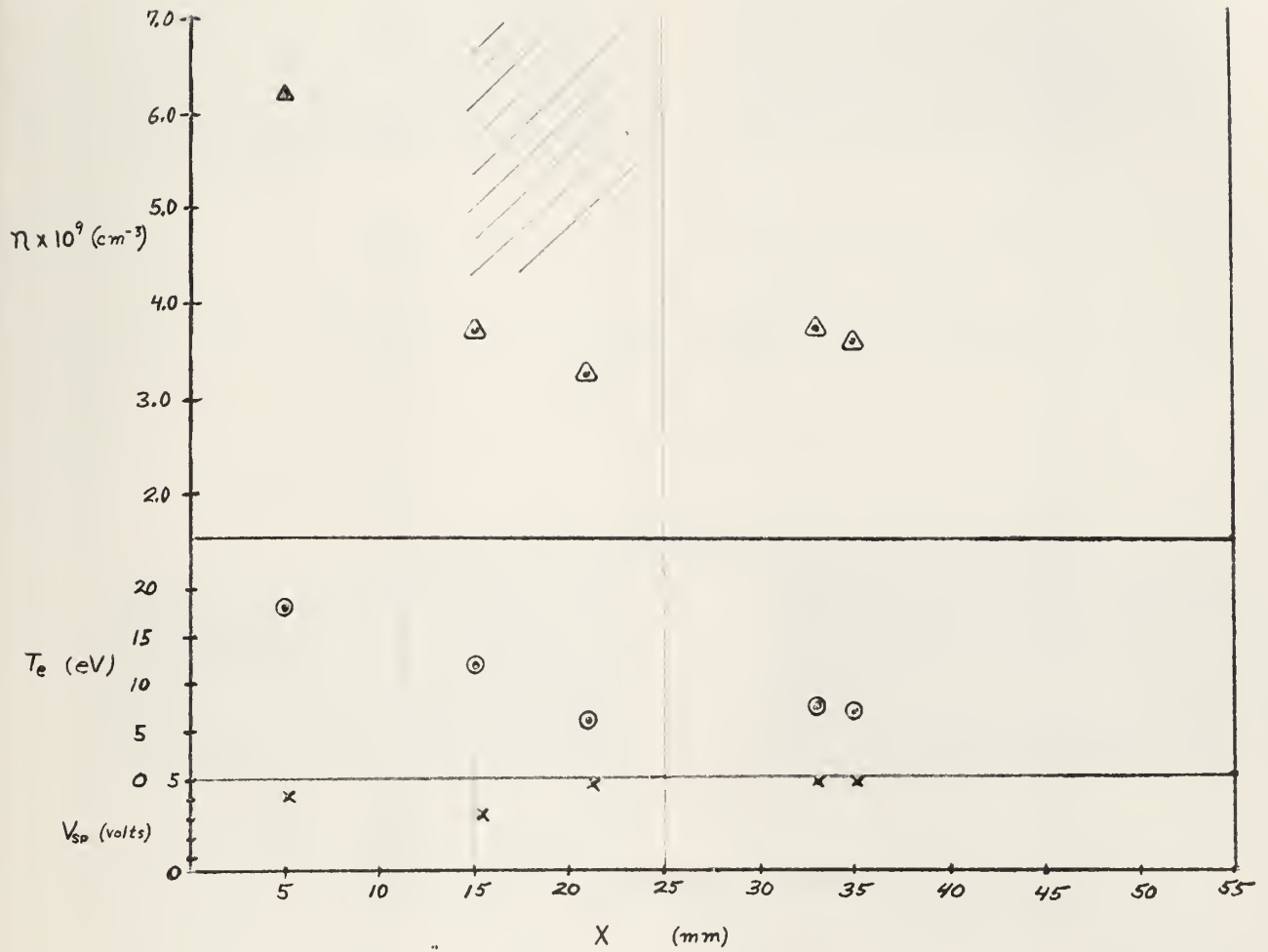


Fig. 35. Electron density, n , electron temperature, T_e , and space potential, V_{sp} , vs distance, Run 2

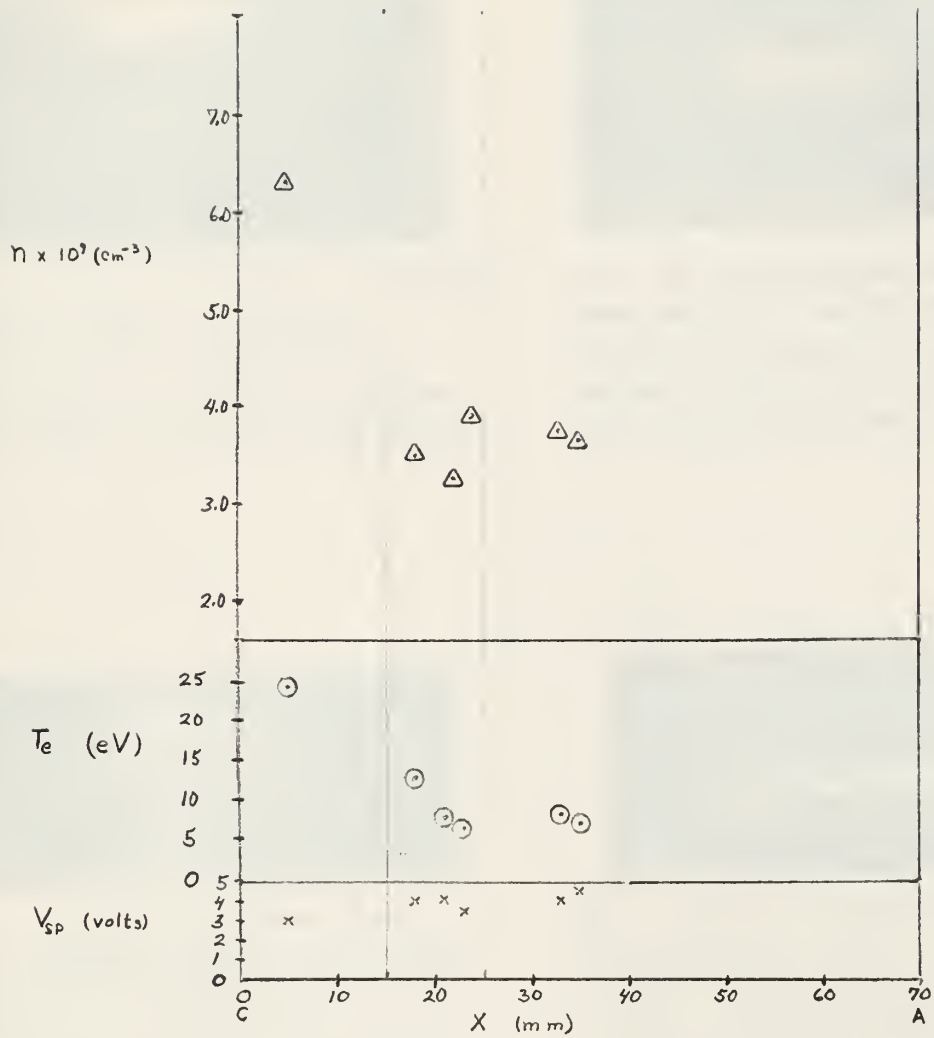


Fig. 36. Electron density, n , electron temperature, T_e , and space potential, V_{sp} , vs distance, Run 2



Fig. 37. Ion Oscillations 5 mm from cathode. Scale 005 Volt/cm vertical; 5 micro-sec/cm horizontal. Tube pressure 10 microns, Discharge current 65 milliamperes.



Fig. 38. Ion Oscillations 18 mm from cathode. Scale .02 Volt/cm vertical; 5 micro-sec/cm horizontal. Tube pressure 10 microns, Discharge current 65 milliamperes.



Fig. 39. Ion Oscillations 21 mm from cathode. Scale .02 Volt/cm vertical; 5 micro-sec/cm horizontal. Tube pressure 10 microns, Discharge current 65 milliamperes.



Fig. 40. Ion Oscillations 33 mm from cathode. Scale .02 Volt/cm vertical; 5 micro-sec/cm horizontal. Tube pressure 10 microns, Discharge current 65 milliamperes.



Fig. 41. Ion Oscillations 28 mm from cathode. Scale .02 Volt/cm vertical; 5 micro-sec/cm horizontal. Tube pressure 10 microns, Discharge current 65 milliamperes.

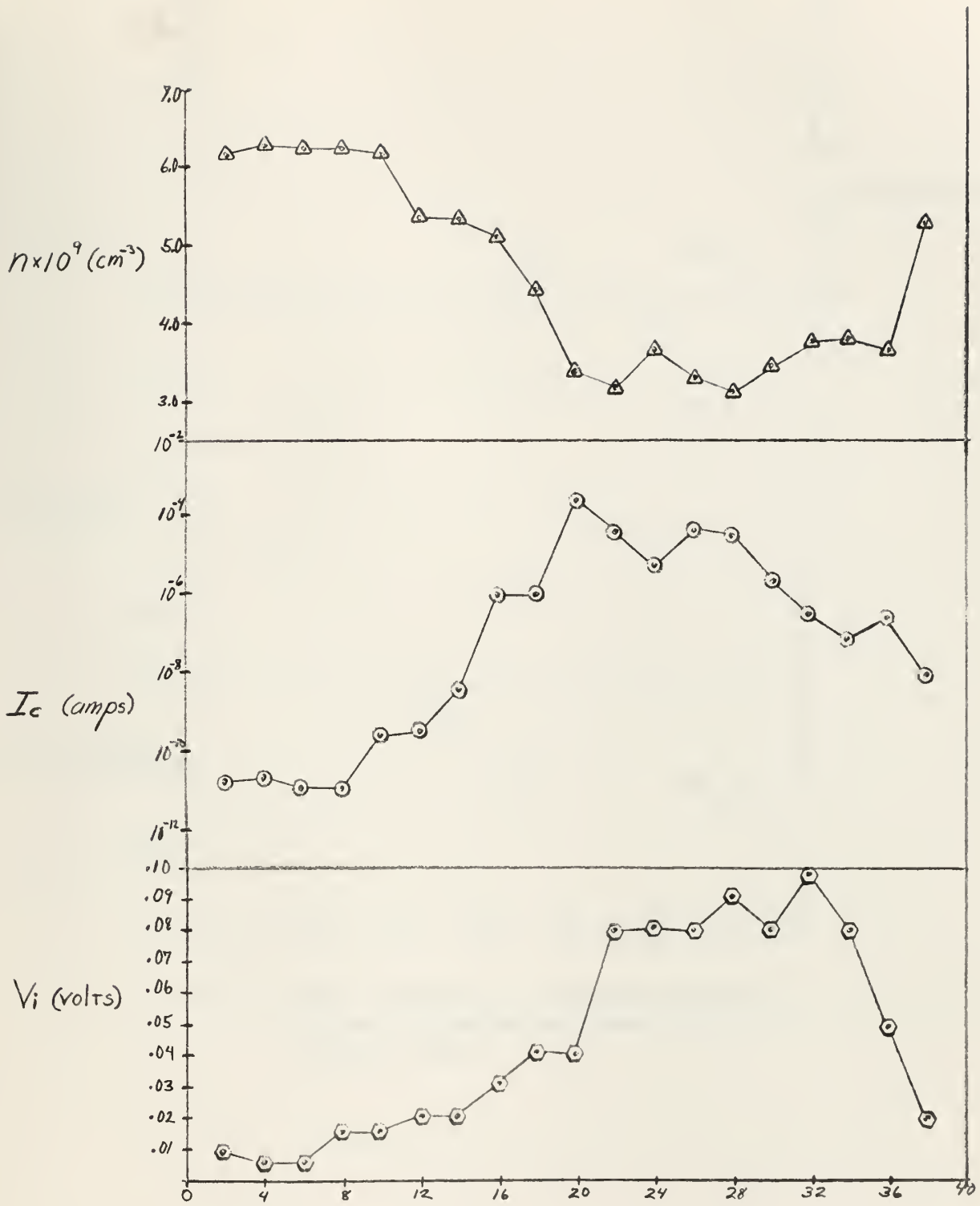


Fig. 42 Electron density, n , detector current, I_c , Ion oscillation amplitude, V_i , vs distance, Run 1

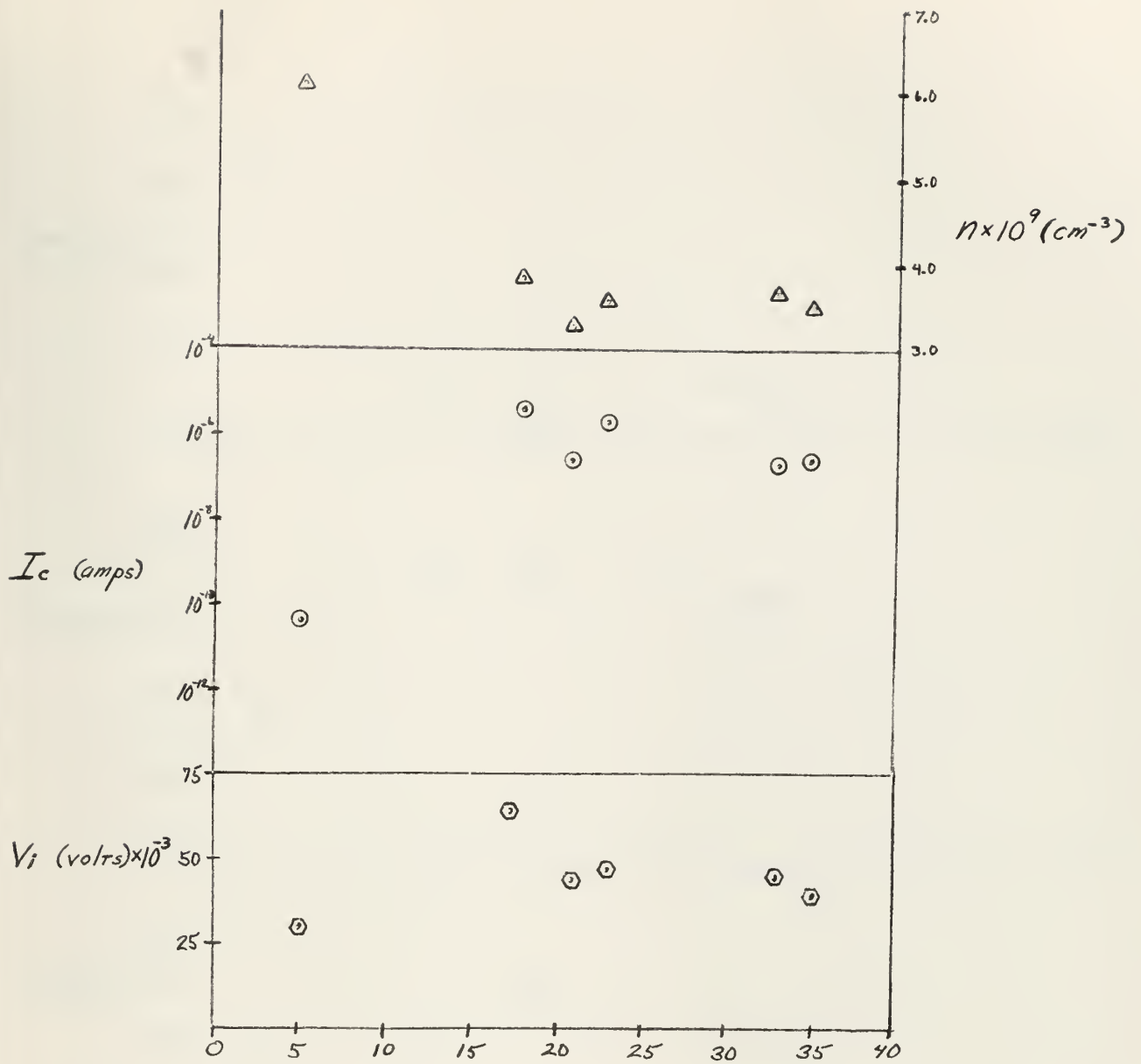


Fig. 43. Electron density, n , detector current, I_c , and ion oscillation amplitude, V_i , vs distance; Run 2

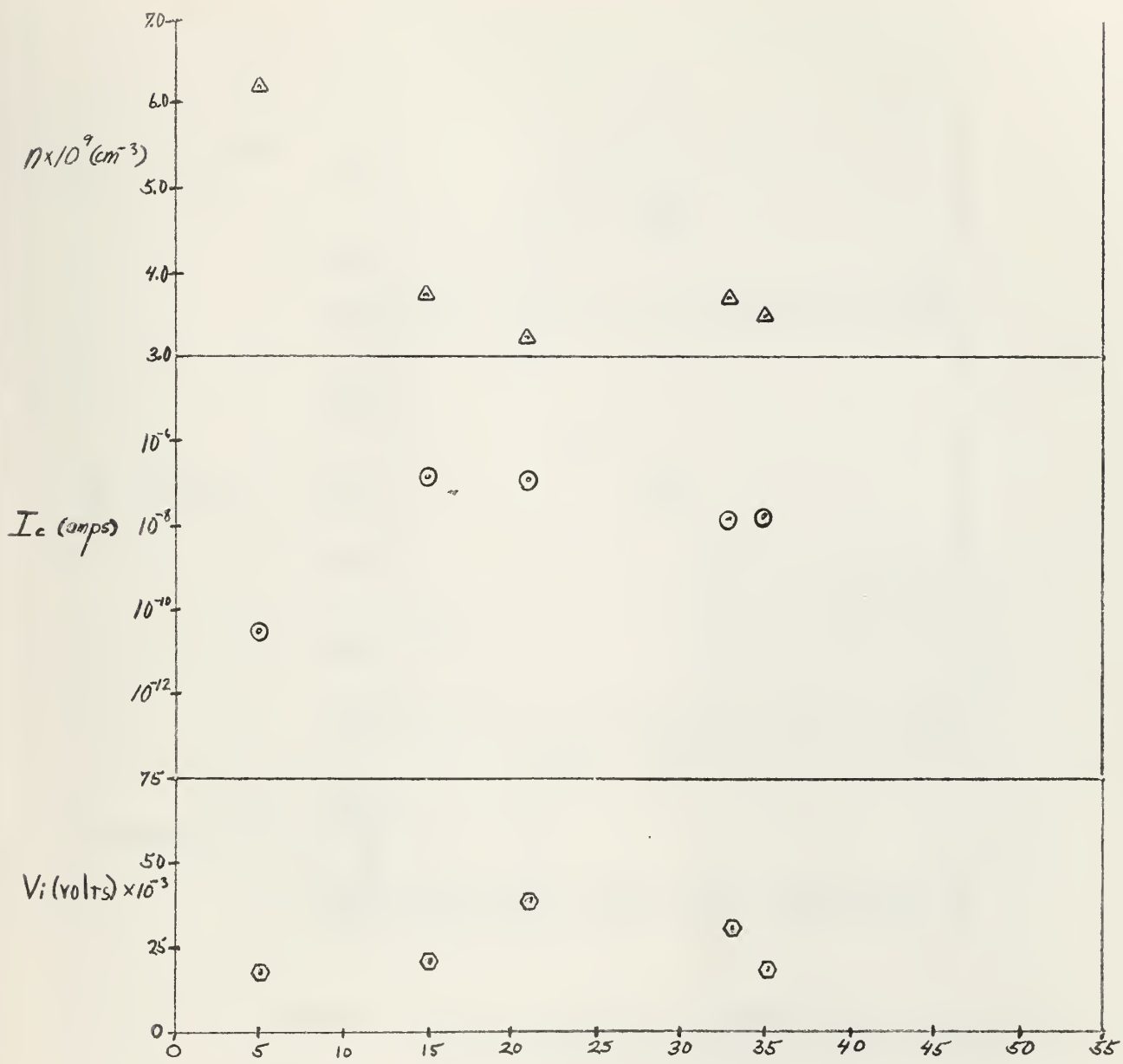


Fig. 44. Electron density, n , detector current, I_c , and ion oscillation amplitude, V_i , vs distance; Run 2

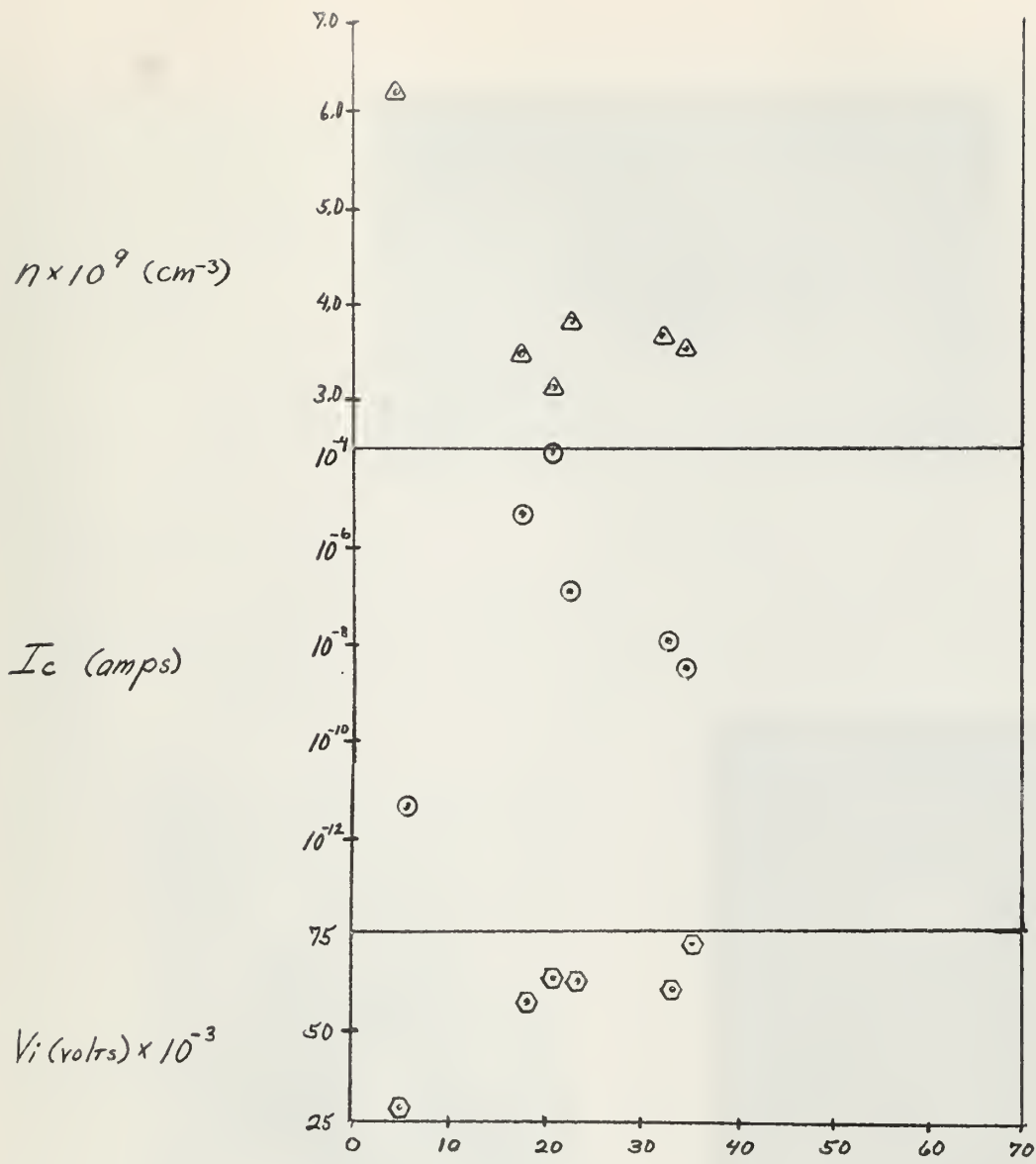


Fig. 45. Electron density, n , detector current, I_c , and ion oscillation amplitude, V_i , vs distance; Run 2



Fig. 46 a.



Fig. 46 b.

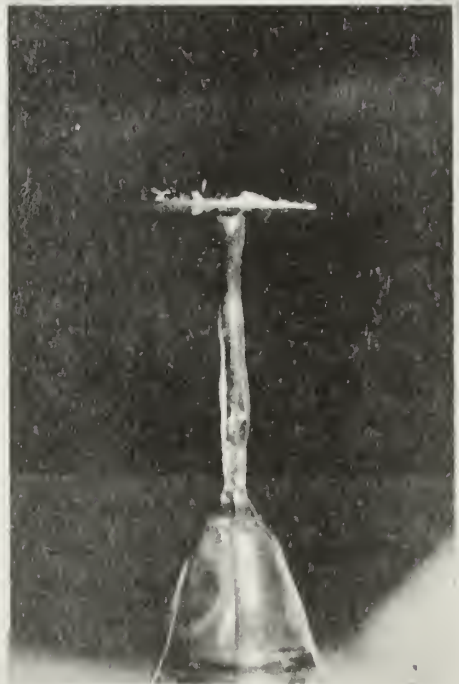


Fig. 46 c.

Fig. 46 a, b, c. Contaminated sections of the tube and internal structures
a. Deposition of copper on glass envelope
b. and c. Deposition of copper and copper oxides on tantalum anode

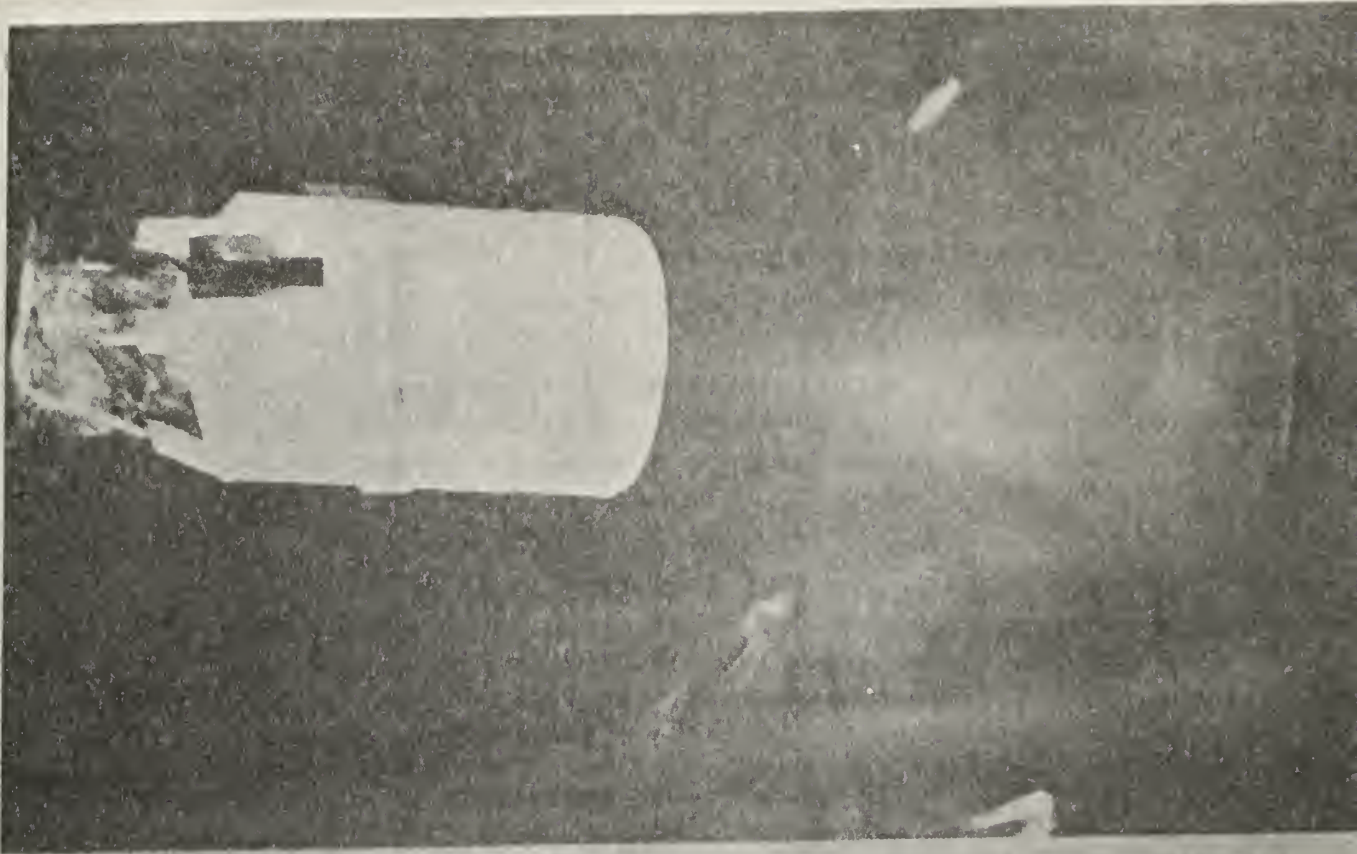


Fig. 47. Photograph of normal glow discharge in 10 microns of Neon. Illustrating the glowing region of maximum interaction. Anode to Cathode spacing 40 millimeters, Discharge current 65 milliamperes probe withdrawn. Photograph taken through didymium filter.

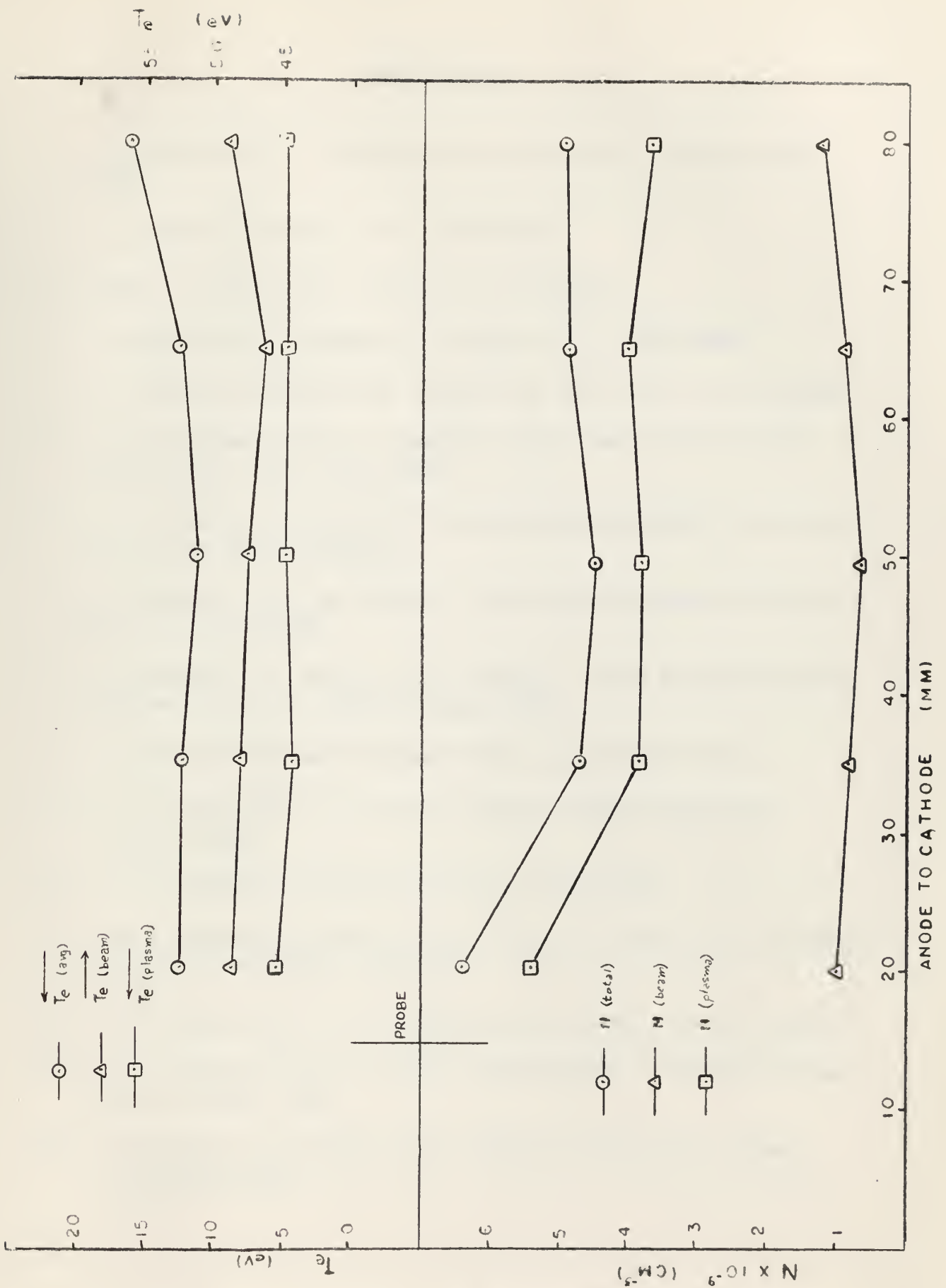


Fig. 48. Electron temperature, T_e , and electron density n , vs anode to cathode separation, probe position fixed at 15.5 mm.

BIBLIOGRAPHY

1. I. Langmuir and H. Mott-Smith, *Gen. Elec. Rev.* 449 (July-Dec 1924)
2. I. Langmuir, *Phys. Rev.* 26, p. 585 (1925)
3. Arthur F. Dittmer, *Phs. Rev.* 28, p. 507 (1926)
4. Lewi Tonks and I. Langmuir, *Phys. Rev.* 33, p. 195 (1929)
5. H. J. Merrill and Harold W. Webb, *Phys. Rev.* 55, p. 1191 (1939)
6. E. B. Armstrong and K. G. Emeleus. *Proc. Inst. E. E. (London)* 96 Pr III, No. 43, p. 390 (1949)
7. T. R. Neill and K. G. Emeleus, *Proc. Royal Irish Acad.*, 53, Sect. A No. 13, p. 197-219 (1951)
8. R. A. Bailey and K. G. Emeleus, *Proc. Royal Irish Acad.*, 57, Sect. A, No. 5, p. 58, (1955)
9. T. K. Allen, R. A. Bailey, K. G. Emeleus, *British Journal of Applied Physics*, Vol. 6, p. 320-322 (Sept. 1955)
10. M. A. Easley, *Journal of Applied Physics* 22, 590-593 (1951)
11. N. L. Oleson and C. G. Found, *Journal of Applied Physics* 20, 416-417 (1949)
12. M. J. Druyvestyn, *Zeits. Phys.* 29, p. 903 (1958)
13. John F. Waymouth *Probe Methods for Plasma Diagnostics*, University Microfilms, Ann Arbor, Michigan
14. R. H. Sloane and E. I. R. MacGregor, *Phil. Mag.* 18, 193, (1934)
15. R. L. F. Boyd and N. D. Twiddy, *Physics Dept.*, University College London (5 Sept. 1958)
16. K. Takayama, H. Ikegami, and S. Miyozaki: *Phys. Rev. Letters* 5, 238-240 (1960)

17. W. P. Allis, *Electronic Waveguides*, (Microwave Research Institute Symposium Series, Vol. VII, Polytechnic Press, Brooklyn, (1958) 149-155
18. D. W. Mahaffey, G. C. McCulloch, A. Garascadden, K. G. Emeleus, *Proceedings of the Royal Irish Academy*, Vol. 61, Sect. A, No. 9 (1961)
19. L. H. Putnam and H. D. Collins, *Plasma Oscillations in a Low Pressure Argon Discharge*, U. S. Naval Postgraduate School Thesis, (1961) and *Phys. Rev. Letters*, Vol. 7, No. 3, 77-79 (1961)
20. J. D. Cobine, *Gaseous Conductors*, 563-564, McGraw-Hill Book Co., Inc., New York and London (1941)
21. R. B. Brode, *Reviews of Modern Physics* 5, 257 (1933)
22. A. von Engel, *Ionized Gases*, 33, Clarendon Press, Oxford (1955)
23. D. Bohm and E. P. Gross, *Phys. Rev.* 75, 1851-1865, *Phys. Rev.* 79 992 (1950)
24. D. Looney and S. Brown, *The Excitation of Plasma Oscillations*, Technical Report No. 273, *Phys. Rev.* Vol. 93, No. 5, 965-969 (1954)
25. R. A. Demirkhanov, A. K. Gevorkov and A. P. Popov, *The Interaction of a Beam of Charged Particles with a Plasma*, Proc. Fourth International Conference on Ionization Phenomena in Gases, Uppsala 1959, North Holland Pub. Co., Amsterdam (1960)
26. G. D. Boyd, L. M. Field, and R. W. Gould, *Phys. Rev.* 109, 1393 (1958)
27. L. Alexoff, and R. V. Neidigh, *Proceedings Fifth International Conference on Ionization Phenomena in Gases*, Munich 1961, North Holland Pub. Co., Amsterdam (1961)
28. Laurence S. Hall, *Probes and Magnetic Pumping in Plasma* (Doctoral Thesis) University of California Lawrence Radiation Laboratory; Published by Dept. of Commerce, Washington, D. C. (1961)

29. Lewi Tonks and I. Langmuir, *Phys. Rev.* 33, p. 202, (1929)
30. Robert W. Young, *Frequencies of Simple Vibrators and Musical Scales*, p. 3-102, *American Institute of Physics Handbook*, Maple Press, (1957)

APPENDIX

Late in this work an effort was made to establish whether electron oscillations could be detected near the cathode in an Argon discharge. A discharge was established for this purpose at a pressure of 8.7 ± 0.2 microns with a current of 90 milliamperes.

No oscillations were detected within 5mm of the cathode at these values of current and pressure. Oscillations were detected near the center of the discharge as found by Putnam and Collins in last year's work. These oscillations reached a maximum detector current intensity of 2×10^{-4} amperes at a position 15mm from the cathode.

We have also been able to calibrate the pressures we have reported, which were based on our modification of the Veeco vacuum gauge. This modified vacuum gauge circuit described in this paper was calibrated with a McLeod gauge. It was determined that the response of the Veeco gauge was not linear as assumed. All pressures reported in this paper as 10 microns of Hg. must therefore be corrected to read 58 ± 1 micron. It was also determined that this non-linear response occurred for the gases Argon and Helium, although the factors for correction were not the same for the various gases. The pressure for Argon, reported above, we believe is accurate within the limits specified.

This increased pressure of Neon in our tube would result in a mean free path for electrons in Neon on the order of 1.1 to 1.5 cm, however, the phenomena described in section three of the work we believe is still valid. Further experiment in anode cathode spacing down to slightly less than 7mm

indicated little if any effect on the discharge characteristics. The only noticeable effect was a visible shortening of the plasma column which normally fills the greater part of the length of our tube. For these very small spacings the plasma surrounded the anode and cathode in the rough form of a sphere with a diameter of approximately 5cm.

thesA355

Plasma oscillations in a low pressure ne



3 2768 001 90972 4

DUDLEY KNOX LIBRARY